

American Journal of Science

DECEMBER 2007

GEOCHRONOLOGIC CONSTRAINTS ON THE CHRONOSTRATIGRAPHIC FRAMEWORK OF THE NEOPROTEROZOIC HUQF SUPERGROUP, SULTANATE OF OMAN

SAMUEL A. BOWRING*[†], JOHN P. GROTZINGER****, DANIEL J. CONDON****,
JAHANDAR RAMEZANI*, MARK J. NEWALL^{§,§§}, and PHILIP A. ALLEN^{§§§}

ABSTRACT. The Huqf Supergroup, Sultanate of Oman, contains an important record of Neoproterozoic history, including evidence for two glaciations, a massive reorganization of the global carbon cycle, and the Ediacaran-Cambrian transition. New U-Pb geochronologic data provide precise constraints on the age of several key stratigraphic levels in the Neoproterozoic Huqf Supergroup and its subjacent crystalline basement rocks. The basement ages constrain an interval of felsic magmatism to have occurred from at least 840 Ma to approximately 810 Ma. Detrital zircons from several stratigraphic levels within the Huqf Supergroup yield ages in excess of 2.5 Ga, suggesting proximity of Archean crust during the Neoproterozoic evolution of the eastern Arabian Peninsula. Volcanic ash beds intercalated within the Huqf Supergroup were dated in the Oman Mountains, and in several subsurface wells (South Oman Salt Basin). Glacial deposits of the Abu Mahara Group in the Oman Mountains (Ghubrah Formation) contain volcanoclastic rocks that are approximately 713 Ma; overlying syn-glacial turbiditic sandstones of the Fiq Formation yield a suite of detrital zircon dates ranging from 920 to 664 Ma so that deposition of at least the upper Fiq must have post-dated 664 Ma. In the South Oman Salt Basin, volcanoclastic deposits intercalated within glaciogenic strata of the Fiq Formation yielded zircons, the youngest of which is about 645 Ma. These data indicate two distinct episodes of glaciation at approximately 713 and <645 Ma.

The uppermost Ara Group of the Huqf Supergroup contains multiple ash beds within its carbonate strata, where an age of roughly 547 Ma is reported for rocks that occur above strata marked by a pronounced negative (-12‰) to positive (+4‰) excursion in carbon isotope composition. Higher in the Ara sequence, three distinct ash beds dated at about 543 Ma, 542 Ma, and 541 Ma closely approximate the Ediacaran-Cambrian boundary in Oman. The dramatic carbon isotope excursion of ~16 permil in the Shuram Formation (middle Nafun Group) has a firm maximum age of approximately 620 Ma as provided by detrital zircon ages from the base of the formation. Interpolation and downward extrapolation from the Ara Group ages, coupled with correlation to other global strata, suggests the base of the Shuram C-isotope excursion to be on the order of 560 Ma, with an estimated duration of approximately 5 to 11 m.y. This excursion is inferred to post-date the last well-

*Department of Earth, Atmospheric and Planetary Sciences, Massachusetts Institute of Technology, Cambridge, Massachusetts 02139, USA

**Current Address: Division of Earth and Planetary Sciences, California Institute of Technology, Pasadena, California 91125, USA

***Current Address: NERC Isotope Geoscience Laboratories, British Geological Survey, Keyworth, NG12 5GG, United Kingdom

§Petroleum Development Oman, Box 81, Muscat, PC 113, Oman

§§Current Address: Shell Egypt, Heliopolis, Cairo, Egypt

§§§Department of Earth Science and Engineering, Imperial College, London SW7 2AZ, United Kingdom

[†]Corresponding author: sbowring@mit.edu

documented Neoproterozoic glaciation (about 582 Ma) and is broadly coincident with the appearance of complex organisms in the fossil record.

INTRODUCTION

The Neoproterozoic Era was characterized by major shifts in the carbon isotopic composition of seawater (Kaufman and Knoll, 1995; Halverson and others, 2005) often associated with major glaciations and subsequent appearance of macroscopic organisms in the fossil record. The base of the Ediacaran Period is defined by the termination of a globally extensive Marinoan glaciation, and its top by the base of the Cambrian demarcated by the first occurrence of *Treptichnus pedum*. The boundary is broadly coincident with an extinction event and a distinctive negative $\delta^{13}\text{C}$ excursion (Amthor and others, 2003; Knoll and others, 2004). This interval of time contains a record of global biological and geochemical events, beginning with the origin and diversification of the enigmatic Ediacaran soft-bodied biota (for example Narbonne, 2005) and ending with the development and extinction of the first weakly calcified metazoans (Germs, 1972; Grotzinger and others, 1995; Amthor and others, 2003). During the later part of the Ediacaran Period (approximately 578 – 542 Ma) macroscopic metazoan fossils appear in the rock record, which broadly coincides with one of the most profound shifts of the carbon isotopic composition of seawater in Earth history (Burns and Matter, 1993; Workman and others, 2002; Condon and others, 2005; Fike and others, 2006). Determining a detailed history of the Neoproterozoic is crucial for understanding global-scale interactions between life and environment.

The Huqf Supergroup in the Sultanate of Oman captures a record of the middle to late Neoproterozoic, but until now has lacked detailed chronostratigraphic context. It is well exposed in the Oman Mountains, Huqf and Mirbat areas (fig. 1) (McCarron, ms, 2000; Leather and others, 2002; Cozzi and others, 2004a; Le Guerroue and others, 2005) and also occurs in the subsurface where numerous boreholes penetrate Ediacaran to Cambrian age strata (see for example Mattes and Conway Morris, 1990; Amthor and others, 2003). The Huqf Supergroup contains distinctive Neoproterozoic glacial deposits and associated cap carbonate(s), which are overlain by thick siliciclastic and carbonate shelf strata. These carbonates contain a dramatic carbon isotopic ($\delta^{13}\text{C}$) excursion of ~ 6 permil, and are in turn overlain by evaporites and carbonates that contain the Ediacaran-Cambrian boundary. Fossils include acritarchs preserved in the lower and middle Huqf (Butterfield, 2001) and the late Ediacaran index fossils *Cloudina* and *Namacalathus* (Amthor and others, 2003), as well as biomarker evidence for sponges in rocks inferred to be pre-Marinoan (Love and others, 2005).

Huqf Supergroup strata also include zircon-bearing volcanic rocks, some of which were dated previously (Brasier and others, 2000; Amthor and others, 2003). This contribution is focused on providing high-precision temporal constraints on the Neoproterozoic of Oman by presenting new age data from its key stratigraphic levels, as well as revised and more precise ages for previously dated ash beds. In addition, detrital zircon dates from siliciclastic lithologies provide maximum depositional age limits for enclosing strata and help characterizing provenance. Considered collectively, the results bear significant implications on the timing of pre-Ediacaran glaciation cycles, as well as Ediacaran global biogeochemical and tectonic events.

GEOLOGIC SETTING

Early Neoproterozoic (<1.0 Ga) crystalline basement of Oman is unconformably overlain by approximately 800 Ma, low-grade, rhyolitic volcanic and associated clastic rocks and strata of the Neoproterozoic to earliest Cambrian Huqf Supergroup (fig. 2) (Gorin and others, 1982; Clarke, 1988; Burns and Matter, 1993; Loosveld and others, 1996; Brasier and others, 2000; Amthor and others, 2003). Overlying strata of the Haima Supergroup, of middle Cambrian to Silurian age (Millson and others, 1996),

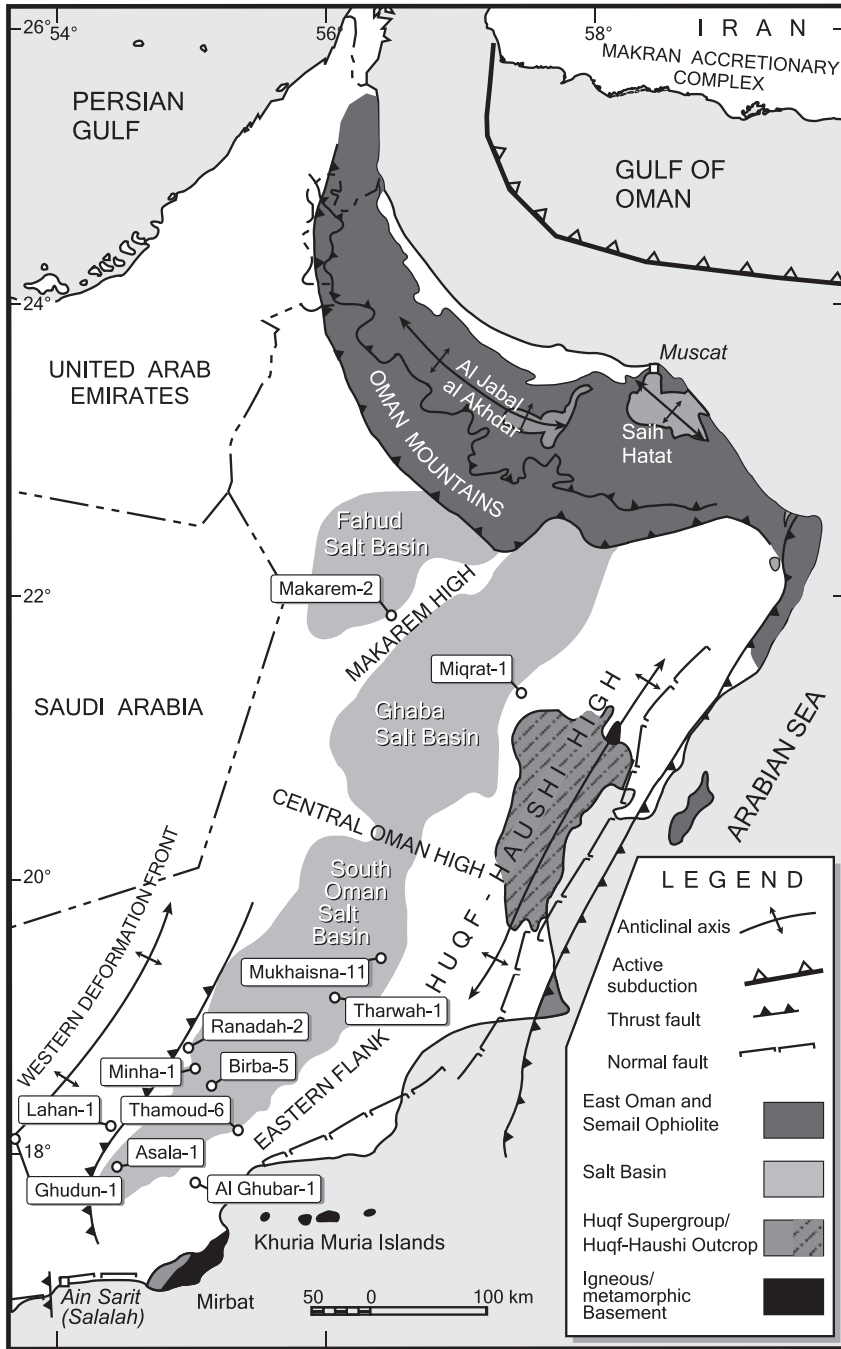


Fig. 1. Simplified geological map showing outcrop study areas, location of key subsurface wells, and major geological features discussed in this paper. Wells in and adjacent to the SOSB outline the zone of major subsidence during Ara Group deposition time. Note the thrust front to the west of the SOSB that marks the eastern boundary of deformation related to uplift along the Western Deformation Front.

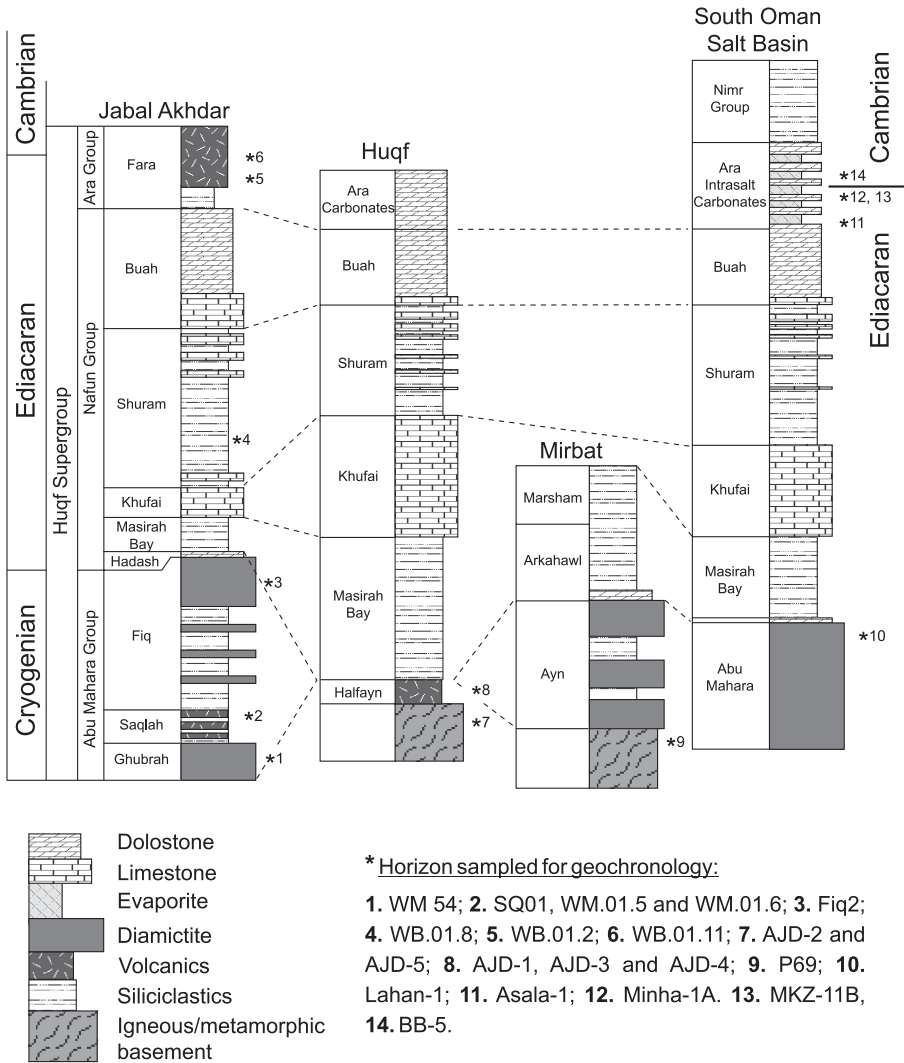


Fig. 2. Lithostratigraphy of Neoproterozoic to early Cambrian rocks in Oman for each of the geographic regions studied (see fig. 1) along with horizons represented by geochronology samples. The SOSB stratigraphic column is a composite of several wells with significant overlap (see figs. 8 and 10, and Amthor and others 2003).

are distinguished from the Huqf Supergroup rocks by a regionally continuous angular unconformity.

The Huqf Supergroup is well-exposed in central and northern Oman, including the Huqf-Haushi area and the Oman Mountains/Jabal Akhdar area (Gorin and others, 1982; Mattes and Conway Morris, 1990; Wright and others, 1990), in the Mirbat area of southern Oman (Kellerhals and Matter, 2003; Mercogli and others, 2006) (fig. 1), and is intercepted in numerous wells in the South Oman Salt Basin. The Huqf Supergroup is subdivided into three groups (fig. 2), which in ascending order are: the Abu Mahara Group (glacial clastics); the Nafun Group, which is subdivided into the Hadash (cap-carbonate), Masirah Bay (shelf clastics), Khufai (peritidal cyclic carbonates), the Shuram (storm-dominated shelf clastics and carbonates) and Buah (storm-dominated

shelf dolostones and limestones) formations; and the Ara Group (several carbonate platforms interlayered with evaporites) (Gorin and others, 1982; Mattes and Conway Morris, 1990; Wright and others, 1990; Schroeder and others, 2005). In general, the outcrops constrain the Abu Mahara and Nafun groups, whereas cores, well logs, and seismic data provide constraints on the thickness and distribution of the Ara Group. In outcrops of the Oman Mountains the volcanoclastic Fara Formation overlies the Buah Formation and is generally considered time equivalent to the Ara Group. Strata of possible Ediacaran-Cambrian boundary age are known only from subsurface data (Amthor and others, 2003; Schroeder and others, 2005). In a few key wells on structural highs both the Abu Mahara and Nafun groups were intercepted, thus providing ties between the surface exposures and the subsurface (Mattes and Conway Morris, 1990; Cozzi and others, 2004a). The Huqf Supergroup preserves several distinct stages of basin development, probably associated with different subsidence mechanisms. The Abu Mahara Group was deposited within localized fault bounded basins, whereas the overlying Nafun Group is laterally extensive reflecting broad, regional subsidence. The Nafun Group-Ara Group boundary marks a shift from this regional subsidence to a tectonic style marked by uplift of large basement blocks that segmented the broader basin into several fault-bounded sub-basins (Immerz and others, 2000).

The Ara Group depositional patterns reflect segmentation of the Nafun basin into three smaller-scale basins within the interior of Oman. This segmentation began at about 550 to 548 Ma, and was accompanied by a shift to a more arid climate and accumulation of salts and carbonates. These basins include the South Oman Salt Basin (SOSB), the Ghaba Salt Basin, and the Fahud Salt Basin (fig. 1). Seismic data indicate that the western margins of these basins are delineated by structurally complex transpressional deformation fronts (Loosveld and others, 1996) of Ara age (late Ediacaran to earliest Cambrian). An upper age limit for deformation is provided by sediments that contain late Cambrian trilobites, derived from uplift and erosion of the western margin. A significant clastic wedge, represented by the Nimr Group, is derived from unroofing of the western margin ("Western Deformation Front", see fig. 1). Clastic sediments of the uppermost Ara Group signal the onset of this event. In contrast, the eastern margins of the salt basins are characterized by onlap and thinning of basin strata onto a structural high located close to the modern-day east coast of Oman. Within the three salt basins, further segmentation occurred, with localized subsidence related to basement-involved block faulting. Within the SOSB the uplifted blocks became sites of carbonate deposition, and down-faulted blocks were overlain with black shale and silicilyte (Amthor and others, 2005). Evaporites blanketed both basins and uplifted blocks. Interlayered carbonates and evaporites of the Ara Group accumulated within these sub-basins creating an ideal geologic setting for the generation, trapping and long-term preservation of hydrocarbons (Al-Siyabi, 2005). The SOSB has long been recognized as a major hydrocarbon province (Morton, 1959), although it was not clear until the mid-1970's that the dominant source rock is of terminal Proterozoic age. Subsequent work demonstrated that this source rock charged not only Proterozoic reservoirs, but also Paleozoic and Mesozoic reservoirs (Al-Marjebi and Nash, 1986).

Several models have been invoked to explain the history of basin evolution and subsidence recorded by the Huqf Supergroup. There is general agreement that the Abu Mahara (bimodal volcanic and clastic sedimentary rocks) accumulated within aurally restricted basins related to regional extension (rifting), however interpretation of the Nafun and Ara groups is less certain. It has been suggested that the aurally extensive Nafun Group deposits reflect subsidence related to post-rift thermal contraction of the lithosphere and creation of a passive continental margin (Allen and Kapellos and others, 1992; Leather, 2006). Grotzinger and others (2002) interpret Abu

Mahara subsidence to relate to regional extension but suggests that the broad, regional subsidence represented by the Nafun Group is related to dynamic depression of the lithosphere associated with subduction of oceanic lithosphere beneath the Arabian plate. Subduction is inferred to have occurred along the northeastern margin of Gondwanaland (eastern Oman) where an Andean margin developed. Although subsidence of the younger Ara Group is generally attributed to regional strike slip faulting associated with Najd tectonism (Al-Husseini and Al-Husseini, 1990), in the subduction model the Ara Group was deposited in troughs created by basement-involved uplift, analogous to the Laramide orogeny of the western U.S., or the Bolivian segment of the Andes where flat slab subduction occurred. Retro-arc uplift and desiccation may have helped produce the Ara evaporite deposits, and the numerous ash beds of the Ara Group are likely airfall equivalents of contemporaneous arc magmatism. Thick sequences of felsic volcanic rocks such as those represented by the Fara Formation (Oman Mountains) and in the subsurface (Ghaba Salt Basin) are all broadly consistent with subduction-related melting of the crust in a retroarc setting (Grotzinger and others, 2002). Given the structurally segmented nature of the basin and the increase in volcanic and volcanoclastic rocks (relative to the underlying Nafun Group), it is unlikely that the Ara Group records simple passive margin subsidence.

All tectonic models for the region are hampered by lack of exposures combined with an incomplete understanding of the temporal evolution of the Huqf Supergroup. The models outlined above make predictions concerning the stratigraphic continuity of certain units and the chronostratigraphic framework developed in this paper provides a means to begin to assess such models. Determining the age and temporal distribution of each of these units is the key to establishing a viable chronostratigraphic framework for the Huqf Supergroup.

U-Pb ANALYTICAL PROCEDURES

Samples collected for geochronological analyses were crushed using a combination of jaw crusher and disc mill followed by washing in water to remove the bulk of the low-density material. Heavy minerals were separated using standard heavy liquid and magnetic techniques. Zircon grains were hand-selected for analysis from the least magnetic fraction based on the absence of cracks, inclusions, and surface contamination. In order to minimize the effects of Pb loss, the grains were subjected to either conventional mechanical air-abrasion (Krogh, 1982) or a version of the thermal annealing and acid leaching (also known as chemical abrasion or CA-TIMS) technique of Mattinson (2005) prior to isotope dilution thermal ionization mass-spectrometry (ID-TIMS) analyses using a mixed ^{205}Pb - ^{233}U - ^{235}U tracer solution (spike). Details of zircon pre-treatment, dissolution and U and Pb chemical extraction procedures are described in Ramezani and others (2007).

U and Pb isotopic measurements were performed on a VG Sector-54 multi-collector thermal ionization mass spectrometer at MIT. Pb and U were loaded together on a single Re filament in a silica-gel/phosphoric acid mixture (Gerstenberger and Haase, 1997). Pb isotopes were measured by peak-hopping using a single Daly photomultiplier detector and U isotopic measurements were made in static mode using multiple Faraday collectors. Mass fractionation for Daly measurements was determined to be $0.25 \pm 0.04\%$ /amu over a wide temperature range based on long-term measurements of the NBS-981 Pb standard. U mass fractionation was calculated in real-time using a double spike. All common Pb was attributed to procedural blank. A sensitivity test shows that the composition of the common Pb has no discernable effect on any of the calculated dates reported in this paper. U blanks were <0.1 pg. Data reduction, age calculation, and the generation of concordia plots were carried out using the algorithms of Ludwig (1980), and the statistical reduction and plotting program ISOPLOT (Ludwig, 1991).

The data presented in this paper was accumulated over a period of about five years during which our analytical protocols have been continuously improving. Most notably we have adopted the chemical abrasion (CA-TIMS) technique (Mattinson, 2005), have participated in the initial stages of a community-based assessment of interlaboratory standards as part of the EARTHTIME project (Condon, 2005), and have refined our U-Pb tracer calibration (Schoene and others, 2006). In cases where the highest possible precision is crucial and where we had sufficient sample material, older data were supplemented with new analyses using the latest techniques.

In the past few years it has become evident that zircon which yields high-precision, statistically equivalent data sets often exhibit slight age discordance ($^{207}\text{Pb}/^{206}\text{Pb}$ dates are a minimum of 0.2% older than the U-Pb dates), likely due to imprecision in one or both of the U decay constants (Mattinson, 2000; see also a recent review in Schoene and others, 2006). In many previous studies of lower Paleozoic zircons plagued with Pb loss that is inferred to have occurred in geologically recent times, $^{207}\text{Pb}/^{206}\text{Pb}$ dates have been considered the best estimate for the age of a discordant population. In this case, uncertainties in the decay constants could be ignored if the dates are not compared with dates calculated using other chronometers. However, it now appears that discordance related to radiation damage and Pb loss can very often be effectively eliminated through the CA-TIMS technique (Mundil and others, 2004; Mattinson, 2005; Schoene and others, 2006). A data set for a single population of zircons for which Pb loss has been eliminated is manifested by a coherent cluster of data (equivalent in the terminology of Ludwig, 1998), in which all the scatter can be accounted for by analytical uncertainty. In these cases the weighted mean $^{206}\text{Pb}/^{238}\text{U}$ date is generally the most precise and accurate and thus preferred for the purpose of fine-scale stratigraphic correlation, as well as calculating rates and/or durations of sediment accumulation. For some samples, equivalent data sets were not obtained and we instead rely on either the $^{207}\text{Pb}/^{206}\text{Pb}$ or the upper concordia intercept date as the best estimate of age. Errors for U-Pb dates are reported in the following format: $\pm X(Y)[Z]$, where X is the internal or analytical uncertainty in the absence of all systematic error (tracer calibration and decay constants), Y includes the tracer calibration error (using a conservative estimate of the 2σ standard deviation of 0.05% for the Pb/U ratio in the tracer), and Z includes the additional decay constant errors of Jaffey and others (1971). For $^{207}\text{Pb}/^{206}\text{Pb}$ dates, tracer calibration errors are negligible and Y is not reported (so it reads $\pm X[Z]$). The MSWD (mean square of the weighted deviates: York, 1967, 1969) of the weighted mean $^{206}\text{Pb}/^{238}\text{U}$ date is calculated prior to the addition of systematic uncertainties. All data are presented in Appendix 1, concordia plots for selected samples are shown in figures 3 and 4, and calculated dates and associated uncertainties for critical samples are summarized in table 1. When considering relative ages of different samples (for example when determining sediment accumulation rates) it is crucial to use dates calculated using a single decay scheme, in which case decay constant uncertainties can be effectively ignored. Alternatively, the decay constant uncertainties must be taken into account for each of the dates being compared.

In this study we present a large number of U-Pb dates for single detrital zircons separated from a number of lithologies. Some were collected as possible volcanic ashes, whereas others were intentionally sampled to examine provenance. The detrital dates provide maximum age constraints on the depositional age, in addition to providing information on the age of the source terrains supplying detritus. Although pre-treatment techniques (air abrasion and CA-TIMS) were employed to minimize the effects of Pb loss, detailed studies of certain samples (such as WM 54, see below) demonstrate the difficulty in completely eliminating it for certain zircons. Thus, for detrital zircons the $^{207}\text{Pb}/^{206}\text{Pb}$ date provides the best estimate for the age of the zircon and avoids the potential problem of underestimation (by potentially many tens

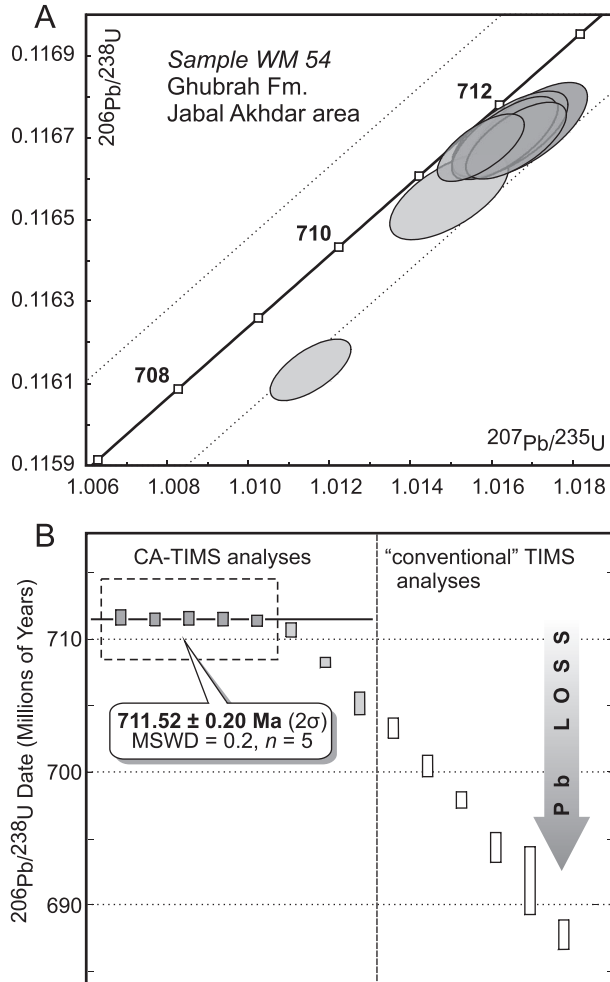


Fig. 3. U-Pb single-zircon data from sample WM 54, volcaniclastic tuff from the glaciogenic Ghubrah Formation. Analyses used in age calculation are in dark gray. (A) Concordia plot showing the five concordant analyses in addition to two analyses that are slightly discordant (light gray ellipses). Not all data are shown. Dashed line represents uncertainty in U decay constants. (B) Plot of $^{206}\text{Pb}/^{238}\text{U}$ dates for single zircon analyses showing the effect of Pb loss. Note that for this sample the CA-TIMS technique was much more effective in overcoming Pb loss compared to the conventional air abrasion technique.

of millions of years) when utilizing the $^{206}\text{Pb}/^{238}\text{U}$ age for zircons that have suffered Pb loss. While potentially confusing to the non-geochronologist, the main point of this discussion is that one needs to know the type of U-Pb date being reported before it can be compared with either other U-Pb dates or dates derived from other chronometers. Somewhat paradoxically, this state-of-affairs is a direct result of our ability to make increasingly more precise analyses; as recent as five years ago this level of resolution was not possible.

Two other analytical techniques are often employed for detrital zircon geochronology, laser-ablation ICPMS and ion microprobe (SIMS). While these techniques are able to produce a large amount of data in relatively short periods of time, they do so with much less precision than ID-TIMS. However, these techniques are particularly useful for establishing a spectrum of detrital dates in order to fingerprint provenance.

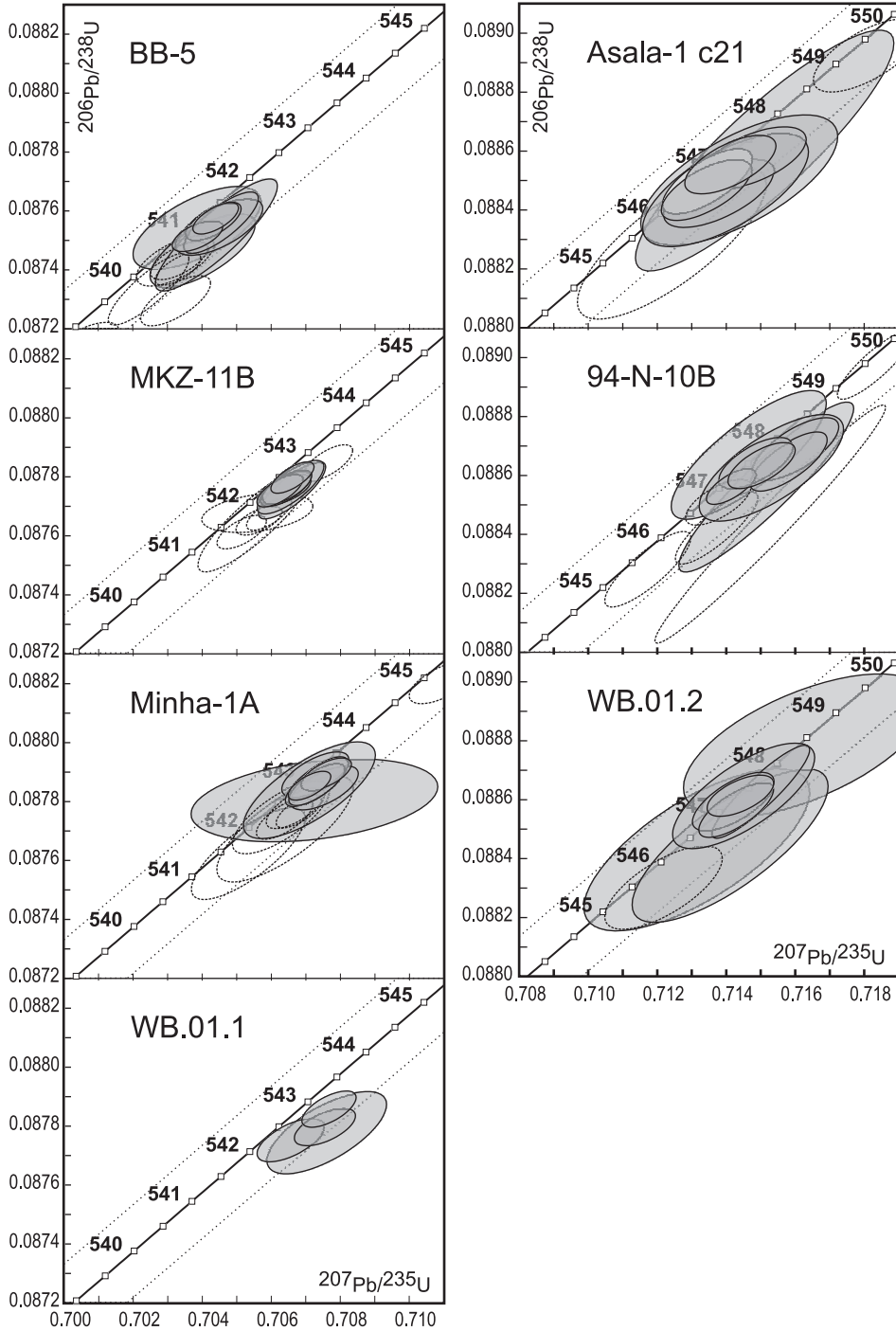


Fig. 4. Concordia plots for U-Pb zircon data from Ara Group and Fara Formation ash beds and volcanic rocks (data outside the plot ranges are not shown). Sample 94-N-10B is an ash bed from the Nama Group, Namibia (see Grotzinger and others, 1995). Shaded ellipses signify analyses used in the weighted mean $^{206}\text{Pb}/^{238}\text{U}$ age calculations. Straight dashed lines represent uncertainty in U decay constants.

TABLE 1
Summary of high-precision age results

Sample	Group	Lithostratigraphic Unit	Number of analyses ^[1]	²⁰⁶ Pb/ ²³⁸ U date (Ma)	± X (Myr) ^[2]	± Y (Myr) ^[3]	± Z (Myr) ^[4]	MSWD	²⁰⁷ Pb/ ²⁰⁶ Pb date (Ma)	± X (Myr) ^[2]	± Z (Myr) ^[4]	MSWD
BB-5		A4 Carbonate (lower)	18,8,15	541.00	0.13	0.21	0.81	1.0	542.68	0.46	1.2	0.58
MKZ-11B		A3 Carbonate (upper)	16,8,12	542.33	0.11	0.19	0.79	0.50	544.10	0.40	1.2	0.31
Minha-1A	Ara	A3 Carbonate (lower)	17,8,14	542.90	0.12	0.20	0.80	0.62	544.38	0.45	1.2	0.37
Asala-1 c21		A0 carbonate	12,8,10	546.72	0.21	0.29	0.89	0.92	548.90	0.98	1.7	0.63
WB.01.1		Fara	10,4,7	542.54	0.45	0.53	1.13	2.6	545.94	0.68	1.4	0.83
WB.01.2		Fara	17,8,9	547.23	0.28	0.36	0.96	1.3	548.27	0.80	1.6	0.44
94-N-10B	Nama	Kuibis	15,8,12	547.36	0.23	0.31	0.91	1.4	549.34	0.82	1.6	2.2
WM 54	Abu Mahara	Ghubrah	24,5,12	711.52	0.20	0.31	1.09	0.18	714.08	0.52	1.5	0.38
Makarem-2		Syenite intrusion	4,2,4	695.10	1.60	1.70	2.47	1.3	698.68	0.50	1.5	0.53
Salalah 13	Intrusive	Leger granite	9,4,7	726.12	0.40	0.51	1.31	0.79	730.22	0.96	2.0	1.2
P69		Pegmatitic vein in basement	5,3,5	808.92	0.33	0.45	1.34	1.0	811.32	0.54	1.7	0.17

Notes: [1] Number of zircon analyses; total, included in calculation of Pb/U age, included in calculation of Pb/Pb age.

[2] Uncertainty due to internal (analytical) errors only.

[3] Uncertainty including internal errors and tracer calibration error.

[4] Uncertainty including internal errors, tracer calibration error and U decay constant uncertainties of Jaffey and others (1971).

Even the most precise $^{206}\text{Pb}/^{238}\text{U}$ LA-ICPMS and ion-microprobe dates are often characterized by one-sigma errors of 1 to 2 percent making the detection of Pb loss and subtle inheritance difficult at best. In general, for Neoproterozoic age rocks, these *in-situ* techniques rely on the highest precision $^{206}\text{Pb}/^{238}\text{U}$ dates as the best estimate of the age of the grain. It is therefore worth noting that between relative imprecision and the inability to detect subtle Pb loss, it is possible that dates are often younger than the true zircon crystallization age (see for example Zhang and others, 2005).

LITHOSTRATIGRAPHIC AND GEOCHRONOLOGIC CONSTRAINTS

In the following section we present new U-Pb zircon geochronologic data from the igneous/metamorphic basement, the overlying Abu Mahara Group, Nafun Group and Ara Group of Oman. These data are used to constrain depositional ages, as well as to characterize source regions for detrital zircons.

Basement Rocks

There are three outcrop areas in Oman where crystalline basement and overlying Neoproterozoic sedimentary rocks are exposed. The two most prominent localities are Al Jobah in the Huqf-Haushi outcrop belt of east-central Oman and in the Mirbat area of southern Oman near Salalah (fig. 1). At Al Jobah approximately 35 meters of felsic volcanic and shallow marine sedimentary rocks of the Halfayn Formation (Dubreuilh and others, 1992) overlie penetratively deformed granodioritic rocks. The felsic volcanic rocks have been correlated with the Ghadir Manquil Formation of the Oman Mountains (Bell, 1993; Pilcher and Buckley, 1995), as well as with trachytic volcanic rocks recovered from a core in the Khufai Dome of the Huqf outcrop belt. Previous geochronologic data including a K-Ar date of 654 ± 12 Ma on the trachytic volcanic rocks (Gorin and others, 1982) and a Rb-Sr whole-rock date of 562 ± 42 Ma (Dubreuilh and others, 1992) on samples of rhyolite from the Halfayn Formation implied that the overlying sedimentary rocks were much younger. Our U-Pb zircon results show a limited range for dates from both granodioritic basement and the overlying felsic volcanic rocks and indicate that both are considerably older than earlier estimates.

Zircon from five samples from the Al Jobah area, including two of the underlying granodioritic basement (AJD2 and ADJ5), two of felsic volcanic rocks (AJD1 and AJD3) in the Halfayn Formation, and a sedimentary breccia (AJD4), were analyzed. Samples of the Al Jobah granodiorite (AJD2 and ADJ5) yielded large, euhedral zircons that scatter near the concordia curve (Appendix table 1). The data are consistent with minor amounts of inheritance of slightly older zircon combined with Pb loss. The youngest grains have $^{207}\text{Pb}/^{206}\text{Pb}$ dates at approximately 824 Ma which we interpret as the best estimate of the age of the intrusion. Four zircons were analyzed from sample AJD1, a light-green rhyolitic ignimbrite with well-preserved primary volcanic textures. $^{207}\text{Pb}/^{206}\text{Pb}$ dates range from about 823 to 850 Ma indicating the predominance of xenocrystic grains in the sampled population. Zircons from this sample are indistinguishable from the underlying basement, but given the combined effects of Pb loss and inheritance it is difficult to precisely estimate the eruptive age. Four zircons were analyzed from a sample of a red rhyolitic ash-flow tuff (AJD3) stratigraphically below AJD1 and, like AJD1, there is evidence for inheritance of older zircons from the basement. AJD4 is a sample of light-gray volcanoclastic and calcareous breccia and conglomerate stratigraphically above AJD1. The four zircons analyzed in AJD4 yielded $^{207}\text{Pb}/^{206}\text{Pb}$ dates that range in age from 827 Ma to 840 Ma, older than the underlying rhyolites. All samples have variably complex U-Pb systematics that preclude precise age determination, however the data strongly suggests that these non-deformed, low-grade rocks are approximately 823 Ma and slightly older.

Previous geochronological investigations of basement in the Mirbat region resulted in a Rb-Sr 'isochron' age of 554 ± 10 Ma from a combination of samples from

both granodioritic dikes and an unfoliated alkaline (Leger) granite cutting 800+ Ma old basement (Platel and others, 1992). This 'isochron' age led to the inference that the overlying Mirbat Formation was younger than roughly 550 Ma. However, between the fact that unrelated samples were combined to calculate an isochron and consideration of the emerging Neoproterozoic chronostratigraphic framework, this young age was thought anomalous and these rocks were targeted for U-Pb geochronology.

A sample of a pegmatitic granitic vein (P69) was collected at Mirbat where the Ayn Member of the Mirbat formation rests unconformably on deformed, foliated gneissic basement. This foliated gneiss has been dated at approximately 815 Ma (Mercogli and others, 2006). Sample P69 occurs about 3 meters below the contact, where sub-vertical light pink pegmatite veins, striking E-W, cross-cut an older foliated gneissic unit and are in turn truncated by the sub-Ayn unconformity. Five zircons were analyzed and yield a weighted mean $^{207}\text{Pb}/^{206}\text{Pb}$ date of $811.3 \pm 0.6[1.7]$ Ma (MSWD = 0.17), similar in age to basement samples dated in the north, indicating a magmatic link between the basement exposures in the north and Mirbat.

The Leger granite is a non-foliated granite that cross-cuts the older basement and is unconformably overlain by Cretaceous carbonates. It is inferred to have also been truncated by the Mirbat Formation, which pinches out before reaching the Leger granite (Wuersten and others, 1991). Nine single grains of zircon were analyzed (five air-abraded and four CA-TIMS) from a sample of the Leger granite (Salalah 13) and yield a weighted mean $^{207}\text{Pb}/^{206}\text{Pb}$ date of $730.2 \pm 1.0[2.0]$ Ma ($n = 7$, MSWD = 1.2), with the four most concordant analyses (all CA-TIMS) yielding a weighted mean $^{206}\text{Pb}/^{238}\text{U}$ age of $726.1 \pm 0.4(0.5)[1.3]$ Ma (MSWD = 0.79) (Appendix table 1 and table 1). We interpret these data as the crystallization age of the granite. Since the Mirbat Formation glacial deposits have no observable contact with this granite, it is not clear whether it is a stratigraphic or intrusive relationship. Therefore, this age cannot be used to constrain the age of the Ayn glacials.

These samples give us a glimpse into the age of the low-grade arc basement to the Huqf Supergroup in this region which is based on the age of the granodiorite, volcanic and inherited zircons in the rhyolites, and the detrital zircons in the volcanoclastic sedimentary rocks. As is discussed below, clasts of felsic porphyries from diamictites near Mirbat, as well as detrital zircons from clastic rocks throughout the sections yield abundant zircons in this age range, again suggesting widespread distribution of these felsic volcanic rocks.

Abu Mahara Group and Correlatives

The glaciogenic Abu Mahara Group is known principally from the Oman Mountains in north Oman (fig. 1). It also has been intercepted in several subsurface wells in central Oman. In south Oman the Abu Mahara Group is thought to correlate with the Mirbat Formation.

Mirbat Formation.—Glacial diamictites are found in south Oman in the Mirbat region east of Salalah (fig. 1), where they form part of a <1 km-thick succession overlying a complex igneous and metamorphic basement (Lees, 1928; Kellerhals and Matter, 2003). The glacially influenced Mirbat Formation has been correlated with the Abu Mahara Group in the Huqf and Jabal Akhdar regions (Loosveld and others, 1996). The Mirbat Formation consists of three members known as Ayn (Lower, ~400 m thick), Arkahawl (Middle, ~300 m thick) and Marsham (Upper, <300m thick). Glaciogenic lithologies are found principally in the Lower (Ayn) Member (Kellerhals and Matter, 2003), where they dominate the stratigraphy. Clasts in the Ayn diamictite are composed of felsic porphyry, granite, and rhyolite, but dominated by rhyolites with centimeter-sized feldspar phenocrysts, similar to the Halfyn volcanic rocks in the Huqf area. The glaciogenic Ayn Member is locally overlain by a very thin (<30 cm), clastic-textured, silty limestone, or by a <1 m-thick, stromatolitic limestone characterized by light carbon isotopic composition (-4%), interpreted to represent a poorly

developed 'cap' carbonate (Kellerhals and Matter, 2003). In other locations, the carbonate is entirely missing.

In an attempt to constrain the maximum age of the basal Ayn Member, sample P70 was collected about 2 meters above the unconformity, where the Ayn Member consists of coarse, cross-bedded sandstone with intercalated finer-grained silty lenses. Sample P72 represents some of this finer-grained silty material. Two zircon grains from sample P70 are nearly concordant with $^{207}\text{Pb}/^{206}\text{Pb}$ dates of 747 ± 2 Ma and 749 ± 2 Ma; the rest of the zircons range from 777 Ma to 832 Ma again consistent with derivation from the basement rocks. Sample P72 has two grains at 828 and 844 Ma. The detrital zircon suite from P70 and P72 are consistent with local derivation, however the two youngest grains indicate that sediment accumulation did not begin until after about 747 Ma and provide a maximum for the age of the overlying glacial deposits.

Rieu and others (2006) refer to unpublished U-Pb data from detrital zircons near the base of the lower member of the Ayn Formation as indicating a maximum depositional age of 722 ± 12 Ma, although no analytical details are presented. Figure 2 of Rieu and others (2006) indicate that the detrital zircon dates are from within the lowermost diamictites. This is at least circumstantial evidence that the diamictites of the lower Ayn Formation are best correlated with the Ghubrah. Two rhyolite clasts were sampled from the diamictites of the upper part of the Ayn Member near Mirbat (sample OM-01-05 and Salalah 11). The diamictite is dominated by unfoliated clasts of rhyolite porphyry from a stratigraphic level about 20 meters below the possible cap carbonate. Three zircons were analyzed; the systematics are complex but similar to the samples from the Huqf Area where granites and rhyolites from the basement yield similar results. Two of the analyzed zircons (z1 and z2) from sample OM-01-05 overlap within uncertainties and indicate a $^{207}\text{Pb}/^{206}\text{Pb}$ date of 810 ± 2 Ma. Salalah 11 is a sample of a non-deformed, rhyolite porphyry clast (5 cm in diameter) that was collected from the lower part of the diamictite. We have dated 3 zircons from this sample and although they have some scatter as a result of inheritance, they indicate a $^{207}\text{Pb}/^{206}\text{Pb}$ date of about 800 Ma, essentially the same as OM-01-05. In addition, the dates and discordance patterns are similar to those obtained from granites and rhyolites from the Huqf (Al Jobah) area. It should be noted that these dated clasts are identical to ones used in Rb-Sr studies that were interpreted to indicate a much younger age (approximately 560 Ma) for this sequence of rocks (A. Matter, personal communication).

Ghubrah Formation.—The Abu Mahara Group is exposed in the Jabal Akhdar region (fig. 1) and comprises three distinct lithostratigraphic units: the glaciogenic Ghubrah Formation, which is unconformably overlain by the volcanogenic Saqlah Formation, which itself is overlain by the glaciogenic Fiq Formation (Rabu, 1993; Le Guerroue and others, 2005) (fig. 2). The presence of an angular unconformity between the Ghubrah Formation and overlying Saqlah Formation suggests a hiatus between the earlier glaciation (Ghubrah Formation) and subsequent volcanism (Saqlah Formation) and glaciation (Fiq Formation).

Outcrops of the Ghubrah Formation are limited to the Jabal Akhdar region in the Oman Mountains (Leather and others, 2002). A tuffaceous sandstone from the Ghubrah Formation, approximately 200 m below the Saqlah Member in Wadi Mistal, yielded a U-Pb zircon upper intercept age of $723 +16/-10$ Ma (Brasier and others, 2000). Resampling (sample WM 54) and analysis of zircons from the same bed was undertaken in order to increase the precision of the published date and to evaluate the nature of the zircon population. The rock yielded a zircon population of uniform color and size with well-developed crystal forms indicating little or no evidence for mixing and reworking (Brasier and others, 2000). Nevertheless, even though this unit is a distinctive, uniform layer within the diamictite, we stress that it is a clastic rock and could contain a still younger population of zircons. A total of twenty-four single grain

zircons were analyzed following the analytical procedures outlined above. A subset of twenty-one zircons from this sample define a discordia with an upper intercept of $714.2 \pm 0.6[5.0]$ Ma and a lower intercept of 46 ± 15 Ma (MSWD = 1.04) (fig. 3). A subset of five analyses defines a cluster of equivalent points at the upper end of the discordia array. These five analyses yield a weighted mean $^{206}\text{Pb}/^{238}\text{U}$ date of $711.52 \pm 0.20(0.31)[1.09]$ Ma (MSWD = 0.18). The $^{206}\text{Pb}/^{238}\text{U}$ date is about 0.4 percent younger than the $^{207}\text{Pb}/^{206}\text{Pb}$ date, consistent with the results from Schoene and others (2006) for the difference in the two U decay schemes (that is, the discordance is not an artefact of Pb loss), indicating that chemical abrasion has effectively eliminated Pb loss. The remaining three analyses are variably discordant with older $^{207}\text{Pb}/^{206}\text{Pb}$ ages indicating a small xenocrystic component. Although the upper intercept age of 714.2 ± 0.6 Ma is younger than the previously attained upper intercept date of $723 +16/-10$ Ma, there is an overlap when the uncertainties are considered. We suggest that the most concordant zircon analysis reported in Brasier and others (2000) most likely reflects a minor xenocrystic component combined with Pb loss and thus biased the upper intercept date. Our data set of twenty four single-crystal analyses indicates a minor component (about 15%) of older crystals. However, given the uniform nature of both the age (discounting the effect of post-depositional Pb loss) and morphology of the crystals we believe this to represent a population of volcanic zircons and that the U-Pb dates are the best estimate for the depositional age of the tuffaceous graywacke.

This interpretation can be evaluated by dating zircons obtained from adjacent strata composed of obviously detrital facies. A sample of a sandstone clast in the diamictite (WM.01.02) immediately above the tuffaceous graywacke and a sample of diamictite matrix (WM.01.03) were collected to examine the detrital population and to see if they were significantly different from the tuffaceous graywacke. Five zircon grains were analyzed for the sandstone clast and range in age from 815 to 828 Ma consistent with derivation from the basement and distinctly different from the 713 Ma grains from the volcanoclastic rock (WM 54). The sandstone matrix yielded a population ($n = 4$) with $^{207}\text{Pb}/^{206}\text{Pb}$ dates at 756 Ma. Interestingly, these grains are younger than exposed and dated basement rocks, and therefore could be derived from rift-related magmatic rocks.

In summary, although there are limited exposures of “basement” in Oman, they provide important constraints on the maximum age of the overlying Huqf Supergroup and point to a major gap in the record perhaps related to unroofing and erosion some time between approximately 800 and 713 Ma. Detrital zircon suites show prominent peaks at about 800 Ma consistent with derivation from the volcano-plutonic complex exposed in northern Oman. The age of the Ayn glacial deposit must be younger than approximately 750 Ma and perhaps younger than 722 ± 11 Ma (Rieu and others, 2006), and the Ghubrah Formation is constrained at about 713 Ma although the duration of diamictite accumulation remains unconstrained. As the relationship between the Leger Granite and the Ayn Member cannot be directly observed its age cannot be used as a constraint on the timing of glacial sediment accumulation. Importantly, these results (ages of diamictite clasts and Leger granite) indicate the roughly 550 Ma Rb-Sr “isochron” constructed from a mixture of samples from the Leger granite diamictite clasts represents a mixing line with no geochronological significance.

Saqlah, Fiq and Hadash Formations.—The Saqlah Formation comprises mafic volcanics and volcanoclastic sandstones with local accumulations of pillow basalts (Le Guerroue and others, 2005). The overlying Fiq Formation consists of a heterolithic suite of glaciomarine sediments (Leather and others, 2002; Allen and others, 2004) that are in turn overlain by the transgressive cap carbonate Hadash Formation. Negative $\delta^{13}\text{C}$ values (~ -6 to -2%) from the Hadash Formation (Leather and others, 2002), combined with the occurrence of pseudo-tepee structures, are characteristic of

other Marinoan-type cap carbonates (Kennedy and others, 1998; Hoffman and Schrag, 2002; Allen and Hoffman, 2005; Halverson and others, 2005).

Detrital zircons were analyzed in an attempt to better constrain the age of the Saqlah (SQ01) and Fiq Formations (FIQ2). Sample SQ01, was collected at Wadi Mistal (Oman Mountains, fig. 1), from approximately 20 meters above the base of the Saqlah directly below a basalt interval. Sample FIQ2 was a siliciclastic lithology collected from the overlying Fiq Formation. Seven zircons were analyzed from SQ01, three grains yield $^{207}\text{Pb}/^{206}\text{Pb}$ dates of about 750 Ma, the remaining four grains at approximately 800 to 830 Ma (Appendix table 1, fig. 5). Twelve single grains were analyzed from sample FIQ2 and the $^{207}\text{Pb}/^{206}\text{Pb}$ dates obtained were: one grain at about 920 Ma, ten

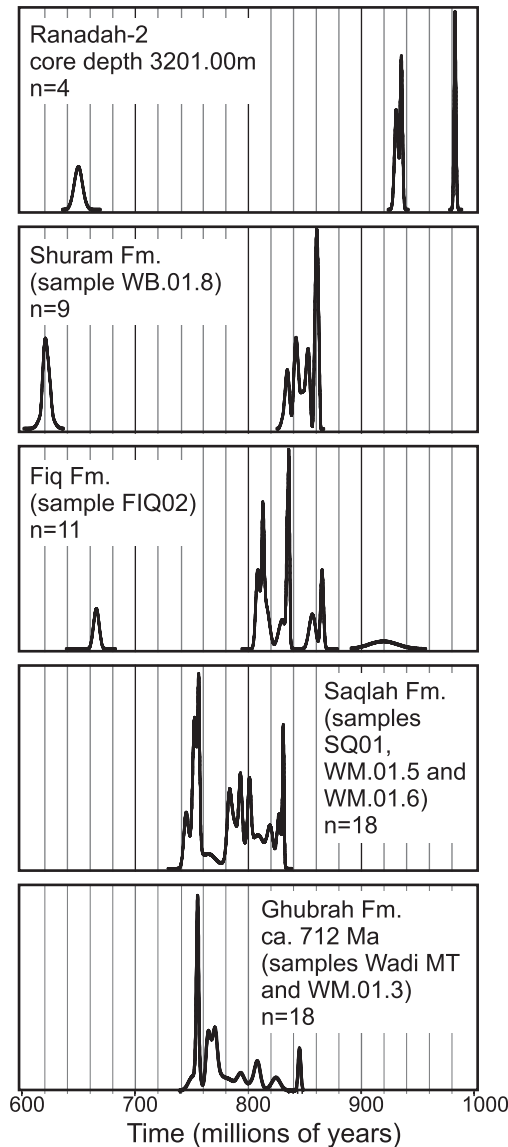


Fig. 5. Probability distribution function (PDF) plots of detrital zircon analyses.

grains were in the range 810 to 860 Ma and one grain yielded an approximately 664 Ma age (Appendix table 1, fig. 5).

Two samples of possible volcanic ash (WM.01.05 and WM.01.06) were collected from the Saqlah Formation and zircons analyzed. Three grains were analyzed from sample WM.01.05 (approximately 782 Ma, 786 Ma, and 826 Ma) whereas six grains were analyzed from sample WM.01.06 (approximately 750 Ma, 752 Ma, 756 Ma, 792 Ma, 800 Ma and 818 Ma). These zircons have ages similar to that of the underlying diamictite indicating that they most likely reflect reworking and inheritance of material during deposition.

Glacial deposits of the Lahan-1 well.—The Lahan-1 well was drilled in 2003 along the southwest margin of the SOSB (fig. 1) to a depth of 6032 m (fig. 6). At 3910 m depth

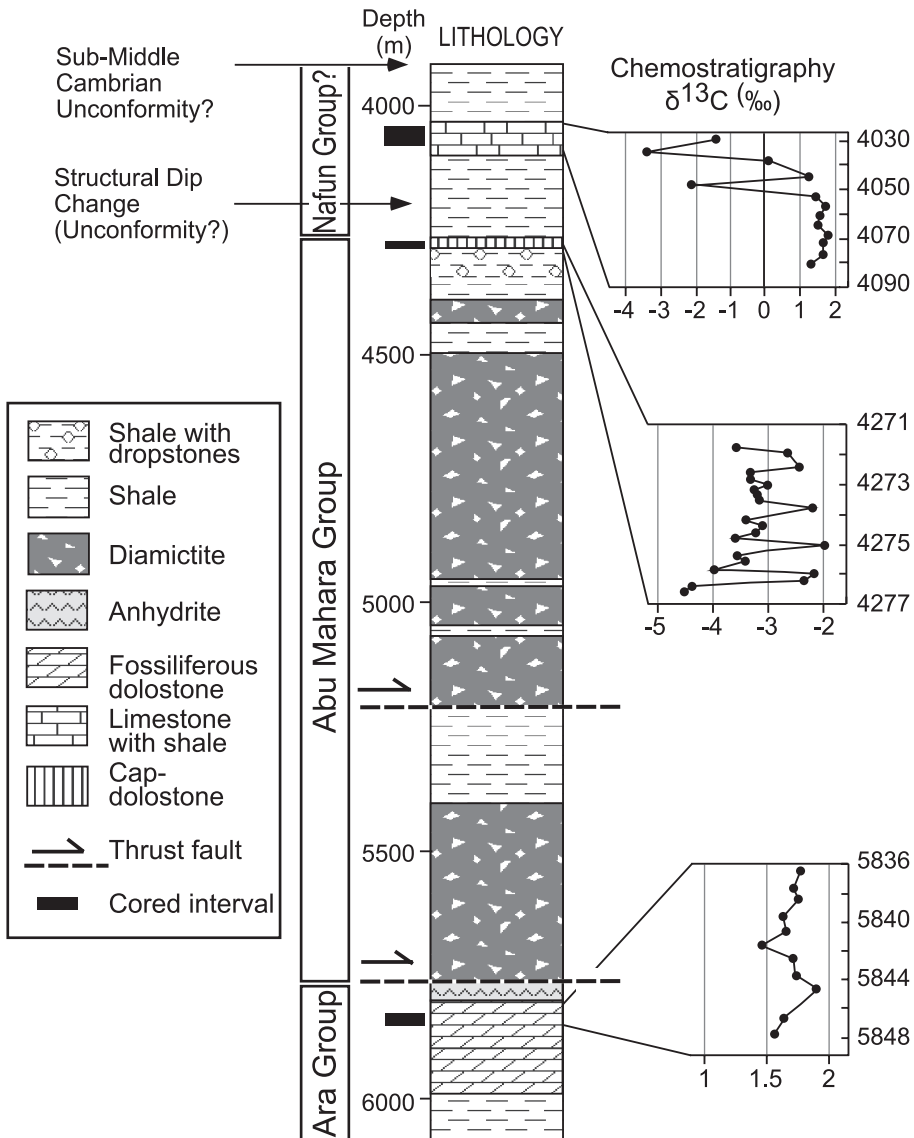


Fig. 6. Lithostratigraphy and carbon isotopic variability of cored intervals along the Lahan-1 well. Depths are meters along hole below derrick floor.

(along hole below derrick floor) the well intercepted a seismically defined regionally extensive angular unconformity at the base of the Haima Supergroup, composed of Middle Cambrian to Silurian siliciclastic facies (Fortey, 1994; Millson and others, 1996). Strata intercepted beneath the unconformity belong to the late Neoproterozoic Nafun and Abu Mahara groups, comprising a large anticline detached at a depth of 5760 m above flat-lying evaporites and fossiliferous carbonates of the Ara Group. Thrust faulting is constrained to be Early Cambrian in age, most likely associated with convergence along the western margin of the basin (Immerz and others, 2000; Grotzinger and others, 2002). Abu Mahara strata may be imbricated as suggested by the fault at 5204 m depth, revealed through the analysis of borehole dip meter data. However, above this level, dip meter data provide no evidence for structural repetition.

During drilling of the well, one 10 cm diameter core and two 7.5 cm diameter cores were obtained ranging in length from 6 to 27 m. The deepest core (5830 to 5848 m; fig. 6) intercepted fractured and dolomitized platform carbonates of the Ara Group containing both *Cloudina* and *Namacalathus*. These fossils are known only from strata of approximately 548 to 542 Ma in age (Grant, 1990; Grotzinger, 2000; Amthor and others, 2003). These strata, in addition to overlying anhydrites, are interpreted as the autochthonous footwall. Above the detachment, shales alternate with thick intervals of diamictite as shown by high-resolution borehole image data. A second core was obtained near the base of the thickest of these diamictites at a depth of 5123 to 5129 m (fig. 6). This core reveals a continuous interval of massive, matrix-supported diamictite (fig. 7A). The broad range of grain size, poor sorting, matrix-supported texture, and common occurrence of fractured or angular clasts is consistent with a glaciogenic origin.

The shallowest core is the longest (4271 – 4298 m; fig. 6) and straddles the facies boundary at 4276.2 m between dropstone-bearing, fine-grained dominantly siliciclastic facies and abruptly overlying cap dolostone facies. The siliciclastic facies (22 m preserved in core) include shales, laminated siltstones, pebbly shales and siltstones, lonestone-bearing laminated siltstones (fig. 7B), rare m-thick laminated dolostone beds, and several thin green colored volcanic ash and siltstone layers (fig. 7C). The carbonate facies (5 m preserved in core) include basal fine dolostones with scattered barite laths and pervasive framboidal pyrite, which pass upward into crudely laminated fine dolostones. The lower few meters of the carbonate unit exhibit an early diagenetic overprint of spar-filled sheet cracks; this overprint diminishes upward so that overlying carbonates are unbrecciated. The carbonates were sampled every 20 cm for their carbon isotopic content, which reveals a set of moderately negative values of –2 to –4.5 permil. The facies, diagenetic textures and isotopic content of these dolostones are all compatible with the unique attributes of other carbonates that cap Marinoan-type Neoproterozoic glacial successions globally (Kennedy, 1996; Hoffman and others, 1998; Hoffman and Schrag, 2002). These carbonates are correlated with the Hadash cap carbonate in the Jabal Akhdar area.

Thin (3 to 5 mm thick), fine-grained, green colored volcanic ash or siltstone layers (fig. 7C) occur at a depth of 4285 m to 4284.18 m, just 9 m below the cap dolostone, within the succession of shales and siltstones containing dropstones. U-Pb dating of zircons separated from one of these horizons yield a range of dates from approximately 718 Ma to 645 Ma, however there is significant scatter within this population (Appendix table 1). The earliest analyses (z1, z7 and z4) have relatively low radiogenic/common Pb ratios in part because of the very small size they were not abraded prior to analysis. Subsequent analyses utilizing the CA-TIMS approach are more precise, nonetheless all of the analyses indicate groupings at 715 to 718 Ma, one at 675 Ma and another at about 645 Ma. Although these thin horizons were sampled as potential volcanic ash beds, the scatter in the dataset and small number of ‘young’

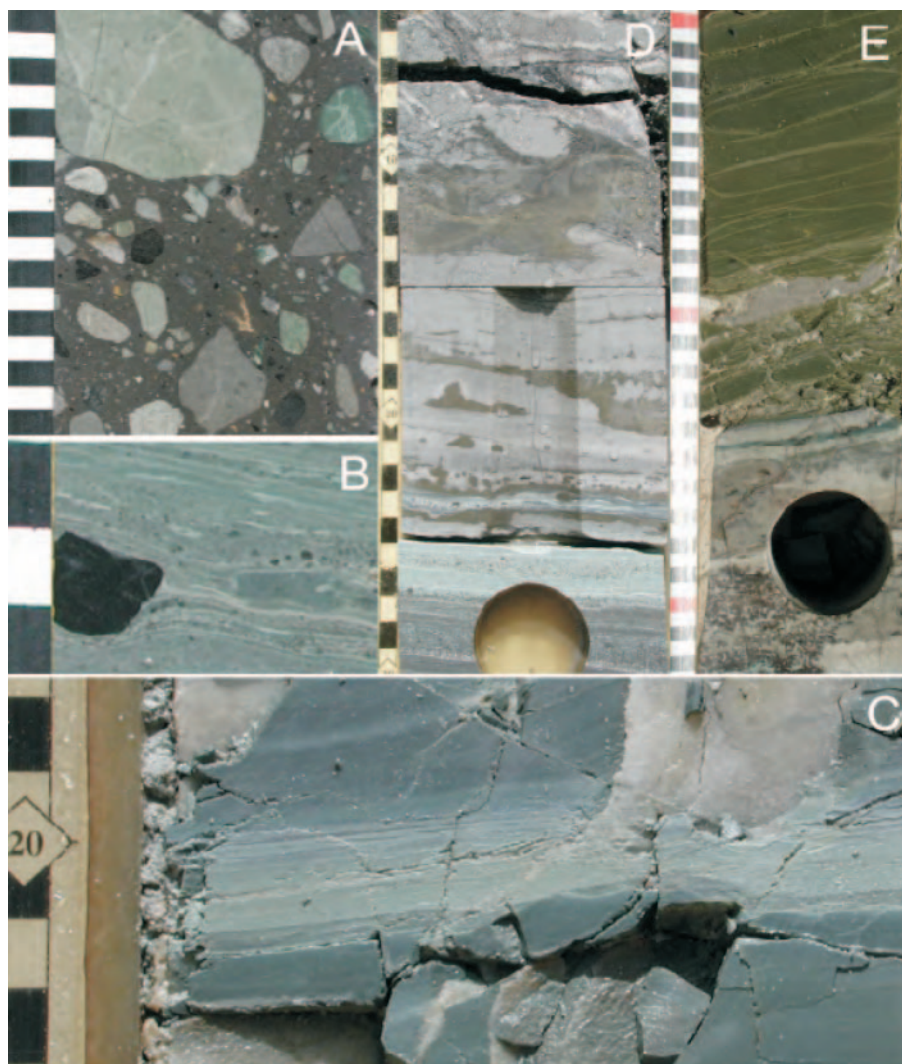


Fig. 7. Sedimentary facies and ash interlayers of the Huqf Supergroup in subsurface. All scales are in centimeters. (A) Diamictite in the Lahan-1 well, Core 2, at a depth of 5124.7 m. (B) Lonestone in the Lahan-1 well, Core 1, at a depth of 4276.52 m. (C) Possible ash bed in Lahan-1 well, Core 1, at a depth of 4284.21 m. (D) Cap carbonate in the Lahan-1 well, Core 1 at a depth of 4276.0 – 4276.3 m. Note abrupt transition from sandy siltstone to dolostone, about 7 cm from the bottom of photograph. Uppermost part of photograph shows sheet cracks, filled with coarse, white, dolospar cement. Intervening core is marked by nodules and discontinuous laminae of framboidal pyrite. (E) Ash bed in Asala-1 well, at a depth of 3851.0 m. Note apple-green color, which contrasts with underlying light gray dolostones and blue-green shales. Depths are meters along hole below derrick floor.

grains ($n = 5$) means that assigning a depositional age to this interval is not straightforward: if they are primary volcanic zircons the approximately 645 Ma population represents the depositional age. Alternatively, even the youngest zircons could be detrital or xenocrystic, providing a maximum age constraint of about 645 Ma. At present we consider the 645 Ma age as a maximum age for the Lahan-1 glacial unit at this stratigraphic level.

When the geochronological data from Lahan-1 is combined with the youngest age of detrital zircons in the Fiq Formation in the Jabal Akhdar region (664 Ma), it strongly

suggests that the Fiq glacial deposits were widespread across Oman, and that the age of glacial deposition is 645 Ma or younger and consistent with a Marinoan assignment. In the subsurface, several other wells (Ghadir Manquail-1, Miqrat-1, Thamoud-6) intercept diamictites, overlain by thin capping carbonates, which in turn are overlain by characteristic Nafun Group units (see below). These new results suggest that these glacial deposits are also of Fiq age, and that numerous extensional basins were filled with glaciogenic strata.

Nafun Group

No volcanic lithologies suitable for dating have been observed in the Nafun Group rocks despite extensive examination of outcrops and material from the sub-surface. In order to better constrain the age of the Shuram Formation, detrital zircons were analyzed (sample WB.01.8) with the objective of identifying the youngest grains, which would constrain the maximum age of the horizon sampled. Nine single grains were analyzed from siltstones collected from a shale-rich horizon about 5 meters above the base of the Shuram Formation in the Jabal Akhdar. One grain yielded a date of approximately 2 Ga, six grains ranged between 830 and 860 Ma and two grains yielded dates of about 620 Ma (fig. 5). The two youngest grains provide a maximum age constraint for the Shuram Formation at the horizon sampled. In addition, four zircons were analyzed from a sample of the Buah Formation (sample WB.01.6), two of which yielded ages of about 780 Ma, the other two about 1.6 Ga.

Ara Group

The Ara Group represents at least six (A1-A6) 3rd-order cycles of carbonate/evaporite sedimentation in a tectonically active basin (Mattes and Conway Morris, 1990) in addition to a basal, pre-evaporitic carbonate (A0). The Precambrian-Cambrian boundary is interpreted to occur within the A4 cycle, at the base of the A4 carbonate unit. Carbonates occupy positions within the basin center (in addition to flanks) and vary in thickness from 50 to 200 m. They formed during relative highstands in sea level characterized by mostly unrestricted conditions, exemplified by biohermal facies containing *Cloudina* and *Namacalathus* body fossils. Carbonate platforms were formed during transgressive to highstand accommodation conditions, superimposed upon a progressive, long-term accommodation increase that forced platforms within each cycle to occupy progressively less area (Grotzinger and Amthor, 2002; Schroeder and others, 2005). Platform facies include microbial boundstones, intraclast-peloid-oid grainstone-packstone, and mudstone. These pass laterally into thrombolite sheet and mound facies, which pass downslope into turbiditic mudstones that interfinger with deep-water microbial laminites in the most distal settings (Schroeder and others, 2005). Deposition of overlying thick and laterally extensive basin-center evaporites occurred during drawdown and low stands in sea level. Ara evaporites include 10 to 20 m thick anhydrites, and 100's of meters thick halite and potash salts (Mattes and Conway Morris, 1990). Toward the eastern flank of the Ara salt basin, the basin-center evaporites pinch out. The Ara evaporites do not occur as basin-filling wedges onlapping basin margin carbonates, but blanket the isolated carbonate platforms. This requires that evaporite deposition occurred during strong tectonic subsidence, creating enough accommodation space so that low stand evaporites could overlap earlier high stand carbonates (Grotzinger and Amthor, 2002).

In an attempt to further refine and expand upon the ages of the Ara Group volcanic ash beds (upper A3C and lower A4C) published in Amthor and others (2003) we applied the CA-TIMS technique to additional zircons recovered from samples MKZ-11B (upper A3C) and BB-5 (lower A4C). In addition, we collected ash beds from two stratigraphic levels lower in the Ara Group; Minha-1A in the lower part of the A3 carbonate, and Asala-1c21 in the middle of the lowermost A0 unit (fig. 8).

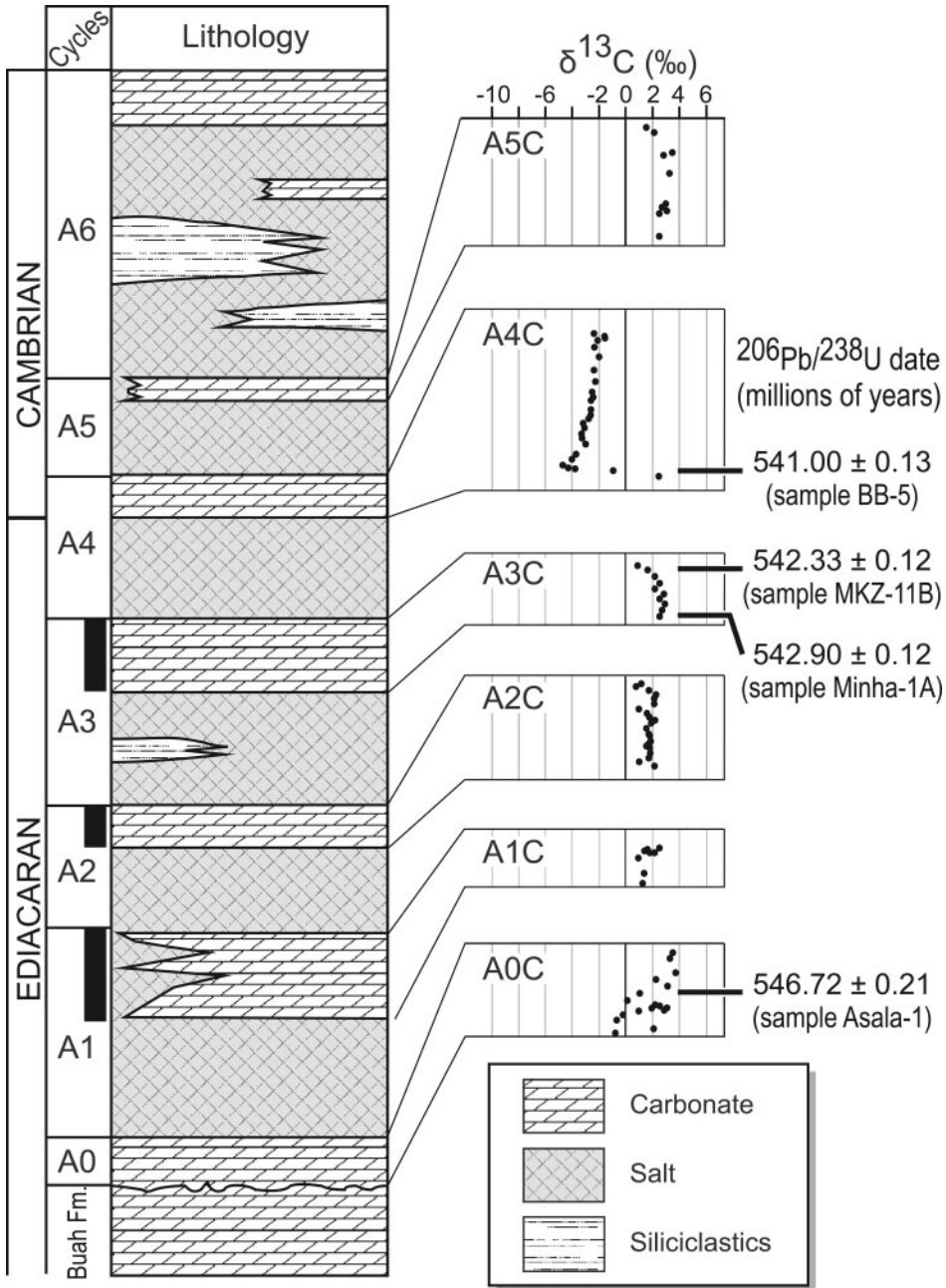


Fig. 8. Stratigraphy of the Ara Group carbonate-evaporite cycles showing carbon isotope data, stratigraphic distribution of *Cloudina* and *Namacalathus* fossils (black bars on left column) and weighted mean $^{206}\text{Pb}/^{238}\text{U}$ dates of ash beds (see text for details). Carbon isotope data are from Amthor and others (2003) and represent a composite of data from three wells: A0C to A3C, Sabsab-1; A4C, Birba-5; A5C, Birba North-1. The sharp negative $\delta^{13}\text{C}$ anomaly (base of A4C) is interpreted as being correlative with the Ediacaran-Cambrian boundary.

Twelve single zircons were analyzed from sample Asala-1c21 the lowermost unit of the Ara Group. The sample was collected from the middle of the A0 unit, which is approximately 60 to 70 meters thick and consists of shaly and tuffaceous carbonates, and unconformably overlies the Buah Formation. Eight new analyses employing the CA-TIMS technique resulted in a well defined cluster of equivalent analyses with a weighted mean $^{206}\text{Pb}/^{238}\text{U}$ date of $546.72 \pm 0.21(0.29)[0.89]$ Ma ($n = 8$, MSWD = 0.92) and a weighted mean $^{207}\text{Pb}/^{206}\text{Pb}$ date of $548.90 \pm 0.98[1.7]$ Ma ($n = 10$, MSWD = 0.63) (fig. 4 and table 1). This ash occurs within the A0 unit and therefore closely constrains the age of the basal Ara Group. The age of Asala-1c21 provides a constraint on the age of the $\sim +4\%$ $\delta^{13}\text{C}$ peak reached following the Shuram excursion (fig. 8), and occurs just above the zero crossing following the end of the +4 permil excursion (fig. 9). An ash bed with a similar chemostratigraphic context occurs within the Nama Group (sample 94-N-10B: Grotzinger and others, 1995); however it occurs within the falling limb of the +4 permil excursion and therefore we would expect it be slightly older than Asala-1c21. In order to test the correlation of the $\delta^{13}\text{C}$ isotopic excursion between Oman and Namibia, we analyzed additional zircons from 94-N-10B (Lower Hoogland Member, Nama Group) using the CA-TIMS method in order to improve upon the precision. Eight single zircon crystals define a cluster of equivalent analyses with a weighted mean $^{206}\text{Pb}/^{238}\text{U}$ date of $547.36 \pm 0.23(0.31)[0.91]$ Ma ($n = 8$, MSWD = 1.4). A slightly larger group of analyses yield a weighted mean $^{207}\text{Pb}/^{206}\text{Pb}$ date of $549.3 \pm 0.8[1.6]$ Ma ($n = 12$, MSWD = 2.2) (fig. 4). Grotzinger and others (1995) reported a weighted mean $^{207}\text{Pb}/^{206}\text{Pb}$ date of 548.8 ± 0.3 Ma (MSWD = 0.08) using a combination of discordant multi- and single-grain analyses from the same mineral separate. The consistency of the geochronological results for Asala-1c21 and 94-N-10B in terms of their predicted relative stratigraphic positions and chemostratigraphic context indicates that these Late Neoproterozoic $\delta^{13}\text{C}$ fluctuations reflect globally synchronous variations in seawater chemistry (fig. 9) and that the drop from +4 to 0 permil occurred in less than 1 million years.

Sample Minha-1A was collected 3 meters above the base of the A3 carbonate unit which itself is approximately 100 to 125 meters thick. Seventeen single zircons (all CA-TIMS analyses) were analyzed from this sample, three were distinctly xenocrystic, but the remaining fourteen yielded a $^{207}\text{Pb}/^{206}\text{Pb}$ weighted mean date of $544.4 \pm 0.5[1.2]$ Ma ($n = 14$, MSWD = 0.37), a subset of which are equivalent with a weighted mean $^{206}\text{Pb}/^{238}\text{U}$ date of $542.90 \pm 0.12(0.20)[0.80]$ Ma ($n = 8$, MSWD = 0.62).

Amthor and others (2003) presented geochronological constraints on two samples from the Ara Group, sample MKZ-11B which occurs 9 meters below the top of the A3 carbonate unit, and sample BB-5 from 1 meter above the base of the overlying A4 carbonate. Additional zircons from both of the samples were analyzed using the CA-TIMS methods to improve precision. Zircons from sample MKZ-11B with equivalent U/Pb dates have yielded a weighted mean $^{206}\text{Pb}/^{238}\text{U}$ date of $542.33 \pm 0.11(0.19)[0.79]$ Ma ($n = 8$, MSWD = 0.50) and weighted mean $^{207}\text{Pb}/^{206}\text{Pb}$ date of $544.10 \pm 0.4[1.2]$ Ma ($n = 12$, MSWD = 0.31). Zircons from sample BB-5 yield a weighted mean $^{206}\text{Pb}/^{238}\text{U}$ date of $541.00 \pm 0.13(0.21)[0.81]$ Ma ($n = 8$, MSWD = 1.0) and weighted mean $^{207}\text{Pb}/^{206}\text{Pb}$ date of $542.68 \pm 0.46[1.2]$ Ma ($n = 15$, MSWD = 0.58). Dates for these Ara Group samples are summarized in table 1, with most concordant analyses plotted in figure 4. The Ediacaran/Cambrian boundary in Oman is interpreted to closely coincide with the BB-5 ash bed (Amthor and others, 2003); these new results suggest the boundary, therefore, may be closer to 541 Ma (in $^{206}\text{Pb}/^{238}\text{U}$ years) than the 542 Ma estimate reported by Amthor and others (2003).

Fara Formation

The Fara Formation consists of three lithologies (McCarron, ms, 2000): a lower unit (~ 140 m thick) composed of black, finely-laminated siliceous shale and chert with some interbedded carbonate breccias; a middle unit composed of volcanoclastic

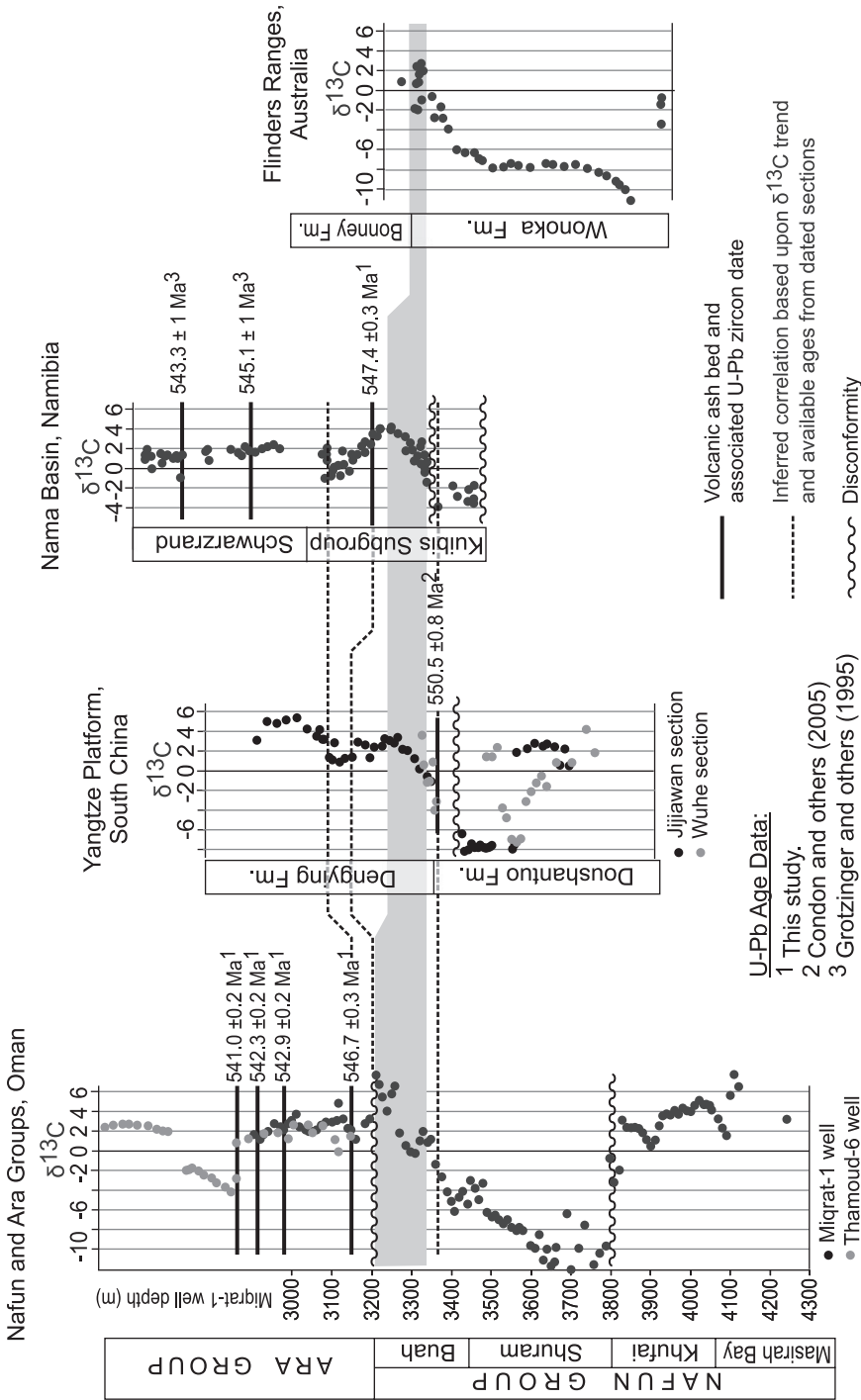


Fig. 9. Correlation of Neoproterozoic carbon isotope data from Nafun and Ara Groups (Oman: Burns and Matter, 1993; Amthor and others, 2003), Nama Group (Namibia: Grotzinger and others, 1995), Doushantuo/Dengying Formations (China: Condon and others, 2005) and Wonoka Formation (Australia: Calver, 2000) combined with $^{206}Pb/^{238}U$ zircon dates from ash beds.

tuffaceous litharenites; and an upper unit of interbedded volcanoclastic sediments and volcanic ignimbrites featuring welded tuffs with black fiamme. Our own observations of this unit include evidence for slumping, as represented by syn-sedimentary small-scale folds, and other downslope transport is indicated by graded, coarse sedimentary breccias. However, the presence of intercalated feldspathic-lithic hummocky cross-stratified sandstones indicates reworking and deposition above storm wave base.

Prior to the current study, Brasier and others (2000) obtained a U-Pb (zircon, ID-TIMS) upper intercept age of 544.5 ± 3.3 Ma on an ignimbrite sample from 200 meters above the base of the Formation. In order to further improve the precision of this age and correlation with the Ara Group (see above) two samples were collected: WB.01.1 from the top of the Fara Formation, and WB.01.2, a recollection of the ignimbrite sample(s) analyzed by Brasier and others (2000) that occurs 200 meters above the base of the Formation. Zircons from both samples display varying degrees of Pb loss, which was minimized with the application of CA-TIMS. Ten zircons from WB.01.1 were analyzed, one of which was older and discordant. However, the remaining points yield a weighted mean $^{207}\text{Pb}/^{206}\text{Pb}$ of $545.94 \pm 0.68[1.4]$ Ma ($n = 7$, MSWD = 0.83) with four concordant (see above) analyses yielding a weighted mean $^{206}\text{Pb}/^{238}\text{U}$ date of $542.54 \pm 0.45(0.53)[1.1]$ Ma ($n = 4$, MSWD = 2.6) (fig. 4). Seventeen zircon analyses from WB.01.2, six of which were distinctly older (approximately 800 – 900 Ma), yield a weighted mean $^{207}\text{Pb}/^{206}\text{Pb}$ date of $548.3 \pm 0.8[1.6]$ Ma ($n = 9$, MSWD = 0.44), with eight concordant analyses yielding a weighted mean $^{206}\text{Pb}/^{238}\text{U}$ date of $547.23 \pm 0.28(0.36)[0.96]$ Ma ($n = 8$, MSWD = 1.3) (fig. 4 and table 1).

Previously, the Fara Formation had been considered to be equivalent to the Athel Silicilyte in the SOSB, which is in turn regarded as a possible equivalent to the A4 carbonate/evaporite cycle. However, the results obtained here indicate that the Fara Formation is chronologically equivalent to much of the Ara. Indeed, the age of the lower ignimbrites (WB.01.2) of the Fara Formation predates by approximately 0.5 m.y. the age of the A0 carbonates (see Asala-1c21 above), which are known to contain abundant felsic tuffs. The Fara age of about 548 Ma could coincide exactly with the transition between the Nafun and Ara groups, which is marked by a regional unconformity and onset of volcanism and fault-related subsidence.

Detrital Zircons, Western Deformation Front and Southern Oman

Detrital zircons from four siliciclastic samples of uncertain lithostratigraphic affinity were analyzed in order to determine maximum depositional age and provide information of the age of the source terrains supplying the clastic sediment. In general, these samples consist of detritus that may have been derived from erosion of the uplifting Western Deformation Front (see fig. 1 for location), which forms the western margin of the Ara salt basins.

Sample OM-01-4 was collected from deformed and mildly metamorphosed sandstone turbidites exposed at the base of the escarpment at Ain Sarit (fig. 1). Five single grains were analyzed yielding ages of approximately 1.43 Ga, 2.43 Ga, 2.45 Ga, 2.47 Ga and 3.0 Ga. Sample Tharwah-1 consists of shale sampled from a depth of 3390.0 meters depth (Tharwah-1 well; fig. 1) at the A0 stratigraphic level. Three single zircon grains were analyzed each giving ages of about 2.58 Ga. Sample Ranadah-2 consists of fine, fluvial sandstones in the upper Ara Group, and was collected from a depth of 3201.00 meters (Ranadah-2 well; fig. 1). Four single zircons were analyzed yielding ages of approximately 650 Ma (one grain), 940 Ma (two grains) and 980 Ma (one grain). In the context of the constraints outlined above, the youngest zircon at about 650 Ma constrains this sample to being equivalent to Saqlah Formation or younger. Sample Ghudun-1 was recovered from TD cuttings at the base of the Ghudun-1 well (depth of 2509.8 to 2659.4 meters). Fourteen single zircon grains were analyzed from this sample and record a wide range of ages: approximately 620 Ma (two grains), 640 Ma (one grain), 720 Ma (one grain), 760 Ma (one grain), 970 Ma (two grains), 1.02-1.06 Ma

(two grains), 1.75 Ga (two grains), 2.09 Ga (one grain), 2.39 Ga (one grain) and 2.52 Ga (one grain). Again, in the context of the constraints outlined above, the approximately 620 Ma grain confines this interval to be either Nafun equivalent or younger. These results are summarized in figure 5.

DISCUSSION

The data presented in this study provide the basis for the first comprehensive chronostratigraphic framework for the Neoproterozoic of Oman. This framework is required for understanding the relationships between tectonic, climatic and paleobiologic events recorded in these rocks and their relationship to other similar global data sets for this interval.

Basement Terrains

The age of the crystalline basement exposed in Oman is important in understanding the tectonic history and source region for detrital zircons in younger stratigraphy. Although basement exposures in Oman are restricted to the Huqf and Mirbat areas, their geological history is broadly consistent with that inferred from western Saudi Arabia. The geochronology and isotope systematics of Yemen, Saudi Arabia, and Somalia have been discussed by several authors (Windley and others, 1996; Whitehouse and others, 2001; Mercolli and others, 2006). The older crystalline basement in Yemen is characterized by seven major domains separated by N-NE trending boundaries (Whitehouse and others, 2001). In general there are fragments of Archean crust within a collage of early to mid-Neoproterozoic arc terranes of the Arabian-Nubian shield. From a combination of U-Pb zircon and Pb and Nd isotope systematics, there is evidence for Archean crust in Yemen that ranges in age from about 2.6 to >3.0 Ga.

The history of arc and microcontinent accretion in Saudi Arabia spans from approximately 820 Ma to 750 Ma followed by collisional assembly of a collage of continental fragments including parts of Sri Lanka, Seychelles, and India to form the East African orogen from approximately 750 to 640 Ma (Meert and Van Der Voo, 1997; Meert, 2003). Subsequently, the region was affected by post-assembly extension along an approximately N-S axis (Meert, 2003). The Huqf Supergroup of Oman spans the time of early assembly and regional extension (approximately 750–630 Ma). Although the record is sparse in Oman, it would appear that following the amalgamation at about 800 Ma (recorded by igneous activity reflecting an active magmatic arc: Mercolli and others, 2006), there is little preserved record until <750 to about 713 Ma (Gubrah Formation) and most is younger (Saqlah-Fiq Formations, Nafun and Ara Groups).

Constraints on Neoproterozoic Glaciations

The Huqf Supergroup contains evidence for two distinct Neoproterozoic glaciations. Based upon the data of Brasier and others (2000) the Ghubrah Formation has previously been considered to reflect a 'Sturtian' age glaciation. Other examples of Sturtian-type glaciations occur in Australia (Sturt Formation), Congo Craton (Chuos Formation), Western Laurentia (Rapitan Formation) and are commonly associated with ironstones and $\delta^{13}\text{C}$ -depleted cap-carbonates (see Evans, 2000, for an exhaustive review). In Namibia the Chuos Formation (Congo Craton) overlies Naauwpoort volcanics that have yielded a U-Pb (zircon, ID-TIMS) age of 746 ± 2 Ma (Hoffman and others, 1996). Clasts from the Rapitan Formation of Canadian Cordillera and Pocatello Formation of southeastern Idaho (Western Laurentia) have yielded U-Pb zircon ages of 755 ± 18 Ma (ID-TIMS, Ross and Villeneuve, 1997) and 717 ± 9 Ma (ion-microprobe, Fanning and Link, 2004), respectively, both providing maximum age constraints for Sturtian-type glacial deposits. Minimum age constraints on Sturtian-type deposits come from units in China where the Tiesiao Formation, interpreted as a glaciogenic diamictite, is overlain by a volcanic tuff bed dated by the U-Pb (ID-TIMS) method at 663 ± 4 Ma (Zhou and others, 2004) and in Australia where black shales

overlying glacial deposits yield Re-Os dates of 643 and 657 Ma (Kendall and others, 2006). Our approximately 713 Ma age from the Ghubrah Formation represents the first direct high precision constraint for a 'Sturtian' age Neoproterozoic glacial deposit. However it should be noted that it remains unclear whether deposition of the Ghubrah Formation was associated with ironstones or dark, organic-rich cap-carbonate that are considered hallmarks of Sturtian-type deposits (Kennedy and others, 1998). Furthermore, given the current data set, it remains unclear whether the Sturtian-type glacials represent a single, globally synchronous glacial epoch. Kendall and others (2006) suggest that the Sturtian ice age was diachronous and/or there were multiple glaciations from about 650 to >700 Ma.

The ages of Marinoan-type glacial deposits, as characterized by their overlying light-colored dolostone cap carbonates with distinctive physical attributes (Hoffman and Schrag, 2002), have been constrained in China, Namibia and Canada. In China an age of 663 ± 4 Ma (U-Pb ID-TIMS zircon) has been obtained on an ash that occurs well below the Nantuo tillite (Zhou and others, 2004) and an age of 635 ± 1 Ma (U-Pb ID-TIMS zircon) has been obtained on an ash *within* the cap carbonate (Lower Dolomite Member) of the Doushantuo Formation (Condon and others, 2005). In central Namibia the Ghuab Formation, considered an archetypal example of a Marinoan-type deposit (Halverson and others, 2005), has yielded an age of 635 ± 1 Ma (U-Pb ID-TIMS zircon) from within its dropstone-bearing lithology (Hoffmann and others, 2004). In western Canada the Icebrook Formation has been constrained to be older than a 608 ± 5 Ma Re-Os isochron age (MSWD = 1.2) derived from overlying black shales (Kendall and others, 2004). In Australia where the type-Marinoan and base Ediacaran GSSP occur, the emerging picture is more complex (Schaefer and Burgess, 2003; Calver and others, 2004; Kendall and others, 2004, 2006). A third, younger, Neoproterozoic glaciation is preserved in successions from Avalonia, Laurentia, Baltica and possibly western Australia and China. These include the Sqaantum Tillite of southern New England (Thompson and Bowring, 2000), Gaskiers Formation of Newfoundland (Bowring and others, 2003), Lower Southern Highland Group of northern Ireland (Condon and Prave, 2000; McCay and others, 2006), Moelv Tillite of southeast Norway (Bingen and others, 2005), Egan Formation of western Australia (Grey and Corkeron, 1998), and Quruqtagh Group of eastern Tianshan (Xiao and others, 2004). Geochronological constraints from this "Gaskiers glaciation" are limited to the Gaskiers Formation itself, which yields an age for glaciation of about 582 Ma (Bowring and others, 2003; unpublished data).

Maximum age constraints of approximately 660 Ma and 645 Ma have been determined for the glaciomarine Fiq Formation and Lahan-1 dropstone-bearing siltstones, respectively. Both glacial units are overlain by tan-colored, dolomitic, cap carbonates that record negative $\delta^{13}\text{C}$ values characteristic of other Neoproterozoic post-glacial cap carbonates world-wide (Kennedy and others, 1998; Hoffman and Schrag, 2002). Within the context of our present understanding of the chronology of Neoproterozoic glaciations (for example, Bowring and others, 2003) there are two possible interpretations of the Fiq/Lahan-1 glacial(s): they represent a Marinoan age glaciation which terminated at about 635 Ma, or they reflect a younger Ediacaran Period glaciation and are broadly correlative to the approximately 582 Ma Gaskiers Formation. Given the nature of the cap carbonate and its similarities to other Marinoan-type cap carbonates most workers interpret the Fiq Formation as reflecting a Marinoan-type glaciation (Leather and others, 2002; Le Guerroue and others, 2005). In the context of the present geochronologic constraints, we feel this is the most straightforward interpretation. Thus, the simplest working hypothesis for the Abu Mahara Group is that the older, Ghubrah glacial deposits correspond, based upon direct age constraints, to the Sturtian event and that the younger, Fiq Formation glacial deposit represents the Marinoan event. Inference on the latter is based largely upon

maximum age constraints combined with the nature of the respective cap carbonate. However the exact age of onset, and therefore duration, of the event remains unconstrained.

Calibrating Terminal Ediacaran History

Geochronological calibration of the Ara Group, when combined with published data from the Nama Group (Southern Namibia) and Doushantuo Formation (China) permit refined evaluation of terminal Ediacaran history (551 – 542 Ma). Chemostratigraphic data from Oman, Australia, Namibia and China indicate a globally extensive carbon isotope excursion of ~16 permil (the “Shuram excursion”). The top of this excursion is constrained at about 551 Ma (Condon and others, 2005) in China where an ash bed has been dated just below the cross-over to positive $\delta^{13}\text{C}$ values. It must be noted, however, that this excursion involves crossing a substantial facies boundary which could possibly coincide with a sequence boundary, as well. Subsequent to this excursion $\delta^{13}\text{C}$ values increase to +4 permil before decreasing to +2 permil where they remain invariant until the Precambrian-Cambrian boundary (Grotzinger and others, 1995; Amthor and others, 2003). This decrease from +4 to +2 permil is constrained by interstratified ash beds in both the Ara and Nama Groups; the ashes have yielded $^{206}\text{Pb}/^{238}\text{U}$ dates indicating that the variations in $\delta^{13}\text{C}$ reflect globally synchronous and correlated changes in seawater composition. Weakly calcified metazoans (*Cloudina*, *Namacalathus*, and *Namapoikia*) occur just below the +4 permil zenith in the Nama Group and are prevalent throughout the +2 permil ‘plateau’ characterized by reefs inhabited by *Cloudina* and *Namacalathus* in the Nama Group, Ara Group and Dengying Formation (fig. 9). In China, macroscopic algae (Miaohe Biota) occur within the top of the Doushantuo Formation contemporaneous with the upper part of the excursion.

Amthor and others (2003) reported U-Pb dates on an Ara ash bed (sample BB-5) that occurs within carbonate strata (A4C) marked by a distinctive negative excursion in carbon isotopes and considered to mark the Ediacaran-Cambrian boundary in Oman. Additional analyses for this A4C ash bed, and a second, subjacent ash-bed (sample MKZ-11B) within the upper A3C, were undertaken as part of this study in order to refine their ages (fig. 4 and table 1). The new analyses reflect use of the CA-TIMS method as well as our new and improved calibration of the U-Pb tracer used for isotope dilution analysis. The best estimates for the age of the BB-5 ash bed are the new weighted mean $^{206}\text{Pb}/^{238}\text{U}$ and $^{207}\text{Pb}/^{206}\text{Pb}$ dates of 541.00 ± 0.13 and 542.68 ± 0.46 Ma, respectively, which supersede the U-Pb Concordia age of 542.0 ± 0.3 Ma reported in Amthor and others (2003) (fig. 4). Similarly, the best estimates for the age of the MKZ-11B ash bed are now the weighted mean $^{206}\text{Pb}/^{238}\text{U}$ and $^{207}\text{Pb}/^{206}\text{Pb}$ dates of 542.33 ± 0.11 Ma and 544.10 ± 0.40 Ma, respectively, which supersede the previously reported U-Pb Concordia age of 542.6 ± 0.3 (fig. 4).

Duration of Ara Group Carbonate-Evaporite Cycles

In addition to the ages reported above for the base of the A4C and the top of the A3C units, we have also obtained an age for an ash bed (Minha-1A) at the base of the A3C unit (see above and fig. 8). The three Ara Group ages (BB-5, MKZ-11B, and Minha-1A) allow estimation of the sediment accumulation rates for the A3C carbonate unit and the overlying A4 evaporite unit. Furthermore, an additional ash bed (Asala-1c21) is located in the middle of the A0 unit (see above and fig. 8), which allows us to constrain the duration of three and a half carbonate-evaporite cycles. The combination of the four ages from the Ara allows an estimate of the average duration of each carbonate-evaporite cycle, in addition to directly constraining the accumulation rates of the A3 carbonate unit and the A4 evaporite unit.

For the purposes of calculating durations, the same calculated date must be compared between samples. Utilizing the more precise $^{206}\text{Pb}/^{238}\text{U}$ dates, the differ-

ence between the Asala-1c21 age (middle of A0) and the MKZ-11B age (top of A3) is 4.1 to 4.7 m.y., which is taken as the time represented by the upper half of the A0 unit and all of the overlying A1, A2, and A3 units. This yields an average of 1.2 to 1.3 m.y. per carbonate-evaporite cycle. The age difference between BB5 and MKZ-11B constrains the duration of the A4 evaporite half cycle to 1.1 to 1.6 m.y. In contrast, the underlying A3 carbonate half cycle has a calculated duration of 0.3 to 0.8 m.y. (difference between Minha-1A and MKZ-11B) (fig. 8).

Partitioning of Time in the Nafun Group

Deposition of the Abu Mahara Group appears to have occurred in aurally restricted basins, probably associated with regional extension (Loosveld and others, 1996; Le Guerroue and others, 2005). In contrast, stratigraphic and sedimentologic studies of the overlying Nafun Group show facies and thickness distributions consistent with deposition across a broadly subsiding region. The mapped limits of these strata do not show evidence of thinning, or a transition to shoreline or fluvial facies, which indicates that the original basin limits may once have extended well beyond the currently known margins (unpublished data, Petroleum Development Oman). Outcrop and subsurface data indicate that the Nafun Group extends from the Mirbat area in the south of Oman, to the Huqf area in central Oman, and farther north to the Oman Mountains (McCarron, ms, 2000).

The Nafun Group consists, in ascending order, the Hadash Formation (cap-carbonate), Masirah Bay Formation (shelf clastics), the Khufai Formation (shelf carbonates), the Shuram Formation (mixed shelf clastics and carbonates), and the Buah Formation (shelf carbonates) (fig. 2). The Masirah Bay Formation overlies the Hadash Formation in the Oman Mountains, and in turns passes upwards with a gradational contact into the overlying Khufai Formation. The transition from the Hadash Formation into the Masirah Bay is marked by several parasequences in which carbonates progressively thin and siliciclastic shales and siltstones progressively thicken indicating a gradational/conformable transition. These clastics then form several shoaling-upward sequences, capped by tidal sandstones (Huqf area) or deeper water, storm-deposits (Jabal Akhdar) (Allen and Leather, 2006). The Masirah Bay-Khufai Formation transition reflects a deepening (upper Masirah Bay Formation) followed by a prograding, shallowing-upward carbonate ramp succession capped by ooid grainstone shoal and evaporitic peritidal deposits (McCarron, ms, 2000). The Khufai is overlain by the Shuram Formation, which consists of aggradationally-stacked parasequence sets; individual parasequences contain basal wave-rippled siltstone and shales that grade upward into isolated and amalgamated hummocky cross-stratified sandstone beds, often associated with oolitic and intraclastic carbonates. The Shuram Formation grades upward, through increasing carbonate content and decreasing sandstone content, into the Buah formation, which represents a prograding carbonate ramp succession (McCarron, ms, 2000; Cozzi and others, 2004a). In the Buah ramp model, deeper water edgewise conglomerates and mudstones pass upward into ooid-peloid tide-dominated packstone-grainstone facies, with interbedded stromatolite bioherms. In the Jabal Akhdar, the Buah preserves a ramp margin transition, where shallow-water facies pass laterally into deepwater allodapic breccias and associated mudstones. The Buah-Ara contact is everywhere regarded as a regional unconformity, although in the Oman Mountains the Buah may be conformably overlain by the Ara-equivalent Fara Formation (Cozzi and others, 2004a).

The stratigraphy of the Nafun Group provides strong evidence for conformable transitions between the Hadash cap carbonate and the Masirah Bay Formation; between the Masirah Bay Formation and Khufai Formation; and between the Shuram Formation and the Buah Formation. However, the contacts between the Khufai Formation and Shuram Formation, and the Buah Formation and Ara Group, may both represent unconformities (McCarron, ms, 2000; Cozzi and others, 2004a). In addition,

unpublished seismic and well-log data from Petroleum Development Oman (PDO) indicate gentle truncation along these surfaces, providing further evidence for unconformable relations.

The duration of the Buah-Ara unconformity may be short, on the order of 1 m.y. or less, constrained by the inferred age of the top-Buah positive C-isotope excursion which is thought to correlate to Namibia (Cozzi and others, 2004a) where it has been dated at approximately 547 Ma (see above), and the age reported here for the middle of the A0 unit of about 547 Ma (see table 1). In contrast, there are no direct constraints on the amount of time represented by the Khufai-Shuram contact. The base of the Shuram Formation is constrained to being younger than approximately 620 Ma, the youngest detrital zircon data from sample WB.01.6, which is from the base of the Shurham Formation. Detrital zircon data obtained by ion microprobe (SHRIMP II) from a sample below the Shuram-Khufai boundary yielded detrital zircons that have a range of $^{206}\text{Pb}/^{238}\text{U}$ dates between 900 Ma and 600 Ma (one-sigma errors of about 10 Ma), with a youngest zircon component whose weighted mean $^{206}\text{Pb}/^{238}\text{U}$ date was derived by mathematical deconvolution from a mixed age population to be 609 ± 7 Ma (2σ) (Le Guerroue and others, 2006). Given the problem of detecting Pb loss in detrital zircon suites analyzed by *in-situ* methods, caution is urged in accepting 609 ± 7 Ma as a firm maximum constraint until further analyses are carried out. These data are interpreted by the authors to indicate that the “Khufai-Shuram boundary cannot be much older than 600 Ma”. This statement is misleading as the detrital zircon dates only provide a maximum constraint; the boundary must be younger than the youngest detrital zircon in the Khufai. In contrast to our speculations on the age of the Shuram, Le Guerroue and others (2006) used the age of detrital zircons and subsidence modelling to infer an age for the base of the Shuram of 600 Ma and a duration of the large negative carbon isotope excursion of 50 m.y.

Critical to understanding the tectonostratigraphic evolution of the Arabian shield during this interval (Ediacaran to Early Cambrian) is to know how time is partitioned in the Nafun Group and inferentially the subsidence mechanism responsible for generation of accommodation space. In the absence of geochronologic constraints throughout the Nafun the duration of the Shuram-Buah succession can be estimated based on interpolation and downward extrapolation of calibrated tie points on the C-isotope curve. Figure 10 shows a significant reference section for the Huqf Super-group, provided by the Miqrat-1 well. This well is representative of the Nafun Group and was selected because of its important role in constraining major events in the history of the basin (Burns and Matter, 1993). Its thickness is also representative of the more complete sections in the basin. The carbon-isotopic variability for carbonate sediments in the Miqrat-1 well has been determined by Burns and Matter (1993) and, by correlation, ages can be inferred for four stratigraphic points. In order to minimize the uncertainties associated with the geochronological constraints, we utilize the precision of the $^{206}\text{Pb}/^{238}\text{U}$ ages. As we are primarily interested in the *differences* between various dated levels, external sources of uncertainty are not considered. The first, at 546.72 ± 0.21 Ma, is provided by the age of the ash bed located in the middle of the A0 in the Asala-1c21 well; in the Miqrat-1 well this age is assigned to a depth of 3165 m (fig. 10). The second age point, at 547.36 ± 0.23 Ma, is provided by correlation (fig. 9) of the positive carbon isotope anomaly at the top of the Buah (Cozzi and others, 2004b) to the positive carbon isotopic anomaly in the Nama Group (see above). In detail, the Nama ash bed occurs just above the most positive values for this anomaly, where the values are declining rapidly back to the baseline of + 2 permil; in the Miqrat-1 well, this point is assigned to a depth of 3200 m, which corresponds to the Buah-Ara boundary (fig. 10). A third age can be inferred based on correlation to China where Condon and others (2005) obtained an age of 550.5 ± 1.0 Ma (recalculated using the same tracer calibration values for Asala-1c21 and 94-N-10B) for an ash bed in

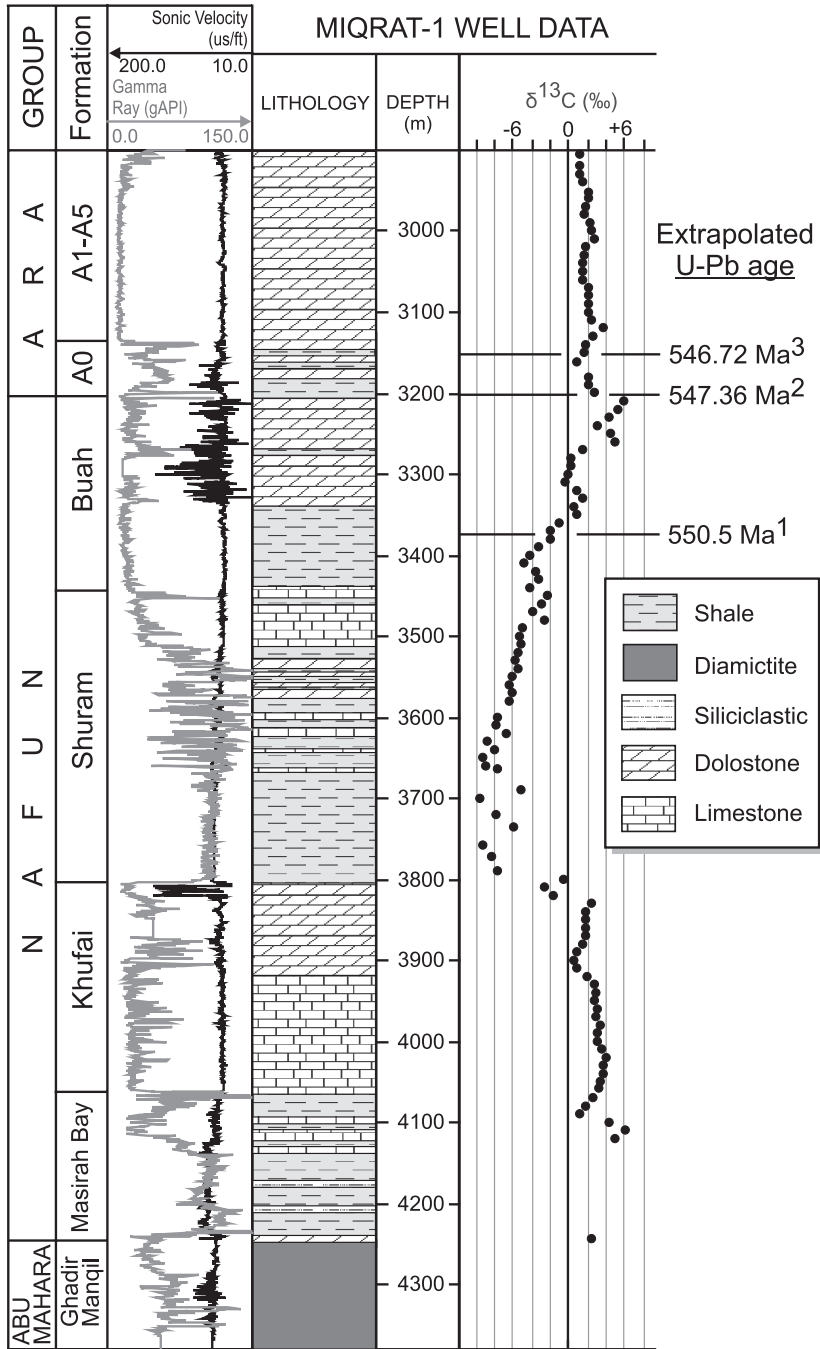


Fig. 10. Wire-line, lithological data (PDO, unpublished) and chemostratigraphy (Burns and Matter, 1993) of the Miqrat-1 well (see fig. 1 for location). This well is used by PDO and outside workers as a reference section for Huqf stratigraphy owing to its substantial thickness and relatively complete stratigraphy. It was also one of the first to be studied for its chemical stratigraphic attributes (Burns and Matter, 1993). Ash bed U-Pb dates on the right are inferred based upon chemostratigraphic correlation: (1) at -3‰ based upon correlation with China (Condon and others, 2005); (2) at directly above $+4\text{‰}$ peak based upon correlation with Nama Group, Namibia (Grotzinger and others, 1995) and (3) within middle of A0 carbonate in the Asala-1 well (this paper). These ages along with their stratigraphic positions are used to estimate sediment accumulation rates by way of linear interpolation. Farther downward extrapolation will then allow inference as to the duration of the Shuram $\delta^{13}\text{C}$ excursion.

the uppermost Doushantuo Formation just below its contact with the overlying Dengying Formation (fig. 9). At this stratigraphic position, the corresponding carbon isotope curve shows an upward shift from strongly negative values on the order of -8 permil to positive values of up to +5 permil. The ash occurs just below carbonates with -3 permil values that increase upwards to slightly positive values and is correlated to the lower Buah Formation in Oman (Condon and others, 2005); in the Miqrat-1 well, this point is assigned to a depth of 3370 m (fig. 10).

When considered in the context of the Miqrat-1 well, these three constraints permit the calculation of sediment accumulation rates for the intervening strata via linear interpolation of thickness between the dated horizons. This analysis is subject to the assumption of depositional continuity both within the upper Nafun Group as well as the sections in Namibia and China which provide time constraints. A first constraint is based upon the thickness of ≥ 35 meters (assuming no significant erosion at the Ara-Buah boundary) between 546.7 ± 0.2 Ma and 547.4 ± 0.2 Ma points yielding rates of approximately 30 to ≥ 100 m/m.y. A second constraint is provided by the interval between the 550.5 ± 1.0 Ma point (3370 m) and the 547.4 ± 0.2 Ma point (3200 m), 170 meters in 1.9 to 4.4 m.y. (considering maximum and minimum differences within confines of analytical uncertainties) yields rates in the order of 40 to 90 m/m.y. Applying these rates to the thickness of the Buah and Shuram Formations (from 3200 m to 3800 m, a thickness of 600 m) yields an inferred duration of approximately 7 to 15 m.y. Using an age of about 547 Ma for the Buah-Ara contact predicts an age for basal Shuram strata of approximately 554 to 562 Ma. Additionally, these rates can be used to estimate the duration of the negative carbon isotope excursion represented by the Shuram and lower Buah formations: picking the zero-crossing points (3800 m to 3370 m; fig. 10) and using the above sediment accumulation rates gives a duration of approximately 5 to 11 m.y. These estimates contrast to those of (Le Guerroue and others, 2006) who derived a 50 m.y. duration for the Shuram excursion based on passive margin thermal subsidence modelling. Our calculations are based upon necessarily simple assumptions such as linear interpolation and extrapolation, however given the absence of geochronologic constraints for the interval of interest (basal part of the Shuram excursion) we feel that these age estimates provide a good first approximation for duration and age of the Shuram excursion.

Le Guerroue and others (2006) assume that the subsidence that provided accommodation space for the Nafun group was driven by post-rift thermal subsidence. For the purposes of their model, they assume that the Shuram/Khufai boundary cannot be much older than 600 Ma, based on a single detrital grain from the upper Khufai with a $^{206}\text{Pb}/^{238}\text{U}$ date of 600 ± 20 (2 σ). In fact, there are no firm constraints for the age of the basal Shuram or subsidence history, which is why we choose to base our estimates for the age and duration of the Shuram anomaly from younger rocks. Our estimates for the duration of the Shuram are obtained by extrapolating downward from the Ara, which provides us with reliable subsidence rates from 547 to 550 Ma. An alternative to a passive margin subsidence model is subsidence induced by tectonic loading and development of a foreland basin. In this model accommodation space would increase with time, not decrease as predicted in a post-rift thermal subsidence model consistent with the record of the Ara Formation. The predicted age of 554 to 562 Ma in our model for the basal Shuram anomaly also explains the apparent absence of any carbon isotopic excursion associated with the older 582 Ma Gaskiers glaciation event in this sequence. In any case, until more direct temporal constraints become available, use of the carbon isotopic record in the Shuram as a global chemostratigraphic reference invites caution.

CONCLUSIONS

The new chronostratigraphic data presented here permit the Huqf Supergroup of Oman to be integrated into the developing global database for the Late Neoprotero-

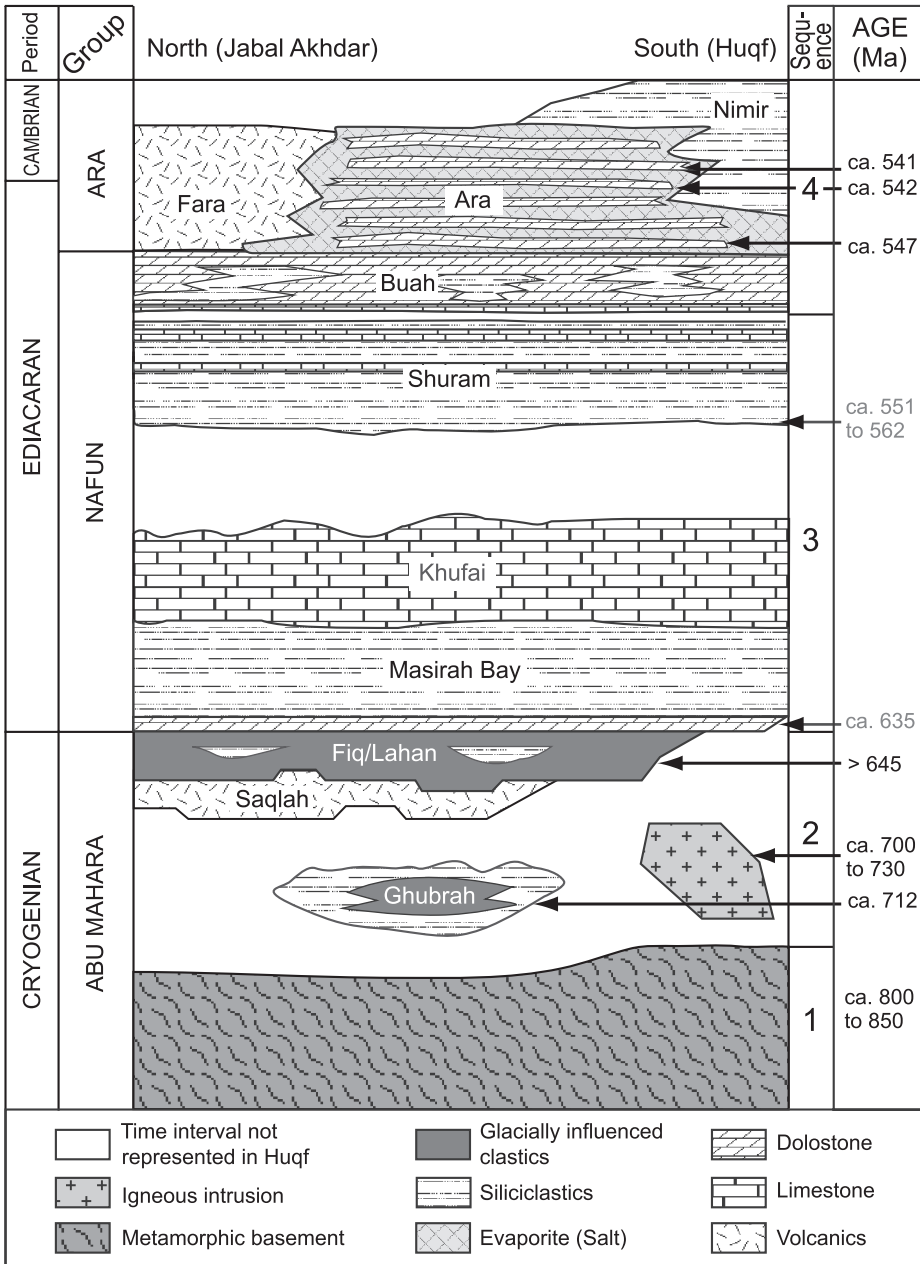


Fig. 11. Interpreted chronostratigraphy of Neoproterozoic rocks in Oman based upon the constraints discussed in this paper. Four major sequences are identified (numbers on the right column): (1) Intraplate magmatism from about 830 to 700 Ma with the main phase occurring approximately 830 to 780 Ma and with minor intrusions being emplaced until about 700 Ma (Mercolli and others, 2006; this paper); (2) The unconformably overlying Abu Mahara Group deposited in aurally restricted basins from >713 Ma to 635 Ma with two phases of glacially influenced sedimentation at roughly 713 Ma (Ghubrah Formation) and 635 Ma (Fiq Formation); (3) Conformable transition into the overlying laterally extensive Nafun Group. An unconformity is recognized within the Nafun Group at the level of Khufai-Shuram interface. The unconformity is recognized in subsurface by seismic reflector truncation (PDO data) and in the outcrop by a karst surface (see McCarron, ms, 2000). The magnitude of the Khufai-Shuram unconformity is uncertain, the age of the lower Shuram Formation being inferred based on the downward extrapolation discussed in the text; (4) Unconformable boundary between the Nafun and Ara Groups is marked by low angle truncations observed in PDO subsurface seismic data, but is constrained to be on the order of 1 m.y. or less (fig. 9). The Nafun-Ara boundary marks a shift from regional subsidence to a tectonic style characterized by uplift of large basement blocks which segmented the broader basin into several fault-bounded sub-basins (Immerz and others, 2000).

zoic Era, including the Ediacaran Period. Evidence for two glacial episodes and the similarities in age and character between the rocks in Oman, Namibia, Australia, and China validate the global and synchronous nature of a large fluctuation in the carbon isotopic composition of seawater at about 560 to 550 Ma used for correlations and inferences with respect to relationships between biology and ocean chemistry.

The evolution of the pre-Huqf Supergroup basement in Oman has a complex history, involving Archean crust in tectonic processes such as the uplift of the western deformation front. Previously, Archean crust has been noted in outcrop at the southern end of the Arabian Peninsula, and these new data suggest the northern extension of these Archean terrains beneath eastern Saudi Arabia and Oman. The younger history of the Oman crystalline basement involves a widespread period of felsic magmatism that spanned at least from 830 to 800 Ma. These rocks may represent development of a continental magmatic arc. Crustal extension, rift-basin development, and limited magmatism was coincident with the development of the Abu Mahara Group between >713 and 635 Ma (fig. 11).

Within the Abu Mahara Group two distinct episodes of glacial deposition occurred at approximately 713 and <645 Ma as constrained by the ages of ash beds intercalated within the Ghubrah and overlying Fiq formations. The younger, Fiq glacial deposit may be widespread in Oman as shown by strata of similar age in the Lahan-1 well (SOSB) and in the Oman Mountains of north Oman. When considered in the context of emerging temporal framework for the Neoproterozoic (for example, Condon and others, 2005; Halverson and others, 2005), these appear to be consistent with the globally recognized Sturtian and Marinoan glacial episodes, the latter of which terminates at approximately 635 Ma and defines the lower bound of the Ediacaran Period.

The dramatic carbon isotope excursion of ~15 permil recorded within the Shuram Formation has a maximum age of 600 Ma. Parts of the “Shuram excursion” can be correlated with the Wonoka anomaly in Australia (Calver, 2000), the Doushantuo Formation of southern China (Condon and others, 2005), and the Omkyk Member (Nama Group) in Namibia (Grotzinger and others, 1995; Workman and others, 2002). Downward extrapolation of new U-Pb data from Oman constrained by local and global correlations suggest this excursion starts at roughly 560 Ma, terminating at about 551 Ma, with an inferred duration of approximately 5 to 11 m.y. There is no evidence that this massive perturbation of the global carbon cycle is related to glaciation but is most likely related to progressive oxygenation of the oceans (Rothman and others, 2003; Condon and others, 2005; Fike and others, 2006). Following the large perturbation of the carbon cycle, the carbon isotopic composition of seawater increase to values of near +4 permil before decreasing to +2 permil where it remains invariant from about 547 Ma to the end of the Ediacaran Period at approximately 542 Ma (Grotzinger and others, 1995; Amthor and others, 2003). It is noteworthy that this interval is characterized by widespread carbonate reefs occupied by the first weakly calcified metazoans (547 Ma onwards), a diverse and complex assemblage of Ediacaran Fauna, and increase in occurrence of trace fossils indicating organisms with the ability to burrow laterally and graze (555 Ma onwards, Martin and others, 2000). These calcified metazoans and the Ediacaran Fauna disappear from the record coincident with a negative excursion in the carbon isotopic composition of seawater at the Precambrian-Cambrian boundary (Amthor and others, 2003).

The Fara Formation, exposed in the Oman Mountains, contains ignimbrites and felsic volcanoclastic sediments, yielding ages of approximately 547 Ma at its base to 542 Ma at the top. This confirms that the Fara Formation and Ara Group (SOSB) are broadly contemporaneous (fig. 11). The base Fara Formation/Ara Group marks a change from broad regional subsidence (Nafun Group) to deposition within arially restricted, fault-bounded basins coincident with the onset of felsic magmatism.

APPENDIX 1
U-Pb isotopic data for the analyzed zircon samples

Sample	Fract'ns ^[1]	Pb _c ^[2]	Pb* ^[2]	Th	U	Ratios ^[5]					Age (Ma)		corr.	coef.		
						²⁰⁶ Pb/ ²⁰⁴ Pb ^[3]	²⁰⁸ Pb/ ²⁰⁶ Pb ^[4]	²⁰⁶ Pb/ ²³⁸ U	²⁰⁷ Pb/ ²³⁵ U	±	²⁰⁷ Pb/ ²⁰⁶ Pb (2σ%)	±			²⁰⁶ Pb/ ²³⁸ U	²⁰⁷ Pb/ ²³⁵ U
BB-5 - ash bed, 1m above base of A4 carbonate unit, Ara Group (3045 meters depth, Birba-5 Well)																
z7	aa	0.8	12	0.24	753.7	0.136	0.103753	(.29)	1.11450	(.39)	0.07791	(.25)	636.37	760.34	1144.5	0.773
z6	aa	0.4	19	0.49	1166.3	0.153	0.087790	(.21)	0.70682	(.33)	0.05839	(.24)	542.45	542.86	544.6	0.674
z20	ca	2.6	34	0.33	2153.4	0.103	0.087560	(.10)	0.70455	(.12)	0.05836	(.08)	541.09	541.50	543.3	0.794
z18	ca	2.0	40	0.38	2536.9	0.118	0.087545	(.09)	0.70449	(.15)	0.05836	(.11)	541.00	541.47	543.5	0.652
z4	aa	1.5	47	0.37	2946.0	0.115	0.087517	(.18)	0.70441	(.20)	0.05838	(.10)	540.84	541.42	543.9	0.873
z17	ca	0.4	289	0.38	18025.6	0.120	0.087574	(.05)	0.70438	(.08)	0.05834	(.06)	541.18	541.41	542.4	0.654
z19	ca	1.0	80	0.26	5145.7	0.080	0.087564	(.06)	0.70433	(.09)	0.05834	(.07)	541.12	541.37	542.4	0.662
z16	ca	1.2	37	0.52	2226.4	0.165	0.087465	(.12)	0.70401	(.18)	0.05838	(.13)	540.53	541.18	543.9	0.692
z15	ca	0.4	157	0.27	10059.8	0.086	0.087514	(.05)	0.70386	(.09)	0.05833	(.07)	540.82	541.09	542.2	0.595
z8	aa	0.4	28	0.26	1798.4	0.080	0.087542	(.13)	0.70384	(.22)	0.05831	(.16)	540.98	541.08	541.5	0.645
z22	ca	0.5	108	0.35	6779.6	0.109	0.087430	(.06)	0.70332	(.10)	0.05834	(.07)	540.32	540.77	542.7	0.650
z13	ca	0.5	138	0.47	8384.7	0.147	0.087402	(.05)	0.70329	(.08)	0.05836	(.06)	540.15	540.76	543.3	0.673
z2	aa	0.8	57	0.38	3529.5	0.121	0.087294	(.08)	0.70322	(.12)	0.05843	(.08)	539.51	540.71	545.8	0.696
z1	aa	1.4	63	0.54	3759.3	0.168	0.087429	(.08)	0.70321	(.13)	0.05833	(.10)	540.32	540.71	542.3	0.643
z21	ca	3.1	70	0.22	4586.7	0.069	0.087333	(.11)	0.70245	(.14)	0.05834	(.07)	539.74	540.25	542.4	0.848
z14	ca	0.5	129	0.81	7218.5	0.255	0.087142	(.07)	0.70057	(.12)	0.05831	(.09)	538.62	539.13	541.3	0.644
z5	aa	2.3	34	0.72	1932.5	0.231	0.085843	(.42)	0.69025	(.44)	0.05832	(.13)	530.91	532.95	541.7	0.956
z3	aa	4.7	20	0.30	1321.4	0.095	0.085611	(.16)	0.68771	(.23)	0.05826	(.15)	529.53	531.42	539.6	0.739
MKZ-11B - ash bed, 9m below top of A3 carbonate unit, Ara Group (2194.4 meters depth, Mukhaizna-11 Well)																
z7	aa	2.7	28	0.44	1667.8	0.166	0.093438	(.16)	0.80624	(.22)	0.06258	(.13)	575.84	600.34	694.0	0.786
z6	aa	0.3	107	0.47	6489.5	0.149	0.087798	(.07)	0.70893	(.10)	0.05856	(.07)	542.50	544.11	550.9	0.721
z17	ca	10.5	14	0.60	856.9	0.190	0.087786	(.22)	0.70816	(.27)	0.05851	(.15)	542.43	543.66	548.8	0.839
z15	ca	0.6	208	0.53	12443.8	0.167	0.087847	(.06)	0.70762	(.08)	0.05842	(.06)	542.79	543.33	545.6	0.682
z22	ca	0.4	299	0.60	17598.9	0.188	0.087796	(.05)	0.70660	(.07)	0.05837	(.05)	542.49	542.72	543.7	0.692
z5	aa	0.7	91	0.55	5406.4	0.174	0.087754	(.09)	0.70659	(.11)	0.05840	(.07)	542.24	542.72	544.8	0.811
z23	ca	1.7	119	0.54	7119.7	0.169	0.087764	(.08)	0.70655	(.11)	0.05839	(.07)	542.30	542.70	544.4	0.771

APPENDIX 1
(continued)

Sample	Fract ^{ns} [1]	Pb _c [2] (pg)	Pb _e *[2] Pb _e	Th U	²⁰⁶ Pb/ ²⁰⁴ Pb ^[3]	²⁰⁸ Pb/ ²⁰⁶ Pb ^[4]	Ratios ^[5]		Age (Ma)				corr. coef.			
							±	(2σ%)	²⁰⁷ Pb/ ²³⁵ U	±	(2σ%)	²⁰⁶ Pb/ ²³⁸ U		²⁰⁷ Pb/ ²³⁵ U	²⁰⁷ Pb/ ²⁰⁶ Pb	
MKZ-11B - ash bed, 9m below top of A3 carbonate unit, Ara Group (2194.4 meters depth, Mukhaizna-11 Well)																
z16	ca	1.1	104	0.54	6201.5	0.169	0.087765	(.05)	0.70646	(.08)	0.05838	(.06)	542.31	542.64	544.0	0.676
z18	ca	0.8	128	0.62	7526.1	0.195	0.087759	(.06)	0.70641	(.08)	0.05838	(.06)	542.27	542.61	544.1	0.683
z13	ca	0.5	430	0.56	25553.6	0.175	0.087757	(.05)	0.70637	(.09)	0.05838	(.07)	542.26	542.59	543.9	0.564
z19	ca	1.4	117	0.58	6935.0	0.182	0.087753	(.05)	0.70624	(.08)	0.05837	(.06)	542.23	542.51	543.7	0.694
z20	ca	1.3	120	0.58	7117.4	0.181	0.087672	(.05)	0.70591	(.07)	0.05840	(.05)	541.76	542.32	544.6	0.696
z21	ca	0.3	257	0.62	15064.3	0.193	0.087650	(.05)	0.70563	(.08)	0.05839	(.06)	541.62	542.15	544.4	0.600
z1	aa	1.0	95	0.52	5728.2	0.163	0.087677	(.06)	0.70558	(.19)	0.05837	(.18)	541.78	542.12	543.5	0.337
z3	aa	2.6	29	0.55	1726.1	0.172	0.087650	(.16)	0.70550	(.19)	0.05838	(.09)	541.62	542.07	543.9	0.808
z2	aa	0.9	123	0.50	7443.3	0.158	0.087611	(.05)	0.70513	(.08)	0.05837	(.06)	541.39	541.85	543.7	0.651
Minha-1 A - ash bed, 3m above base of A3 carbonate unit, Ara Group (3988.3 meters depth, Minha-1 Well)																
z1	aa	0.6	312	0.41	18288.2	0.135	0.308431	(.09)	5.00381	(.13)	0.11766	(.09)	1733.0	1820.0	1921.0	0.701
z19	aa	4.2	10	0.48	616.8	0.149	0.093649	(.18)	0.76646	(.26)	0.05936	(.18)	577.08	577.73	580.3	0.736
z9a	ca	0.6	87	0.72	4995.4	0.225	0.088203	(.07)	0.71092	(.11)	0.05846	(.08)	544.90	545.29	546.9	0.624
z18	aa	0.2	169	0.73	9670.5	0.227	0.087892	(.05)	0.70759	(.08)	0.05839	(.07)	543.06	543.31	544.4	0.619
z8	ca	0.8	84	0.83	4661.3	0.260	0.087846	(.07)	0.70752	(.11)	0.05841	(.09)	542.78	543.27	545.3	0.637
z10	ca	1.5	146	1.05	7734.1	0.330	0.087866	(.08)	0.70731	(.10)	0.05838	(.07)	542.90	543.15	544.2	0.763
z4	aa	0.4	202	0.79	11334.3	0.247	0.087857	(.07)	0.70730	(.09)	0.05839	(.06)	542.85	543.14	544.4	0.731
z20	aa	0.5	56	0.70	3231.8	0.218	0.087891	(.07)	0.70727	(.11)	0.05836	(.08)	543.05	543.12	543.4	0.658
z17	aa	3.0	27	0.88	1512.7	0.276	0.087803	(.13)	0.70724	(.41)	0.05842	(.39)	542.53	543.11	545.5	0.327
z21	aa	0.3	259	0.57	15386.0	0.178	0.087853	(.05)	0.70710	(.07)	0.05837	(.05)	542.83	543.02	543.9	0.642
z16	aa	2.3	25	1.31	1287.6	0.411	0.087837	(.15)	0.70709	(.22)	0.05838	(.15)	542.73	543.02	544.2	0.724
z3	aa	0.5	155	0.37	9694.2	0.115	0.087765	(.05)	0.70679	(.08)	0.05841	(.06)	542.31	542.84	545.1	0.694
z12	ca	1.1	93	0.72	5300.1	0.226	0.087777	(.07)	0.70669	(.10)	0.05839	(.07)	542.38	542.78	544.5	0.685
z13	ca	2.2	21	1.00	1163.9	0.313	0.087707	(.17)	0.70639	(.23)	0.05841	(.15)	541.96	542.60	545.3	0.766
z2	aa	0.6	111	0.41	6893.5	0.128	0.087742	(.07)	0.70638	(.09)	0.05839	(.07)	542.17	542.60	544.4	0.704
z5	aa	1.0	73	0.58	4349.8	0.182	0.087746	(.12)	0.70627	(.16)	0.05838	(.11)	542.19	542.53	543.9	0.735
z6	aa	1.0	73	1.18	3771.2	0.369	0.087622	(.15)	0.70532	(.19)	0.05838	(.12)	541.46	541.96	544.1	0.778

APPENDIX 1
(continued)

Sample	Fract ^{ns} [1]	Pb _c [2] (pg)	Pb* ^[2] Pb _c	Th U	$\frac{^{206}\text{Pb}^{[3]}}{^{204}\text{Pb}}$	$\frac{^{208}\text{Pb}^{[4]}}{^{206}\text{Pb}}$	Ratios ^[5]				Age (Ma)					
							\pm (2 σ %)	$\frac{^{207}\text{Pb}}{^{235}\text{U}}$	\pm (2 σ %)	$\frac{^{207}\text{Pb}}{^{206}\text{Pb}}$	\pm (2 σ %)	$\frac{^{206}\text{Pb}}{^{238}\text{U}}$	$\frac{^{207}\text{Pb}}{^{235}\text{U}}$	$\frac{^{207}\text{Pb}}{^{206}\text{Pb}}$		
															corr. coef.	
Asala-I core 21 - ash bed, middle of A0 carbonate unit, Ara Group (3847 meters depth, Asala-I Well)																
z12	ca	10.5	13	0.60	759.7	0.191	0.088624	(.27)	0.71884	(.47)	0.05883	(.38)	547.39	549.98	560.7	0.604
z1	ca	0.5	35	0.62	2038.3	0.196	0.088923	(.11)	0.71807	(.18)	0.05857	(.13)	549.17	549.53	551.1	0.670
z10	ca	1.1	20	0.63	1207.9	0.198	0.088600	(.38)	0.71510	(.43)	0.05854	(.20)	547.25	547.77	549.9	0.890
z9	ca	0.8	40	0.59	2358.5	0.186	0.088575	(.10)	0.71478	(.18)	0.05853	(.14)	547.11	547.58	549.6	0.588
z13	ca	8.2	16	0.62	962.7	0.194	0.088500	(.20)	0.71437	(.33)	0.05854	(.24)	546.66	547.34	550.2	0.668
z8	ca	0.5	42	0.64	2468.0	0.200	0.088552	(.09)	0.71411	(.15)	0.05849	(.12)	546.97	547.19	548.1	0.638
z6	ca	1.1	13	0.56	773.3	0.178	0.088408	(.61)	0.71398	(.73)	0.05857	(.38)	546.11	547.11	551.3	0.850
z5	ca	0.5	39	0.57	2300.0	0.179	0.088466	(.11)	0.71397	(.27)	0.05853	(.20)	546.46	547.10	549.8	0.670
z11	ca	0.8	34	0.53	2083.3	0.166	0.088455	(.11)	0.71377	(.18)	0.05852	(.14)	546.39	546.98	549.4	0.629
z4	ca	0.4	78	0.48	4778.7	0.149	0.088496	(.10)	0.71344	(.15)	0.05847	(.10)	546.64	546.79	547.4	0.705
z7	ca	0.6	56	0.64	3262.6	0.199	0.088467	(.10)	0.71341	(.15)	0.05849	(.11)	546.46	546.77	548.1	0.657
z3	ca	1.1	37	0.56	2231.9	0.176	0.088285	(.24)	0.71239	(.31)	0.05852	(.20)	545.39	546.17	549.4	0.776
94-N-10B - ash bed from Lower Hoogland Member, Nama Group, Namibia (see Grotzinger and others, 1995)																
z2	ca	1.2	74	0.53	4442.2	0.166	0.089105	(.09)	0.72048	(.13)	0.05864	(.10)	550.24	550.95	553.9	0.685
z9	ca	1.1	137	0.47	8352.1	0.148	0.088974	(.11)	0.71830	(.12)	0.05855	(.06)	549.46	549.66	550.5	0.865
z14	ca	0.6	41	0.58	2455.9	0.183	0.088689	(.10)	0.71601	(.14)	0.05855	(.10)	547.78	548.31	550.5	0.708
z20	ca	2.9	39	0.53	2372.3	0.166	0.088646	(.09)	0.71580	(.13)	0.05856	(.09)	547.52	548.19	551.0	0.739
z5	ca	0.7	24	0.57	1452.5	0.177	0.088624	(.17)	0.71530	(.24)	0.05854	(.17)	547.40	547.89	549.9	0.723
z7	ca	0.8	34	0.55	2020.8	0.174	0.088433	(.37)	0.71526	(.38)	0.05866	(.08)	546.26	547.87	554.5	0.979
z15	ca	2.0	30	0.54	1797.9	0.171	0.088559	(.27)	0.71515	(.29)	0.05857	(.11)	547.01	547.80	551.1	0.923
z16	ca	1.6	57	0.55	3439.7	0.172	0.088632	(.07)	0.71502	(.11)	0.05851	(.08)	547.44	547.72	548.9	0.670
z17	ca	0.6	74	0.55	4450.6	0.170	0.088642	(.08)	0.71484	(.12)	0.05849	(.09)	547.50	547.62	548.1	0.662
z13	ca	1.6	17	0.57	1043.1	0.177	0.088668	(.20)	0.71464	(.26)	0.05845	(.15)	547.66	547.50	546.9	0.803
z18	ca	1.2	154	0.53	9228.9	0.167	0.088562	(.06)	0.71413	(.08)	0.05848	(.06)	547.02	547.20	547.9	0.696
z4	ca	0.5	83	0.48	5042.9	0.151	0.088508	(.07)	0.71376	(.11)	0.05849	(.08)	546.70	546.98	548.1	0.675
z11	ca	1.7	51	0.51	3059.3	0.161	0.088420	(.11)	0.71371	(.14)	0.05854	(.07)	546.18	546.94	550.1	0.845
z6	ca	1.0	156	0.47	9533.3	0.146	0.088280	(.12)	0.71171	(.14)	0.05847	(.08)	545.35	545.76	547.5	0.832
z10	ca	1.1	69	0.31	4286.3	0.124	0.069427	(.11)	0.56040	(.13)	0.05854	(.07)	432.70	451.79	550.1	0.854

APPENDIX 1
(continued)

Sample	Fract'ns ^[1]	Pb _c ^[2] (pg)	Pb _c * ^[2]	Th	U	Ratios ^[5]			Age (Ma)			corr.	coef.					
						$\frac{^{206}\text{Pb}^{[3]}}{^{204}\text{Pb}}$	$\frac{^{208}\text{Pb}^{[4]}}{^{206}\text{Pb}}$	$\frac{^{206}\text{Pb}}{^{238}\text{U}}$	\pm	$\frac{^{207}\text{Pb}}{^{235}\text{U}}$	\pm			$\frac{^{206}\text{Pb}}{^{238}\text{U}}$	$\frac{^{207}\text{Pb}}{^{235}\text{U}}$	$\frac{^{207}\text{Pb}}{^{206}\text{Pb}}$		
WB.01.1 - ignimbrite from ca. 200 m above base of the Fara Formation (Jabal Akhdar area)																		
z10	aa	0.6	53	0.26		3163.0	0.159	0.112662	(.09)	1.34056	(.12)	0.08630	(.07)	688.19	863.47	1344.9	0.770	
z7	aa	6.0	10	0.79		557.6	0.252	0.087972	(.34)	0.71212	(.51)	0.05871	(.35)	543.53	546.00	556.3	0.716	
z8	aa	5.6	9	0.51		585.8	0.162	0.087933	(.33)	0.71013	(.40)	0.05857	(.22)	543.30	544.82	551.2	0.837	
z4	aa	1.1	153	0.32		9663.4	0.102	0.087856	(.06)	0.70767	(.09)	0.05842	(.07)	542.85	543.36	545.5	0.640	
z13	aa	1.3	32	0.74		1844.5	0.233	0.087776	(.13)	0.70761	(.20)	0.05847	(.15)	542.37	543.32	547.3	0.683	
z2	aa	0.5	125	0.46		7658.4	0.145	0.087795	(.06)	0.70755	(.10)	0.05845	(.08)	542.49	543.29	546.7	0.593	
z12	aa	1.3	75	0.92		4109.9	0.289	0.087751	(.07)	0.70656	(.11)	0.05840	(.09)	542.22	542.70	544.7	0.626	
z5	aa	0.7	111	0.60		6515.6	0.191	0.086528	(.06)	0.69727	(.09)	0.05844	(.06)	534.97	537.16	546.5	0.747	
z3	aa	4.8	11	0.88		619.8	0.284	0.085890	(.36)	0.69314	(.60)	0.05853	(.46)	531.19	534.68	549.7	0.655	
z1	aa	0.4	83	0.97		4371.6	0.332	0.080819	(.07)	0.65095	(.10)	0.05842	(.08)	501.01	509.06	545.4	0.661	
WB.01.2 - ignimbrite from top of the Fara Formation (Jabal Akhdar area)																		
z16	ca	0.7	45.5	0.62		2721.5	0.190	0.140474	(.09)	1.30589	(.14)	0.06742	(.11)	847.34	848.32	850.9	0.659	
z9	aa	0.5	13.8	0.99		771.6	0.306	0.139410	(.33)	1.29143	(.54)	0.06719	(.40)	841.33	841.93	843.5	0.664	
z21	ca	1.1	41.5	0.76		2406.5	0.233	0.138218	(.19)	1.27588	(.20)	0.06695	(.08)	834.58	835.02	836.2	0.912	
z19	ca	0.8	19.3	0.59		1171.6	0.180	0.137527	(.18)	1.26746	(.30)	0.06684	(.23)	830.67	831.25	832.8	0.638	
z2	aa	0.3	8.3	0.52		528.9	0.161	0.134520	(.39)	1.23351	(.59)	0.06651	(.42)	813.60	815.94	822.3	0.708	
z6	aa	0.5	10.0	0.38		621.3	0.149	0.105098	(.36)	0.95560	(.67)	0.06594	(.53)	644.22	681.01	804.6	0.615	
z14	ca	0.5	16.7	0.76		981.1	0.236	0.088785	(.22)	0.71631	(.41)	0.05851	(.33)	548.35	548.48	549.1	0.600	
z18	ca	1.0	51.5	0.37		3296.1	0.116	0.088626	(.15)	0.71500	(.16)	0.05851	(.07)	547.41	547.71	549.0	0.903	
z7	aa	0.3	45.8	0.87		2563.1	0.273	0.088612	(.17)	0.71450	(.24)	0.05848	(.16)	547.32	547.41	547.8	0.724	
z15	ca	0.4	73.0	0.56		4537.6	0.175	0.088612	(.06)	0.71440	(.11)	0.05847	(.09)	547.32	547.36	547.5	0.601	
z20	ca	0.8	42.1	0.49		2606.9	0.155	0.088565	(.09)	0.71428	(.12)	0.05849	(.09)	547.04	547.29	548.3	0.726	
z8	aa	0.6	50.6	0.37		3253.8	0.115	0.088592	(.09)	0.71419	(.14)	0.05847	(.10)	547.21	547.23	547.4	0.691	
z26	ca	1.5	14.0	0.62		838.3	0.194	0.088443	(.24)	0.71410	(.33)	0.05856	(.21)	546.32	547.18	550.7	0.771	
z23	ca	0.6	25.0	0.56		816.1	0.176	0.088429	(.26)	0.71313	(.38)	0.05849	(.26)	546.24	546.60	548.1	0.715	
z22	ca	1.0	13.2	0.40		1592.1	0.127	0.088300	(.13)	0.71218	(.20)	0.05850	(.14)	545.48	546.04	548.4	0.697	
z5	aa	0.4	9.6	0.34		614.7	0.117	0.081013	(.40)	0.65384	(.82)	0.05853	(.68)	502.17	510.84	549.8	0.570	
z4	aa	1.4	8.3	0.10		568.4	0.068	0.054275	(.61)	0.47154	(.68)	0.06301	(.29)	340.72	392.25	708.6	0.907	

APPENDIX 1
(continued)

Sample	Fract ^{ns} [1]	Pb _c [2] (pg)	Pb _c *[2] Pb _c	Th U	²⁰⁶ Pb/ ²⁰⁴ Pb ^[3]	²⁰⁸ Pb/ ²⁰⁶ Pb ^[4]	Ratios ^[5]				Age (Ma)		corr. coef.			
							±	²⁰⁷ Pb/ ²³⁵ U	±	²⁰⁷ Pb/ ²⁰⁶ Pb (2σ%)	±	²⁰⁶ Pb/ ²³⁸ U		²⁰⁷ Pb/ ²³⁵ U	²⁰⁷ Pb/ ²⁰⁶ Pb	
WB-01.6 - siliciclastic lithology, Buah Formation, Jabal Akhdar area																
z1	aa	0.5	24	0.05	1554.6	0.040	0.113311	(.19)	1.61586	(.24)	0.10343	(.15)	691.95	976.38	1686.5	0.795
z3	aa	0.7	22	0.08	1389.2	0.075	0.085599	(.15)	1.15530	(.19)	0.09789	(.10)	529.46	779.74	1584.2	0.835
z5	aa	0.6	39	0.40	2314.7	0.182	0.086669	(.12)	0.77860	(.19)	0.06516	(.15)	535.81	584.69	779.4	0.648
z4	aa	0.5	5	0.08	351.1	0.102	0.032548	(.58)	0.29402	(1.2)	0.06552	(.97)	206.47	261.72	791.0	0.584
WB-01.7 - siliciclastic rock, Shuram Formation, Jabal Akhdar area																
z2	ca	9.2	30	0.70	1668.1	0.231	0.289664	(.13)	4.47578	(.14)	0.11207	(.07)	1639.9	1726.5	1833.2	0.889
z5	aa	0.5	38	0.47	2292.0	0.145	0.147953	(.13)	1.40612	(.17)	0.06893	(.10)	889.48	891.52	896.6	0.793
z6	aa	1.0	18	0.42	1127.9	0.130	0.146569	(.24)	1.38356	(.32)	0.06846	(.20)	881.70	881.96	882.6	0.770
z4	ca	1.2	72	0.60	4237.9	0.188	0.138957	(.07)	1.29034	(.09)	0.06735	(.06)	838.76	841.45	848.6	0.748
z1	ca	1.3	16	1.48	789.1	0.454	0.139071	(.26)	1.28711	(.47)	0.06712	(.37)	839.41	840.01	841.6	0.611
z3	ca	3.4	18	0.90	998.0	0.281	0.134314	(.19)	1.23544	(.23)	0.06671	(.12)	812.43	816.81	828.8	0.862
WB-01.8 - siliciclastic lithology, Shuram Formation, Jabal Akhdar area																
z8	aa	0.8	21	0.38	1261.9	0.113	0.357411	(.32)	6.17453	(.36)	0.12530	(.15)	1969.9	2000.9	2033.0	0.914
z3	ca	0.6	5	0.43	340.2	0.132	0.142046	(.60)	1.32183	(.92)	0.06749	(.65)	856.22	855.31	853.0	0.708
z5	ca	0.4	309	0.18	20185.4	0.056	0.140584	(.07)	1.31444	(.10)	0.06781	(.07)	847.97	852.08	862.8	0.737
z2	ca	0.6	53	0.29	3358.4	0.089	0.139794	(.10)	1.29629	(.16)	0.06725	(.13)	843.50	844.08	845.6	0.647
z9	aa	0.7	33	0.40	2056.0	0.124	0.138578	(.19)	1.27981	(.25)	0.06698	(.15)	836.61	836.77	837.2	0.782
z10	aa	0.6	161	0.71	9201.5	0.219	0.136930	(.21)	1.26122	(.24)	0.06680	(.11)	827.28	828.46	831.6	0.884
z6	ca	3.2	24	0.48	1477.1	0.154	0.134984	(.17)	1.25761	(.24)	0.06757	(.16)	816.24	826.83	855.4	0.728
z4	ca	0.4	12	0.83	672.3	0.258	0.101879	(.67)	0.85098	(.79)	0.06058	(.40)	625.41	625.19	624.4	0.859
z7	ca	0.8	43	0.80	2400.5	0.249	0.101132	(.10)	0.84358	(.18)	0.06050	(.14)	621.04	621.12	621.4	0.604
Lahan-1 - volcanic ash or siltstone, 9 m below cap dolostone within dropstone bearing shales (4285.2 meters depth, Lahan-1 Well)																
z1	aa	1.9	2	0.96	106.7	0.327	0.101265	(2.1)	0.86785	(2.5)	0.06216	(1.2)	621.82	634.40	679.5	0.862
z7	aa	1.0	2	0.86	141.9	0.292	0.101189	(1.5)	0.86817	(2.3)	0.06223	(1.6)	621.37	634.57	681.9	0.710
z4	aa	2.8	3	0.53	225.6	0.167	0.104810	(.91)	0.88616	(1.6)	0.06132	(1.2)	642.54	644.30	650.5	0.647
z3	ca	0.3	684	1.06	36104.6	0.327	0.105246	(.07)	0.88715	(.09)	0.06114	(.06)	645.08	644.84	644.0	0.735
z10	ca	3.1	30	0.69	1746.2	0.216	0.105256	(.12)	0.88837	(.37)	0.06121	(.35)	645.14	645.49	646.7	0.318

APPENDIX 1
(continued)

Sample	Fract'ns ^[1]	Pb _c ^[2] (pg)	Pb _c * ^[2]	Th	U	Ratios ^[5]				Age (Ma)							
						$\frac{^{206}\text{Pb}^{[3]}}{^{204}\text{Pb}}$	$\frac{^{208}\text{Pb}^{[4]}}{^{206}\text{Pb}}$	$\frac{^{206}\text{Pb}}{^{238}\text{U}}$	\pm (2 σ %)	$\frac{^{207}\text{Pb}}{^{235}\text{U}}$	\pm (2 σ %)	$\frac{^{207}\text{Pb}}{^{206}\text{Pb}}$	\pm (2 σ %)	$\frac{^{206}\text{Pb}}{^{238}\text{U}}$	$\frac{^{207}\text{Pb}}{^{235}\text{U}}$	$\frac{^{207}\text{Pb}}{^{206}\text{Pb}}$	corr. coef.
Lahan-1 - volcanic ash or siltstone, 9 m below cap dolostone within dropstone bearing shales (4285.2 meters depth, Lahan-1 Well)																	
z14	ca	0.4	166	0.74	0.49	9464.5	0.229	0.105370	(.07)	0.88897	(.10)	0.06119	(.07)	645.80	645.81	645.8	0.708
z15	ca	0.7	48	0.49	29	34.9	0.153	0.109358	(.10)	0.93634	(.15)	0.06210	(.10)	669.02	670.97	677.5	0.703
z11	ca	1.3	74	0.47	4479.3	0.145	0.117273	(.22)	1.02285	(.23)	0.06326	(.08)	714.85	715.34	716.9	0.948	
z13	ca	0.6	41	0.05	2864.2	0.014	0.117367	(.09)	1.02307	(.12)	0.06322	(.07)	715.39	715.45	715.7	0.733	
z17	ca	0.8	45	0.60	2680.3	0.187	0.117221	(.10)	1.02319	(.18)	0.06331	(.15)	714.55	715.51	718.6	0.595	
z4	ca	0.3	181	0.49	10974.5	0.151	0.117423	(.06)	1.02428	(.09)	0.06327	(.07)	715.72	716.06	717.1	0.698	
z12	ca	0.8	43	0.57	2559.5	0.175	0.117522	(.11)	1.02488	(.19)	0.06325	(.15)	716.28	716.36	716.6	0.616	
z2	ca	0.5	118	0.48	7161.6	0.149	0.117644	(.08)	1.02700	(.13)	0.06331	(.10)	716.99	717.43	718.8	0.618	
z18	ca	0.7	23	0.53	1366.5	0.164	0.117629	(.16)	1.02751	(.24)	0.06335	(.17)	716.90	717.68	720.1	0.699	
z16	ca	1.3	39	0.60	2281.3	0.187	0.117756	(.10)	1.02797	(.14)	0.06331	(.10)	717.63	717.91	718.8	0.728	
z6	ca	0.7	34	0.55	2029.4	0.170	0.117765	(.15)	1.02838	(.31)	0.06333	(.26)	717.69	718.12	719.5	0.558	
z5	ca	0.3	48	0.70	2777.3	0.212	0.118400	(.27)	1.02908	(.31)	0.06304	(.14)	721.35	718.47	709.5	0.895	
z5	aa	1.1	13	0.63	769.0	0.195	0.147099	(.29)	1.39458	(.45)	0.06876	(.32)	884.68	886.64	891.5	0.697	
Wadi-MT - volcanoclastic lithology, Fiq Formation, Jabal Akhdar area																	
z4	aa	8.5	17	0.60	1025.0	0.190	0.137196	(.24)	1.27315	(.27)	0.06730	(.13)	828.79	833.80	847.2	0.877	
z14	aa	1.1	12	0.80	699.8	0.249	0.134934	(.42)	1.24101	(.58)	0.06670	(.37)	815.95	819.34	828.6	0.760	
z15	aa	0.7	30	0.62	1785.8	0.190	0.135081	(.14)	1.23173	(.28)	0.06613	(.23)	816.79	815.13	810.6	0.576	
z16	aa	0.5	18	0.76	1030.1	0.231	0.134300	(.40)	1.22363	(.61)	0.06608	(.45)	812.35	811.44	809.0	0.675	
z6	aa	1.7	9	0.69	554.0	0.208	0.131991	(.38)	1.18962	(.70)	0.06537	(.56)	799.21	795.78	786.2	0.616	
z12	aa	1.1	12	0.66	698.0	0.210	0.127611	(.36)	1.15642	(.48)	0.06572	(.30)	774.22	780.27	797.6	0.778	
z13	aa	1.9	28	0.84	1584.7	0.262	0.126579	(.14)	1.13365	(.23)	0.06496	(.16)	768.32	769.49	772.9	0.693	
z10	aa	2.2	28	0.41	1734.2	0.127	0.126570	(.14)	1.13002	(.21)	0.06475	(.16)	768.27	767.76	766.3	0.674	
z5	aa	2.3	26	0.26	1667.4	0.080	0.125831	(.13)	1.12553	(.33)	0.06487	(.28)	764.04	765.62	770.2	0.529	
z2	aa	1.4	21	0.19	1378.2	0.061	0.123099	(.18)	1.10005	(.30)	0.06481	(.23)	748.38	753.38	768.2	0.659	
z3	aa	1.3	7	0.88	407.6	0.285	0.121633	(.47)	1.09176	(.62)	0.06510	(.37)	739.96	749.36	777.5	0.798	
z11	aa	2.7	12	0.41	743.3	0.130	0.121131	(.29)	1.07487	(.49)	0.06436	(.37)	737.07	741.13	753.4	0.660	
z1	aa	2.8	3	0.35	199.5	0.120	0.116760	(.11)	1.04993	(.15)	0.06522	(.10)	711.89	728.85	781.4	0.750	

APPENDIX 1
(continued)

Sample	Fract ^{ns} [1]	Pb _c ^[2] (pg)	Pb _c *[2]	Th	U	$\frac{^{206}\text{Pb}}{^{204}\text{Pb}}$ [3]	$\frac{^{208}\text{Pb}}{^{206}\text{Pb}}$ [4]	Ratios ^[5]			Age (Ma)			corr. coef.			
								\pm	$\frac{^{207}\text{Pb}}{^{235}\text{U}}$	\pm (2 σ %)	$\frac{^{207}\text{Pb}}{^{206}\text{Pb}}$	\pm (2 σ %)	$\frac{^{206}\text{Pb}}{^{238}\text{U}}$		$\frac{^{207}\text{Pb}}{^{235}\text{U}}$	$\frac{^{207}\text{Pb}}{^{206}\text{Pb}}$	
Fig2 - siliciclastic lithology, Fiq Formation, Jabal Akhdar Area																	
z5	aa	1.2	10	0.59	0.59	581.1	0.187	0.148764	(.78)	1.43302	(1.5)	0.06986	(1.2)	894.03	902.81	924.4	0.566
z2	aa	1.0	42	0.46	0.46	2592.3	0.141	0.143115	(.10)	1.34142	(.16)	0.06798	(.12)	862.25	863.84	867.9	0.657
z9	aa	1.5	18	0.54	0.54	1078.2	0.166	0.142018	(.29)	1.32587	(.41)	0.06771	(.27)	856.06	857.08	859.7	0.745
z10	aa	0.6	124	0.40	0.40	7651.8	0.125	0.137696	(.06)	1.27223	(.08)	0.06701	(.06)	831.62	833.39	838.1	0.714
z12	aa	0.6	58	1.02	1.02	3113.7	0.316	0.137098	(.09)	1.26606	(.12)	0.06698	(.08)	828.23	830.63	837.1	0.783
z4	aa	0.6	19	0.55	0.55	1150.5	0.173	0.135176	(.26)	1.24634	(.43)	0.06687	(.32)	817.32	821.75	833.8	0.671
z8	aa	0.9	16	0.83	0.83	907.9	0.257	0.135043	(.25)	1.23732	(.37)	0.06645	(.26)	816.57	817.67	820.7	0.706
z7	aa	1.2	12	0.87	0.87	652.9	0.269	0.134509	(.64)	1.22988	(.70)	0.06631	(.26)	813.54	814.28	816.3	0.929
z11	aa	0.6	54	1.00	1.00	2916.5	0.308	0.134399	(.11)	1.22836	(.14)	0.06629	(.09)	812.91	813.59	815.4	0.765
z6	aa	1.3	8	0.81	0.81	458.8	0.273	0.122803	(.86)	1.12143	(1.1)	0.06623	(.60)	746.68	763.66	813.7	0.828
z1	aa	0.6	26	0.67	0.67	1534.3	0.209	0.108281	(.18)	0.92323	(.30)	0.06184	(.23)	662.75	664.07	668.5	0.656
SQ01 - possible volcanic, Saqlah Formation, Jabal Akhdar area																	
z1	aa	0.5	45	0.44	0.44	2753.1	0.149	0.112689	(.10)	0.99688	(.21)	0.06416	(.18)	688.35	702.23	746.9	0.508
z2	aa	2.5	30	0.44	0.44	1790.5	0.143	0.126692	(.11)	1.15118	(.17)	0.06590	(.13)	768.97	777.80	803.2	0.664
z3	aa	0.7	354	0.56	0.56	20862.1	0.178	0.132484	(.06)	1.22058	(.09)	0.06682	(.07)	802.02	810.04	832.2	0.672
z4	aa	1.4	4	1.10	1.10	241.7	0.359	0.127754	(1.4)	1.16968	(1.7)	0.06640	(.89)	775.04	786.50	819.2	0.849
z5	aa	1.1	7	0.76	0.76	403.5	0.232	0.132036	(1.1)	1.19551	(1.3)	0.06567	(.63)	799.47	798.51	795.9	0.879
z6	aa	4.1	53	0.44	0.44	3180.7	0.138	0.123058	(.08)	1.09220	(.15)	0.06437	(.12)	748.14	749.57	753.9	0.582
z7	aa	1.1	41	0.21	0.21	2690.1	0.066	0.120374	(.20)	1.07008	(.26)	0.06447	(.17)	732.72	738.78	757.2	0.768
WM.01.5 - possible volcanic ash, Saqlah Formation, Jabal Akhdar area																	
z1	aa	0.6	17	0.80	0.80	977.5	0.259	0.123720	(.24)	1.11724	(.26)	0.06549	(.09)	751.94	761.65	790.3	0.935
z2	aa	0.7	25	0.81	0.81	1410.0	0.257	0.125498	(.18)	1.13095	(.26)	0.06536	(.18)	762.13	768.21	785.9	0.734
z3	aa	1.7	13	0.40	0.40	798.9	0.127	0.133155	(.30)	1.22623	(.34)	0.06679	(.17)	805.84	812.62	831.2	0.868

APPENDIX 1
(continued)

Sample	Fract'ns ^[1]	Pb _c ^[2] (pg)	Pb* ^[2]	Th	U	Ratios ^[5]				Age (Ma)							
						$\frac{^{206}\text{Pb}^{[3]}}{^{204}\text{Pb}}$	$\frac{^{208}\text{Pb}^{[4]}}{^{206}\text{Pb}}$	\pm	$\frac{^{207}\text{Pb}}{^{235}\text{U}}$	\pm	$\frac{^{206}\text{Pb}}{^{238}\text{U}}$	$\frac{^{207}\text{Pb}}{^{235}\text{U}}$	$\frac{^{207}\text{Pb}}{^{206}\text{Pb}}$				
						(2σ%)	(2σ%)	(2σ%)	(2σ%)	(2σ%)	(2σ%)	(2σ%)	(2σ%)				
WM.01.6 - possible volcanic ash, Saqlah Formation, Jabal Akhdar area																	
z6	aa	3.5	6	0.60	0.60	371.5	0.185	0.135267	(.53)	1.24102	(.63)	0.06654	(.32)	817.85	819.34	823.4	0.863
z9	aa	1.7	9	0.81	0.81	515.6	0.252	0.131367	(.62)	1.19353	(1.0)	0.06589	(.75)	795.66	797.60	803.0	0.675
z4	aa	1.2	21	0.61	0.61	1223.1	0.190	0.129990	(.20)	1.17699	(.25)	0.06567	(.13)	787.81	789.91	795.8	0.838
z7	aa	0.8	9	0.78	0.78	528.1	0.263	0.122063	(.44)	1.11551	(.89)	0.06628	(.73)	742.43	760.82	815.3	0.582
z5	aa	2.2	37	0.16	0.16	2445.7	0.051	0.122511	(.10)	1.08945	(.13)	0.06450	(.08)	745.00	748.24	757.9	0.801
z1	aa	1.9	23	0.76	0.76	1311.1	0.237	0.122474	(.17)	1.08760	(.28)	0.06441	(.21)	744.78	747.34	755.0	0.664
z8	aa	1.1	7	0.86	0.86	418.7	0.278	0.121337	(.50)	1.08605	(1.1)	0.06492	(.92)	738.26	746.58	771.6	0.558
z3	aa	2.0	7	0.55	0.55	423.2	0.180	0.117641	(.54)	1.04517	(.71)	0.06444	(.45)	716.97	726.49	756.0	0.780
WM 54 - tuffaceous sandstone, Ghubrah Formation, Jabal Akhdar area																	
z19	aa	1.0	6	1.04	1.04	343.1	0.325	0.141281	(.65)	1.32128	(1.0)	0.06783	(.77)	851.90	855.07	863.3	0.675
z15	aa	0.8	173	0.43	0.43	10604.7	0.136	0.124451	(.05)	1.11246	(.09)	0.06483	(.08)	756.13	759.36	768.8	0.549
z4	aa	5.0	11	0.61	0.61	661.6	0.194	0.117318	(.32)	1.02953	(.58)	0.06365	(.47)	715.11	718.69	729.9	0.602
z31	ca	0.5	164	0.42	0.42	10076.0	0.130	0.116720	(.08)	1.01690	(.12)	0.06319	(.08)	711.65	712.35	714.6	0.694
z30	ca	0.7	124	0.57	0.57	7375.7	0.176	0.116692	(.07)	1.01661	(.10)	0.06318	(.07)	711.50	712.21	714.5	0.671
z29	ca	2.1	58	0.64	0.64	3384.1	0.198	0.116709	(.07)	1.01646	(.11)	0.06317	(.08)	711.60	712.13	713.9	0.677
z27	ca	0.6	86	0.78	0.78	4841.9	0.241	0.116698	(.07)	1.01632	(.10)	0.06316	(.07)	711.53	712.06	713.7	0.704
z32	ca	0.5	224	0.58	0.58	13204.6	0.180	0.116676	(.06)	1.01573	(.09)	0.06314	(.06)	711.40	711.76	712.9	0.678
z26	ca	0.7	145	0.66	0.66	8431.2	0.204	0.116556	(.07)	1.01495	(.12)	0.06316	(.09)	710.71	711.37	713.5	0.636
z25	ca	0.5	456	0.43	0.43	27951.0	0.134	0.116131	(.05)	1.01153	(.08)	0.06317	(.06)	708.26	709.65	714.1	0.664
z24	ca	0.8	110	0.42	0.42	6765.6	0.131	0.115597	(.12)	1.00678	(.14)	0.06317	(.06)	705.17	707.25	713.9	0.891
z8	aa	6.1	36	0.82	0.82	2014.1	0.258	0.115274	(.11)	1.00455	(.18)	0.06320	(.14)	703.30	706.12	715.1	0.621
z10	aa	3.3	38	0.53	0.53	2312.6	0.166	0.114779	(.12)	0.99997	(.21)	0.06319	(.17)	700.44	703.79	714.5	0.565
z18	aa	0.8	30	0.75	0.75	1693.9	0.234	0.115026	(.23)	0.99817	(.36)	0.06294	(.27)	701.87	702.88	706.1	0.665
z7	aa	3.0	57	0.47	0.47	3468.9	0.148	0.114336	(.09)	0.99552	(.13)	0.06315	(.10)	697.88	701.53	713.3	0.668
z1	aa	2.8	26	0.44	0.44	1575.2	0.141	0.113716	(.16)	0.99115	(.22)	0.06321	(.14)	694.29	699.31	715.4	0.756
z14	aa	5.9	9	0.74	0.74	516.9	0.236	0.113286	(.37)	0.98760	(.41)	0.06323	(.18)	691.80	697.50	715.9	0.904
z11	aa	0.7	25	0.36	0.36	1590.2	0.115	0.112578	(.16)	0.97954	(.23)	0.06311	(.15)	687.70	693.37	711.8	0.738
z3	aa	1.4	78	0.64	0.64	4520.9	0.206	0.111539	(.08)	0.97088	(.10)	0.06313	(.07)	681.68	688.92	712.6	0.765

APPENDIX 1
(continued)

Sample	Fract'ns ^[1]	Pb _c ^[2]	Pb* ^[2]	Th	U	206Pb ^[3]	208Pb ^[4]	Ratios ^[5]			Age (Ma)				corr.	coef.			
								±	(2σ%)	207Pb	235U	±	(2σ%)	206Pb			238U	207Pb	235U
WM 54 - tuffaceous sandstone, Ghubrah Formation, Jabal Akhdar area																			
z13	aa	2.8	12	0.81	0.81	688.8	0.263	0.111402	(.28)	0.96963	(.36)	0.06313	(.21)	680.89	688.27	712.5	0.815		
z16	aa	0.9	52	0.42	0.42	3200.9	0.142	0.106612	(.08)	0.92708	(.12)	0.06307	(.08)	653.04	666.10	710.5	0.736		
z12	aa	0.9	36	0.59	0.59	2069.5	0.206	0.103548	(.11)	0.90033	(.19)	0.06306	(.15)	635.17	651.90	710.3	0.625		
z20	aa	1.9	4	0.64	0.64	231.1	0.228	0.102956	(.92)	0.89868	(.12)	0.06331	(.75)	631.71	651.02	718.6	0.789		
z6	aa	3.7	20	0.76	0.76	1094.6	0.292	0.092508	(.18)	0.80114	(.33)	0.06281	(.26)	570.35	597.47	701.8	0.618		
WM.01.2 - sandstone clast in Ghubrah Formation, Jabal Akhdar area																			
z4	ca	0.9	61	0.85	0.85	3474.1	0.262	0.136670	(.08)	1.25658	(.13)	0.06668	(.10)	825.81	826.37	827.9	0.665		
z1	ca	1.1	9	0.89	0.89	510.5	0.274	0.136287	(.41)	1.24988	(.53)	0.06651	(.32)	823.63	823.35	822.6	0.797		
z5	ca	0.6	44	0.66	0.66	2586.1	0.204	0.134705	(.09)	1.23101	(.15)	0.06628	(.12)	814.65	814.80	815.2	0.655		
z2	ca	1.9	26	0.78	0.78	1525.2	0.241	0.134087	(.17)	1.22546	(.24)	0.06628	(.17)	811.14	812.27	815.4	0.723		
z3	ca	1.2	29	0.78	0.78	1681.6	0.240	0.133916	(.14)	1.22300	(.20)	0.06624	(.13)	810.17	811.15	813.9	0.757		
WM.01.3 - diamictite matrix, Ghubrah Formation, Jabal Akhdar area																			
z3	ca	0.6	61	0.58	0.58	3675.5	0.181	0.124103	(.16)	1.10293	(.23)	0.06446	(.16)	754.14	754.76	756.6	0.713		
z2	ca	1.3	37	0.37	0.37	2364.7	0.115	0.123995	(.09)	1.10151	(.14)	0.06443	(.10)	753.52	754.08	755.7	0.694		
z1	ca	0.6	122	0.31	0.31	7903.6	0.095	0.123856	(.06)	1.10053	(.09)	0.06444	(.07)	752.72	753.61	756.2	0.645		
z4	ca	1.5	34	0.33	0.33	2218.1	0.102	0.122785	(.10)	1.09114	(.13)	0.06445	(.08)	746.58	749.06	756.5	0.786		
Makarem-2 - syenite intrusion (Makarem-2 well)																			
z2	aa	0.7	1372	0.71	0.71	78320.0	0.221	0.113882	(.05)	0.98486	(.06)	0.06272	(.04)	695.25	696.09	698.8	0.754		
z3	aa	0.6	553	0.57	0.57	32630.8	0.179	0.113838	(.05)	0.98449	(.07)	0.06272	(.05)	695.00	695.91	698.8	0.698		
z1	aa	0.6	344	0.67	0.67	19864.6	0.208	0.113781	(.05)	0.98356	(.08)	0.06269	(.06)	694.67	695.43	697.9	0.635		
z4	aa	0.9	771	0.74	0.74	43689.5	0.230	0.113198	(.05)	0.97893	(.07)	0.06272	(.04)	691.30	693.06	698.8	0.750		
Salalah 11 - rhyolite clast from upper Ayn member, Mirbat area																			
z1	aa	2.9	19	0.92	0.92	1036.2	0.288	0.131894	(.25)	1.20490	(.35)	0.06626	(.24)	798.66	802.85	814.5	0.736		
z2	aa	1.2	53	0.85	0.85	2912.5	0.265	0.130932	(.10)	1.18811	(.14)	0.06581	(.09)	793.18	795.08	800.4	0.753		
z3	aa	2.2	16	0.65	0.65	959.8	0.203	0.131639	(.22)	1.19665	(.32)	0.06593	(.21)	797.21	799.04	804.2	0.746		

APPENDIX 1
(continued)

Sample	Fract'ns ^[1]	Pb _c ^[2]	Pb* ^[2]	Th	U	206Pb ^[3]	208Pb ^[4]	Ratios ^[5]			Age (Ma)			corr.	coef.
								206Pb	238U	± (2σ%)	206Pb	238U	± (2σ%)		
OM-01-5 - rhyolite clast from upper Ayn member, Mirbat area															
z1	aa	1.1	32	0.80	1813.1	0.250	0.131807	1.20128	(.26)	0.06610	(.15)	798.16	801.18	809.5	0.829
z2	aa	0.7	53	0.82	2980.0	0.253	0.131889	1.19938	(.14)	0.06595	(.10)	798.63	800.30	804.9	0.713
z3	aa	0.6	86	0.69	4932.8	0.217	0.130655	1.19138	(.10)	0.06613	(.07)	791.60	796.60	810.6	0.728
z4	aa	3.8	10	0.94	545.6	0.294	0.130369	1.18419	(.45)	0.06588	(.24)	789.97	793.26	802.5	0.840
Salalah 13 - Leger Granite, Mirbat area															
z3	aa	3.0	12	0.35	747.9	0.109	0.119391	1.05113	(.37)	0.06385	(.24)	727.06	729.44	736.8	0.757
z10	ca	0.9	39	0.42	2401.7	0.130	0.119282	1.04758	(.22)	0.06370	(.18)	726.43	727.68	731.6	0.572
z9	ca	1.2	46	0.44	2801.3	0.137	0.119189	1.04670	(.25)	0.06369	(.19)	725.89	727.25	731.4	0.626
z11	ca	2.6	45	0.42	2780.3	0.131	0.119193	1.04524	(.12)	0.06360	(.08)	725.92	726.52	728.4	0.729
z8	ca	0.6	137	0.39	8489.3	0.121	0.118985	1.04464	(.12)	0.06368	(.08)	724.72	726.22	730.8	0.772
z6	aa	1.6	17	0.38	1055.4	0.124	0.118730	1.04385	(.39)	0.06376	(.32)	723.25	725.83	733.8	0.561
z7	aa	5.1	6	0.39	413.4	0.124	0.117577	1.03335	(.73)	0.06374	(.52)	716.60	720.60	733.1	0.709
z5	aa	2.1	25	0.40	1557.1	0.128	0.116681	1.02431	(.23)	0.06367	(.12)	711.43	716.08	730.6	0.866
z2	aa	2.5	20	0.31	1284.9	0.109	0.107623	0.94480	(.31)	0.06367	(.25)	658.93	675.39	730.7	0.601
P69 - pegmatitic granite vien intruding basement, Mirbat area															
z7	ca	0.3	461	0.43	28204.4	0.134	0.133735	1.21995	(.10)	0.06616	(.06)	809.14	809.75	811.5	0.812
z6	ca	1.6	76	0.26	4903.5	0.080	0.133734	1.21981	(.10)	0.06615	(.06)	809.13	809.69	811.2	0.795
z2	ca	1.1	158	0.28	10061.5	0.086	0.133649	1.21916	(.09)	0.06616	(.06)	808.65	809.39	811.4	0.760
z4	ca	1.1	87	0.25	5581.5	0.076	0.133570	1.21811	(.09)	0.06614	(.06)	808.20	808.91	810.9	0.694
z1	ca	1.1	187	0.36	11695.9	0.110	0.133405	1.21698	(.08)	0.06616	(.05)	807.26	808.39	811.5	0.768
P70 - Siliciclastic lithology, Ayn Member, Mirbat Formation, Mirbat area															
z8	ca	0.3	118	0.48	7113.7	0.148	0.137224	1.26475	(.11)	0.06685	(.09)	828.95	830.04	832.9	0.622
z5	aa	0.6	179	0.80	10000.1	0.246	0.136109	1.24988	(.08)	0.06660	(.06)	822.62	823.35	825.3	0.700
z6	ca	0.3	394	0.85	21797.1	0.260	0.136150	1.24903	(.08)	0.06654	(.06)	822.85	822.97	823.3	0.675
z7	ca	0.3	428	0.87	23491.9	0.269	0.131795	1.19550	(.08)	0.06579	(.06)	798.10	798.51	799.7	0.653
z4	aa	0.6	241	0.98	12919.5	0.304	0.127858	1.14817	(.08)	0.06513	(.06)	775.63	776.38	778.5	0.694
z2	aa	4.4	82	0.96	4432.2	0.297	0.122831	1.08772	(.14)	0.06423	(.10)	746.84	747.39	749.0	0.727
z1	aa	0.7	310	0.53	18487.3	0.165	0.122453	1.08321	(.08)	0.06416	(.06)	744.67	745.20	746.8	0.747

APPENDIX 1
(continued)

Sample	Fract'ns ^[1]	Pb _c ^[2]	Pb* ^[2]	Th	U	²⁰⁶ Pb/ ²⁰⁴ Pb ^[3]	²⁰⁸ Pb/ ²⁰⁶ Pb ^[4]	Ratios ^[5]				Age (Ma)					
								±	²⁰⁷ Pb/ ²³⁵ U	±	²⁰⁷ Pb/ ²⁰⁶ Pb	±	²⁰⁶ Pb/ ²³⁸ U	±	²⁰⁷ Pb/ ²³⁵ U		
																(2σ%)	(2σ%)
P72 - Siliciclastic lithology, Ayn Member, Mirbat Formation, Mirbat area																	
z1	ca	0.6	14	0.54	0.44	825.6	0.166	0.136485	(.35)	1.25585	(.54)	0.06673	(.39)	824.76	826.04	829.5	0.696
z5	ca	1.0	14	0.44	0.44	893.5	0.136	0.136128	(.29)	1.25728	(.37)	0.06699	(.21)	822.73	826.68	837.3	0.815
AJD-1 - felsic volcanics, Halfayn Formation, Al Jobah area																	
z4	aa	2.2	12	0.84	0.84	704.2	0.261	0.138393	(.32)	1.28583	(.52)	0.06739	(.38)	835.57	839.45	849.7	0.679
z3	aa	1.4	22	0.58	0.58	1317.0	0.180	0.135407	(.16)	1.24688	(.20)	0.06679	(.11)	818.64	822.00	831.1	0.838
z2	aa	15.0	1	0.83	0.83	90.5	0.262	0.128555	(2.8)	1.16354	(3.1)	0.06564	(1.3)	779.61	783.62	795.1	0.912
z1	aa	5.8	4	0.86	0.86	260.5	0.288	0.124605	(.88)	1.14306	(1.1)	0.06653	(.56)	757.02	773.96	823.1	0.851
AJD-2 - granodioritic basement, Al Jobah area																	
z4	aa	2.3	31	0.77	0.77	1812.4	0.243	0.138449	(.13)	1.28778	(.20)	0.06746	(.15)	835.89	840.31	852.0	0.667
z6	aa	2.9	18	0.88	0.88	1007.7	0.290	0.135881	(.30)	1.28209	(.74)	0.06843	(.66)	821.33	837.78	881.6	0.471
z3	aa	1.7	73	0.67	0.67	4278.7	0.210	0.136222	(.10)	1.25661	(.15)	0.06690	(.11)	823.26	826.38	834.8	0.685
z5	aa	4.6	14	0.87	0.87	793.0	0.267	0.136585	(.26)	1.25373	(.34)	0.06657	(.21)	825.32	825.09	824.5	0.791
z1	aa	1.4	106	0.85	0.85	5973.7	0.263	0.136085	(.10)	1.25308	(.14)	0.06678	(.10)	822.49	824.79	831.0	0.714
AJD-3 - felsic volcanics, Halfayn Formation, Al Jobah area																	
z2	aa	1.1	16	0.76	0.76	911.3	0.240	0.134792	(.27)	1.24642	(.36)	0.06707	(.22)	815.15	821.79	839.8	0.785
z5	aa	3.6	6	0.57	0.57	361.9	0.178	0.134084	(.62)	1.23037	(.78)	0.06655	(.45)	811.12	814.51	823.8	0.816
z1	aa	1.2	11	0.70	0.70	662.5	0.225	0.132708	(.34)	1.22662	(.47)	0.06704	(.31)	803.29	812.80	838.9	0.766
z3	aa	1.0	7	0.65	0.65	412.9	0.206	0.130419	(.53)	1.19023	(.75)	0.06619	(.49)	790.26	796.07	812.4	0.757
z4	aa	1.1	28	0.56	0.56	1715.4	0.175	0.130276	(.15)	1.18344	(.20)	0.06588	(.13)	789.44	792.92	802.7	0.782
AJD-4 - sedimentary breccia, Halfayn Formation, Al Jobah area																	
z5	aa	0.9	24	0.83	0.83	1368.7	0.262	0.135175	(.17)	1.24636	(.26)	0.06687	(.19)	817.32	821.76	833.8	0.691
z4	aa	1.9	36	0.88	0.88	2006.8	0.275	0.134777	(.12)	1.23870	(.21)	0.06666	(.17)	815.06	818.29	827.1	0.611
z3	aa	1.8	14	0.84	0.84	816.4	0.283	0.127136	(.38)	1.17564	(.48)	0.06707	(.28)	771.51	789.28	839.8	0.818
z1	aa	1.4	11	0.90	0.90	632.8	0.320	0.119225	(.42)	1.09992	(.60)	0.06691	(.41)	726.10	753.31	835.0	0.738

APPENDIX 1
(continued)

Sample	Fract'ns ^[1]	Pb _c ^[2]	Pb* ^[2]	Pb _c	Th	U	$\frac{^{206}\text{Pb}^{[3]}}{^{204}\text{Pb}}$	$\frac{^{208}\text{Pb}^{[4]}}{^{206}\text{Pb}}$	$\frac{^{206}\text{Pb}}{^{238}\text{U}}$	Ratios ^[5]		Age (Ma)		corr.	coef.			
										\pm	(2 σ %)	$\frac{^{207}\text{Pb}}{^{235}\text{U}}$	\pm			(2 σ %)	$\frac{^{206}\text{Pb}}{^{238}\text{U}}$	$\frac{^{207}\text{Pb}}{^{235}\text{U}}$
AJD-5 - granodioritic basement, Al Jobah area																		
z1	aa	1.3	33	0.46			2058.7	0.144	0.135695	(.13)	1.25097	(.27)	0.06686	(.23)	820.27	823.84	833.5	0.527
z3	aa	1.1	46	0.88			2557.6	0.273	0.135598	(.19)	1.24881	(.31)	0.06679	(.24)	819.72	822.87	831.3	0.628
z4	aa	3.7	25	0.78			1462.3	0.243	0.134546	(.18)	1.23464	(.47)	0.06655	(.41)	813.75	816.45	823.8	0.495
z2	aa	1.5	23	0.80			1300.6	0.251	0.133381	(.27)	1.22301	(.46)	0.06650	(.35)	807.12	811.15	822.2	0.640
OM-01-4 - siliciclastic lithology, outcrop at base of escarpment, Ain Sarit																		
z5	aa	1.6	269	0.05			16237.7	0.016	0.538483	(.09)	16.6150	(.10)	0.22378	(.04)	2777.1	2912.9	3008.1	0.910
z3	aa	2.5	72	1.36			3508.1	0.389	0.458255	(.12)	10.1775	(.14)	0.16108	(.05)	2431.8	2451.0	2467.0	0.918
z1	aa	1.1	189	0.41			11087.5	0.117	0.449815	(.15)	9.9043	(.16)	0.15969	(.06)	2394.4	2425.9	2452.4	0.920
z2	aa	1.0	143	0.62			7985.2	0.180	0.445382	(.11)	9.6780	(.13)	0.15760	(.06)	2374.7	2404.6	2430.0	0.889
z4	aa	3.0	61	0.60			3610.4	0.188	0.235770	(.11)	2.9287	(.14)	0.09009	(.08)	1364.7	1389.3	1427.4	0.804
Ghudun-1 - siliciclastic lithology, cuttings from 2509.8 to 659.4 meters depth (Ghudun-1 Well)																		
z8	aa	4.8	49	0.27			2904.1	0.104	0.330142	(.09)	6.98560	(.11)	0.15346	(.06)	1839.1	2109.6	2384.9	0.840
z6	aa	0.7	53	0.32			3186.8	0.094	0.375929	(.14)	6.69552	(.15)	0.12917	(.06)	2057.2	2072.0	2086.8	0.926
z1	aa	1.3	43	0.59			2119.8	0.335	0.236483	(.20)	5.43400	(.20)	0.16666	(.22)	1368.4	1890.2	2524.3	0.994
z2	aa	0.6	26	1.36			1289.1	0.403	0.308040	(.20)	4.56472	(.25)	0.10747	(.13)	1731.1	1742.9	1757.0	0.837
z10	aa	1.2	51	0.34			3038.2	0.123	0.250449	(.09)	3.71211	(.16)	0.10750	(.13)	1440.8	1574.0	1757.4	0.574
z13	aa	6.8	4	0.94			257.7	0.289	0.173110	(.77)	1.76080	(.84)	0.07377	(.33)	1029.2	1031.1	1035.2	0.922
z5	aa	2.3	18	0.57			1086.6	0.183	0.169858	(.52)	1.75183	(.59)	0.07480	(.27)	1011.3	1027.8	1063.2	0.888
z11	aa	1.6	18	0.52			1078.0	0.164	0.157433	(.23)	1.59799	(.34)	0.07186	(.24)	942.50	954.39	981.9	0.705
z16	aa	0.7	25	0.44			1500.9	0.141	0.153586	(.17)	1.51011	(.25)	0.07131	(.17)	921.04	934.49	966.3	0.722
z4	aa	1.8	10	0.83			590.0	0.261	0.124424	(.35)	1.11137	(.55)	0.06478	(.40)	755.98	758.83	767.3	0.683
z15	aa	1.6	2	0.50			134.5	0.172	0.110102	(.16)	0.97164	(.22)	0.06400	(.14)	673.34	689.31	741.8	0.767
z7	aa	2.5	19	0.82			1061.8	0.257	0.101094	(.18)	0.84635	(.22)	0.06072	(.12)	620.81	622.64	629.3	0.841
z3	aa	0.7	26	1.83			1157.8	0.579	0.100407	(.19)	0.83913	(.28)	0.06061	(.19)	616.80	618.67	625.5	0.726
z12	aa	1.6	8	0.58			479.5	0.207	0.092575	(.44)	0.78309	(.68)	0.06135	(.49)	570.75	587.24	651.6	0.699

APPENDIX 1
(continued)

Sample	Fract'ns ^[1]	Pb _c ^[2] (pg)	Pb* ^[2]	Th	U	²⁰⁶ Pb/ ²⁰⁴ Pb ^[3]	²⁰⁸ Pb/ ²⁰⁶ Pb ^[4]	²⁰⁶ Pb/ ²³⁸ U	Ratios ^[5]				Age (Ma)			
									±	²⁰⁷ Pb/ ²³⁵ U	±	²⁰⁷ Pb/ ²⁰⁶ Pb	±	²⁰⁶ Pb/ ²³⁸ U	±	²⁰⁷ Pb/ ²³⁵ U
Ranadah-2 - siliciclastic lithology, upper Ara Group (3201.0 meters depth, Ranadah-2 Well)																
z1	aa	0.4	140	0.36	8681.8	0.112	0.162745	(.08)	1.61908	(.11)	0.07215	(.08)	972.02	977.64	990.3	0.725
z2	aa	0.5	46	0.44	2802.4	0.135	0.156284	(.12)	1.51903	(.16)	0.07049	(.10)	936.09	938.08	942.8	0.773
z4	aa	0.6	40	0.85	2214.4	0.268	0.151467	(.14)	1.46913	(.21)	0.07035	(.15)	909.18	917.77	938.5	0.707
z3	aa	0.4	13	0.59	784.9	0.191	0.102092	(.31)	0.86567	(.47)	0.06150	(.34)	626.66	633.22	656.7	0.688
Tharwah-1 - shale lithology at the A0 stratigraphic level (3390.0 meters depth, Tharwah-1 Well)																
z2	aa	1.7	153	0.35	9018.0	0.102	0.476391	(.08)	11.3875	(.09)	0.17337	(.04)	2511.5	2555.4	2590.4	0.870
z1	aa	0.8	188	0.42	10875.6	0.124	0.465469	(.09)	11.0126	(.11)	0.17159	(.06)	2463.7	2524.2	2573.2	0.850
z3	aa	2.0	71	0.20	4295.4	0.062	0.441630	(.17)	10.5106	(.18)	0.17261	(.06)	2357.9	2480.9	2583.1	0.938

Notes: [1] All analyses are single zircon grains or fragments pre-treated either by air abrasion (aa) or combined annealing and chemical leaching (ca). Data used in Pb/U age calculations are in bold.
 [2] Pb_c is total common Pb in analysis. Pb* is radiogenic Pb concentration.
 [3] Measured ratio corrected for spike and fractionation only.
 [4] Radiogenic Pb ratio.
 [5] Corrected for fractionation, spike, blank, and initial common Pb. Mass fractionation correction of 0.25%/amu ± 0.04%/amu (atomic mass unit) was applied to single-collector Daly analyses. Total procedural blank averaged 1.0 pg for Pb and less than 0.1 pg for U.
 Corr. coef. = correlation coefficient.
 Age calculations are based on the decay constants of Jaffey and others (1971).

ACKNOWLEDGMENTS

We thank the Oman Ministry of Oil and Gas for permission to publish this paper. Support was provided by Petroleum Development Oman (PDO). We thank D. Fike, P. Hoffman, A. Maloof, and A. Prave for helpful manuscript reviews. This project has benefited from discussions with colleagues at PDO. We also thank John Paul Breton (BRGM) and Philip Allen (Imperial College) for help with sample collection.

REFERENCES

- Al-Husseini, M. I., and Al-Husseini, S. I., 1990, Origin of the Infracambrian salt basins in the Middle East, *in* Brooks, J., editor, *Classic Petroleum Provinces*: London, The Geological Society, Special Publication, v. 50, p. 279-292.
- Al-Marjebi, A., and Nash, D., 1986, A summary of the geology and oil habitat of the Eastern Flank hydrocarbon province of South Oman: *Marine and Petroleum Geology*, v. 3, p. 306-314.
- Al-Siyabi, H. A., 2005, Exploration history of the Ara intrasalt carbonate stringers in the South Oman salt basin: *GeoArabia (Manama)*, v. 10, p. 39-72.
- Allen, P. A., and Hoffman, P. F., 2005, Extreme winds and waves in the aftermath of a Neoproterozoic glaciation: *Nature*, v. 433, p. 123-127.
- Allen, P. A., and Leather, J., 2006, Post-Marinoan marine siliciclastic sedimentation: The Masirah Bay Formation, Neoproterozoic Huqf Supergroup of Oman: *Precambrian Research*, v. 144, p. 167-198.
- Allen, P. A., Leather, J., and Brasier, M. D., 2004, The Neoproterozoic Fiq glaciation and its aftermath, Huqf Supergroup of Oman: *Basin Research*, v. 16, p. 507-534.
- Amthor, J. E., Grotzinger, J. P., Schroeder, S., Bowring, S. A., Ramezani, J., Martin, M. W., and Matter, A., 2003, Extinction of Cloudina and Namacalathus at the Precambrian-Cambrian boundary in Oman: *Geology (Boulder)*, v. 31, p. 431-434.
- Amthor, J. E., Ramseyer, K., Faulkner, T., and Lucas, P., 2005, Stratigraphy and sedimentology of a chert reservoir at the Precambrian-Cambrian boundary; the Al Shomou Silicilyte, South Oman salt basin: *GeoArabia (Manama)*, v. 10, p. 89-122.
- Bell, A., 1993, The stratigraphy of the Abu Mahara Group (Huqf Supergroup): Muscat, Petroleum Development Oman, 12 p.
- Bingen, B., Griffin, W. L., Torsvik, T. H., and Saeed, A., 2005, Timing of late Neoproterozoic glaciation on Baltica constrained by detrital zircon geochronology in the Hedmark Group, South-east Norway: *Terra Nova*, v. 17, p. 250-258.
- Bowring, S., Myrow, P., Landing, E., Ramezani, J., and Grotzinger, J., 2003, Geochronological constraints on terminal Neoproterozoic events and the rise of metazoans: *Geophysical Research Abstracts*, v. 5, p. 13219.
- Brasier, M., McCarron, G., Tucker, R., Leather, J., Allen, P. A., and Shields, G. A., 2000, New U-Pb zircon dates for the Neoproterozoic Ghubrah glaciation and for the top of the Huqf Supergroup, Oman: *Geology (Boulder)*, v. 28, p. 175-178.
- Burns, S. J., and Matter, A., 1993, Carbon isotopic record of the latest Proterozoic from Oman: *Eclogae Geologicae Helveticae*, v. 86, p. 595-607.
- Butterfield, N. J., 2001, Final report on the subsurface palynology of the Huqf Supergroup, Oman: Muscat, Petroleum Development Oman, 4 p.
- Calver, C. R., 2000, Isotope stratigraphy of the Ediacarian (Neoproterozoic III) of the Adelaide rift complex, Australia, and the overprint of water column stratification: *Precambrian Research*, v. 100, p. 121-150.
- Calver, C. R., Black, L. P., Everard, J. L., and Seymour, D. B., 2004, U-Pb zircon age constraints on late Neoproterozoic glaciation in Tasmania: *Geology (Boulder)*, v. 32, p. 893-896.
- Clarke, M. W. H., 1988, Stratigraphic and rock-unit nomenclature in the oil-producing area of interior Oman: *Journal of Petroleum Geology*, v. 11, p. 5-59.
- Condon, D. J., 2005, Progress report on the U-Pb interlaboratory experiment: *Geochimica et Cosmochimica Acta*, v. 69, p. 319.
- Condon, D. J., and Prave, A. R., 2000, Two from Donegal; Neoproterozoic glacial episodes on the northeast margin of Laurentia: *Geology (Boulder)*, v. 28, p. 951-954.
- Condon, D., Zhu, M., Bowring, S., Wang, W., Yang, A., and Jin, Y., 2005, U-Pb ages from the Neoproterozoic Doushantuo Formation, China: *Science*, v. 308, p. 95-98.
- Cozzi, A., Grotzinger, J. P., and Allen, P. A., 2004a, Evolution of a terminal Neoproterozoic carbonate ramp system (Buah Formation, Sultanate of Oman); effects of basement paleotopography: *Geological Society of America Bulletin*, v. 116, p. 1367-1384.
- Cozzi, A., Allen, P. A., and Grotzinger, J. P., 2004b, Understanding carbonate ramp dynamics using delta ¹³C profiles; examples from the Neoproterozoic Buah Formation of Oman: *Terra Nova*, v. 16, p. 62-67.
- Dubreuilh, J., Platel, J. P., Le Metour, J., Roger, J., Wyns, R., Bechennec, F., and Berthiaux, A., 1992, Geological map of Khaluf, Sheet NF 40-15: Muscat, Oman Ministry of Petroleum and Minerals.
- Evans, D. A. D., 2000, Stratigraphic, geochronological, and paleomagnetic constraints upon the Neoproterozoic climatic paradox: *American Journal of Science*, v. 300, p. 347-433.
- Fanning, C. M., and Link, P. K., 2004, U-Pb SHRIMP ages of Neoproterozoic (Sturtian) glaciogenic Pocatello Formation, southeastern Idaho: *Geology (Boulder)*, v. 32, p. 881-884.
- Fike, D. A., Grotzinger, J. P., Pratt, L. M., and Summons, R. E., 2006, Oxidation of the Ediacaran Ocean: *Nature*, v. 444, p. 744-747.
- Fortey, R. A., 1994, Late Cambrian trilobites from the Sultanate of Oman: *Neues Jahrbuch fuer Geologie und Palaeontologie Abhandlungen*, v. 194, p. 25-53.

- Germs, G. J. B., 1972, New shelly fossils from Nama Group, South West Africa: *American Journal of Science*, v. 272, p. 752-761.
- Gerstenberger, H., and Haase, G., 1997, A highly effective emitter substance for mass spectrometric Pb isotope ratio determinations: *Chemical Geology*, v. 136, p. 309-312.
- Gorin, G. E., Racz, L. G., and Walter, M. R., 1982, Late Precambrian-Cambrian sediments of Huqf Group, Sultanate of Oman: *AAPG Bulletin*, v. 66, p. 2609-2627.
- Grant, S. W. F., 1990, Shell structure and distribution of Cloudina, a potential index fossil for the terminal Proterozoic: *American Journal of Science*, v. 290-A, p. 261-294.
- Grey, K., and Corkeron, M., 1998, Late Neoproterozoic stromatolites in glaciogenic successions of the Kimberley region, Western Australia; evidence for a younger Marinoan glaciation: *Precambrian Research*, v. 92, p. 65-87.
- Grotzinger, J. P., 2000, Facies and paleoenvironmental setting of thrombolite-stromatolite reefs, terminal Proterozoic Nama Group (ca. 550-543 Ma), central and southern Namibia: *Communications of the Geological Survey of South West Africa/Namibia*, v. 12, p. 221-233.
- Grotzinger, J. P., and Amthor, J. E., 2002, Facies and reservoir architecture of isolated microbial carbonate platforms, terminal Proterozoic-early Cambrian Ara Group, South Oman salt basin: *Annual Meeting Expanded Abstracts - American Association of Petroleum Geologists*, v. 2002, p. 67.
- Grotzinger, J. P., Bowring, S. A., Saylor, B. Z., and Kaufman, A. J., 1995, Biostratigraphic and geochronologic constraints on early animal evolution: *Science*, v. 270, p. 598-604.
- Grotzinger, J. P., Al-Siyabi, H. A., Al-Hashmi, R., and Cozzi, A., 2002, New Model for Tectonic Evolution of Neoproterozoic-Cambrian Huqf Supergroup Basins, Oman: *GeoArabia (Manama)*, v. 7, p. 241.
- Halverson, G. P., Hoffman, P. F., Schrag, D. P., Maloof, A. C., and Rice, A. H. N., 2005, Toward a Neoproterozoic composite carbon-isotope record: *Geological Society of America Bulletin*, v. 117, p. 1181-1207.
- Hoffman, P. F., and Schrag, D. P., 2002, The snowball Earth hypothesis; testing the limits of global change: *Terra Nova*, v. 14, p. 129-155.
- Hoffman, P. F., Hawkins, D. P., Isachsen, C. E., and Bowring, S. A., 1996, Precise U-Pb zircon ages for early Damara magmatism in the Summas Mountains and Welwitschia Inlier, northern Damara Belt: *Communications of the Geological Survey of Namibia*, v. 11, p. 47-53.
- Hoffman, P. F., Kaufman, A. J., Halverson, G. P., and Schrag, D. P., 1998, A Neoproterozoic snowball earth: *Science*, v. 281, p. 1342-1346.
- Hoffmann, K. H., Condon, D. J., Bowring, S. A., and Crowley, J. L., 2004, U-Pb zircon date from the Neoproterozoic Ghaub Formation, Namibia; constraints on Marinoan glaciation: *Geology (Boulder)*, v. 32, p. 817-820.
- Immerz, P., Oterdoom, W. H., and El Tonbary, M., 2000, The Huqf/Haima hydrocarbon system of Oman and the terminal phase of the Pan-African Orogeny; evaporite deposition in a compressive setting: *GeoArabia (Manama)*, v. 5, p. 113-114.
- Jaffey, A. H., Flynn, K. F., Glendenin, L. E., Bentley, W. C., and Essling, A. M., 1971, Precision Measurement of Half-Lives and Specific Activities of ²³⁵U and ²³⁸U: *Physical Review C*, v. 4, p. 1889-1906.
- Kapellos, C., Knox, G. J., Borgomano, J., and Mohammed, A. R., 1992, Stratigraphical review of the Huqf Supergroup: *Muscat, Petroleum Development Oman*, 13 p.
- Kaufman, A. J., and Knoll, A. H., 1995, Neoproterozoic variations in the C-isotopic composition of seawater; stratigraphic and biogeochemical implications: *Precambrian Research*, v. 73, p. 27-49.
- Kellerhals, P., and Matter, A., 2003, Facies analysis of a glaciomarine sequence, the Neoproterozoic Mirbat Sandstone Formation, Sultanate of Oman: *Eclogae Geologicae Helvetiae*, v. 96, p. 49-70.
- Kendall, B. S., Creaser, R. A., Ross, G. M., and Selby, D., 2004, Constraints on the timing of Marinoan snowball Earth glaciation by ¹⁸⁷Re/¹⁸⁷Os dating of a Neoproterozoic, post-glacial black shale in Western Canada: *Earth and Planetary Science Letters*, v. 222, p. 729-740.
- Kendall, B., Creaser, R. A., and Selby, D., 2006, Re-Os geochronology of postglacial black shales in Australia; constraints on the timing of "Sturtian" glaciation: *Geology (Boulder)*, v. 34, p. 729-732.
- Kennedy, M. J., 1996, Stratigraphy, sedimentology, and isotopic geochemistry of Australian Neoproterozoic postglacial cap dolostones; deglaciation, ⁸¹³C excursions, and carbonate precipitation: *Journal of Sedimentary Research*, v. 66, p. 1050-1064.
- Kennedy, M. J., Runnegar, B., Prave, A. R., Hoffmann, K. H., and Arthur, M. A., 1998, Two or four Neoproterozoic glaciations?: *Geology (Boulder)*, v. 26, p. 1059-1063.
- Knoll, A. H., Walter, M. R., Narbonne, G. M., and Christie-Blick, N., 2004, A new period for the geologic time scale: *Science*, v. 305, p. 621-622.
- Krogh, T. E., 1982, Improved accuracy of U-Pb zircon ages by the creation of more concordant systems using an air abrasion technique: *Geochimica et Cosmochimica Acta*, v. 46, p. 637-649.
- Le Guerroue, E., Allen, P., and Cozzi, A., 2005, Two distinct glacial successions in the Neoproterozoic of Oman: *GeoArabia (Manama)*, v. 10, p. 17-34.
- Le Guerroue, E., Allen, P. A., Cozzi, A., Etienne, J. L., and Fanning, M., 2006, 50 Myr recovery from the largest negative ⁸¹³C excursion in the Ediacaran Ocean: *Terra Nova*, v. 18, p. 147-153.
- Leather, J., Allen, P. A., Brasier, M. D., and Cozzi, A., 2002, Neoproterozoic snowball Earth under scrutiny; evidence from the Fiq Glaciation of Oman: *Geology (Boulder)*, v. 30, p. 891-894.
- Lees, G. M., 1928, The geology and tectonics of Oman and parts of south-eastern Arabia: *Quarterly Journal of the Geological Society of London*, v. 84, p. 585-670.
- Loosveld, R. J. H., Bell, A., and Terken, J. J. M., 1996, The tectonic evolution of interior Oman: *GeoArabia (Manama)*, v. 1, p. 28-51.
- Love, G. D., Grosjean, E., Fike, D. A., Grotzinger, J. P., Bowring, S. A., Condon, D. J., Lewis, A. N., Stalvies, C., Snape, C. E., and Summons, R. E., 2005, A >90 million year molecular record of Neoproterozoic sponges (Porifera) in the south Oman Salt basin: Seville, Spain, 22nd International Meeting on Organic Geochemistry.

- Ludwig, K. R., 1980, Calculation of uncertainties of U-Pb isotope data: *Earth and Planetary Science Letters*, v. 46, p. 212-220.
- 1991, ISOPLOT; a plotting and regression program for radiogenic-isotope data; version 2.53: U. S. Geological Survey, Open file Report 91-445, p. 39.
- 1998, On the treatment of concordant uranium-lead ages: *Geochimica et Cosmochimica Acta*, v. 62, p. 665-676.
- Martin, M. W., Grazhdankin, D. V., Bowring, S. A., Evans, D. A. D., Fedonkin, M. A., and Kirschvink, J. L., 2000, Age of Neoproterozoic bilaterian body and trace fossils, White Sea, Russia; implications for metazoan evolution: *Science*, v. 288, p. 841-845.
- Mattes, B. W., and Conway Morris, S., 1990, Carbonate/evaporite deposition in the Late Precambrian-Early Cambrian Ara Formation of southern Oman, in Robertson, A. H. F., Searle, M. P., and Ries, A. C., editors, *The geology and tectonics of the Oman region*: London, Geological Society Special Publication, v. 49, p. 617-636.
- Mattinson, J. M., 2000, Revising the “gold standard”—the uranium decay constants of Jaffey et al., 1971: American Geophysical Union, Eos, Transactions, Spring Meeting Supplement, Abstract V61A-02, p. S444-S445.
- 2005, Zircon U/Pb chemical abrasion (CA-TIMS) method; combined annealing and multi-step partial dissolution analysis for improved precision and accuracy of zircon ages: *Chemical Geology*, v. 220, p. 47-66.
- McCarron, M. E. G., ms, 2000, *The sedimentology and chemostratigraphy of the Nafun Group, Huqf Supergroup, Oman*: Oxford, England, University of Oxford, Ph. D. thesis, p. 181.
- McCay, G. A., Prave, A. R., Alsop, G. I., and Fallick, A. E., 2006, Glacial trinity: Neoproterozoic Earth history within the British-Irish Caledonides: *Geology (Boulder)*, v. 34, p. 909-912.
- Meert, J. G., 2003, A synopsis of events related to the assembly of eastern Gondwana: *Tectonophysics*, v. 362, p. 1-40.
- Meert, J. G., and Van Der Voo, R., 1997, The assembly of Gondwana 800-550 Ma: *Journal of Geodynamics*, v. 23, p. 223-235.
- Mercolli, I., Briner, A. P., Frei, R., Schonberg, R., Nagler, T. F., Kramers, J., and Peters, T., 2006, Lithostratigraphy and geochronology of the Neoproterozoic crystalline basement of Salalah, Dhofar, Sultanate of Oman: *Precambrian Research*, v. 145, p. 182-206.
- Millson, J. A., Mercadier, C. G. L., Livera, S. E., and Peters, J. M., 1996, The lower Palaeozoic of Oman and its context in the evolution of a Gondwanan continental margin: London, *Journal of the Geological Society*, v. 153, Part 2, p. 213-230.
- Morton, D. M., 1959, *The geology of Oman*: Proceedings - World Petroleum Congress = Actes et Documents - Congres Mondial du Petrole, p. 277-294.
- Mundil, R., Ludwig, K. R., Metcalfe, I., and Renne, P. R., 2004, Age and timing of the Permian mass extinctions; U/Pb dating of closed-system zircons: *Science*, v. 305, p. 1760-1763.
- Narbonne, G. M., 2005, The Ediacara biota; Neoproterozoic origin of animals and their ecosystems: *Annual Review of Earth and Planetary Sciences*, v. 33, p. 421-442.
- Pilcher, R., and Buckley, R., 1995, An outcrop study of the Huqf Supergroup: Muscat, *Petroleum Development Oman*, 68 p.
- Platel, J. P., Dubreuilh, J., Le Metour, J., Roger, J., Wyns, R., Bechenec, F., and Berthiaux, A., 1992, Geological map of Duqm and Madraça: Oman Ministry of Petroleum and Minerals, sheets NE 40-03/07.
- Rabu, D., 1993, Stratigraphy and structure of the Oman Mountains: Document du Bureau de Recherches Geologiques et Minières, v. 221, 262 p.
- Ramezani, J., Schmitz, M. D., Davydov, V. I., Bowring, S. A., Snyder, W. S., and Northrup, C. J., 2007, High-precision U-Pb zircon age constraints on the Carboniferous-Permian boundary in the southern Urals stratotype: *Earth and Planetary Science Letters*, v. 256, p. 244-257.
- Rieu, R., Allen, P. A., Etienne, J. L., Cozzi, A., and Wiechert, U., 2006, A Neoproterozoic glacially influenced basin margin succession and “atypical” cap carbonate associated with bedrock palaeovalleys, Mirbat area, southern Oman: *Basin Research*, v. 18, p. 471-496.
- Ross, G. M., and Villeneuve, M. E., 1997, U-Pb geochronology of stranger stones in Neoproterozoic diamictites, Canadian Cordillera; implications for provenance and ages of deposition: *Current Research - Geological Survey of Canada, Report: 1997-F*, p. 141-155.
- Rothman, D. H., Hayes, J. M., and Summons, R. E., 2003, Dynamics of the Neoproterozoic carbon cycle: *Proceedings of the National Academy of Sciences of the United States of America*, v. 100, p. 8124-8129.
- Schaefer, B. F., and Burgess, J. M., 2003, Re-Os isotopic age constraints on deposition in the Neoproterozoic Amadeus Basin; implications for the “snowball Earth”: London, *Journal of the Geological Society*, v. 160, p. 825-828.
- Schoene, B., Crowley, J. L., Condon, D. J., Schmitz, M. D., and Bowring, S. A., 2006, Reassessing the uranium decay constants for geochronology using ID-TIMS U-Pb data: *Geochimica et Cosmochimica Acta*, v. 70, p. 426-445.
- Schroeder, S., Grotzinger, J. P., Amthor, J. E., and Matter, A., 2005, Carbonate deposition and hydrocarbon reservoir development at the Precambrian-Cambrian boundary; the Ara Group in south Oman: *Sedimentary Geology*, v. 180, p. 1-28.
- Thompson, M. D., and Bowring, S. A., 2000, Age of the Squantum “tillite,” Boston Basin, Massachusetts; U-Pb zircon constraints on terminal Neoproterozoic glaciation: *American Journal of Science*, v. 300, p. 630-655.
- Whitehouse, M. J., Windley, B. F., Stoesser, D. B., Al-Khribash, S., Ba-Bttat, M. A. O., and Haider, A., 2001, Precambrian basement character of Yemen and correlations with Saudi Arabia and Somalia: *Precambrian Research*, v. 105, p. 357-369.

- Windley, B. F., Whitehouse, M. J., and Ba-Bttat, M. A. O., 1996, Early Precambrian gneiss terranes and Pan-African island arcs in Yemen; crustal accretion of the eastern Arabian Shield: *Geology (Boulder)*, v. 24, p. 131-134.
- Workman, R. K., Grotzinger, J. P., and Hart, S. R., 2002, Constraints on Neoproterozoic ocean chemistry from $\delta^{13}\text{C}$ and $\delta^{17}\text{B}$ analyses of carbonates from the Witvlei and Nama Groups, Namibia in Abstracts of the 12th annual V. M. Goldschmidt conference: *Geochimica et Cosmochimica Acta*, v. 66, 15A, Supplement 1, p. A847.
- Wright, V. P., Ries, A. C., and Munn, S. G., 1990, Intraplatformal basin-fill deposits from the Infracambrian Huqf Group, east central Oman, in Robertson, A. H. F., Searle, M. P., and Ries, A. C., editors, *The Geology and Tectonics of the Oman Region*: London, Geological Society Special Publication, v. 49, p. 601-616.
- Wuersten, F., Flisch, M., Michalski, I., Le Metour, J., Mercolli, I., Matthaues, U., and Peters, T., 1991, The uplift history of the Precambrian crystalline basement of the Jabal J'alan (Sur area): *Petrology and Structural Geology*, v. 5, p. 613-626.
- Xiao, S., Bao, H., Wang, H., Kaufman, A. J., Zhou, C., Li, G., Yuan, X., and Ling, H., 2004, The Neoproterozoic Quruqtagh Group in eastern Chinese Tianshan; evidence for a post-Marinoan glaciation: *Precambrian Research*, v. 130, p. 1-26.
- York, D., 1967, The best isochron: *Earth and Planetary Science Letters*, v. 2, p. 479-482.
- 1969, Least squares fitting of a straight line with correlated errors: *Earth and Planetary Science Letters*, v. 5, p. 320-324.
- Zhang, S., Jiang, G., Zhang, J., Song, B., Kennedy, M. J., and Christie-Blick, N., 2005, U-Pb sensitive high-resolution on microprobe ages from the Doushantuo Formation in south China; constraints on late Neoproterozoic glaciations: *Geology (Boulder)*, v. 33, p. 473-476.
- Zhou, C., Tucker, R., Xiao, S., Peng, Z., Yuan, X., and Chen, Z., 2004, New constraints on the ages of Neoproterozoic glaciations in south China: *Geology (Boulder)*, v. 32, p. 437-440.